論文 / 著書情報
Article / Book Information

題目(和文)	誘発電位を増加させる視覚刺激と脳波を用いたコンピュータインタフェースに関する研究
Title(English)	A Study on Visual Stimulus Increasing Event-Related Potentials and Computer Interfaces Using EEG
著者(和文)	WilaiprasiTheerawit
Author(English)	Theerawit Wilaiprasitporn
出典(和文)	学位:博士(工学), 学位授与機関:東京工業大学, 報告番号:甲第10557号, 授与年月日:2017年3月26日, 学位の種別:課程博士, 審査員:八木 透,伊能 教夫,井村 順一,中島 求,原 精一郎
Citation(English)	Degree:Doctor (Engineering), Conferring organization: Tokyo Institute of Technology, Report number:甲第10557号, Conferred date:2017/3/26, Degree Type:Course doctor, Examiner:,,,,
学位種別(和文)	博士論文
Type(English)	Doctoral Thesis

Tokyo Institute of Technology

Doctoral Thesis

A Study on Visual Stimulus Increasing Event-Related Potentials and Computer Interfaces Using EEG

Supervisor:
Tohru Yagi, Ph.D., Associate Professor

Author:
Theerawit Wilaiprasitporn

A thesis submitted in fulfilment of the requirements for the degree of Doctor of Engineering

in the

Department of Mechanical and Environmental Informatics
Graduate School of Information Science and Engineering

Abstract

Brain–computer interfaces (BCIs) have been actively researched for over two decades. One of the primary goals is to create a non-muscular communication channel for locked-in patients. Electroencephalography (EEG) is a non-invasive technique that is commonly used in BCI measurement systems. Even though BCIs have a long history, their performance is still limited by the low signal-to noise ratio of EEG. A state-of-the-art BCI application is P300-based BCI. P300 refers to a major event-related potential (ERP) component that peaks around 300 ms after visual stimulus. P300 is an electroencephalographic correlate of target recognition in decision-making tasks. The P300 is used in several brain-computer interfaces (BCIs) as a non-motor signal of decisions, such as letter choice in the P300-Speller utility. Accuracy in choice specification depends on the difference in P300 amplitude evoked by target versus non-target stimuli. In this study, I describe visual stimulus factors, *color*, *motion-modulated*, *complexity-modulated* and *orientation-modulated*, all of which enhance the difference in P300 magnitude between target and non-target stimuli for P300-based BCIs. Stimulus arrays incorporating these visual factors may be used for the design of improved P300-based BCIs with greater choice accuracy and speed.

To demonstrate advantage of research findings from visual factor studies, I report the development of a personal identification number (PIN) application using a P300-based BCI. I focus on visual stimulation design for increasing the evoked potential in the brain. Single-channel electroencephalography and a computationally inexpensive algorithm are used for P300 detection. Experimental results showed that my proposed stimulus induces higher P300 amplitude than does a conventional stimulus. For a performance evaluation, I compare two versions of the proposed application, which are based on my 'original P300 BCI' and 'adaptive P300 BCI'. In the adaptive P300 BCI, I introduce a novel algorithm for P300 detection to improve the information transfer rate while maintaining acceptable accuracy. Experiments with 10 healthy participants reveal that the original P300 BCI achieves mean accuracy of 83.5% at 11.4 bits/min and the adaptive version achieves mean accuracy of 86.0% at 18.6 bits/min.

On the basis of BCI and PIN application, I expand my research to hybrid BCI. Here, I propose a hybrid brain/blink computer interface based on a single-channel EEG amplifier. Eyelid closing and hard blink are selected as two possible inputs for control of the interface. A 2-min calibration is required before starting to use the interface. An algorithm for feature extraction and classification is developed for EEG signals from eyelid closing, hard blink, and resting. To evaluate the performance of the interface, I incorporate it into a personal identification number (PIN) application, in both visual

and auditory modes. Experiments with 5 healthy participants reveal that the PIN application based on the interface achieved a mean accuracy of 97.4%. In conclusion, I expect that my investigation will contribute to hybrid brain-computer interface research and technologies in the near future.

At the end of this study, I start side project for future works. I develop a hybrid BCI for drowsiness detection using EEG and electrooculography (EOG). Measurement is done with a single-channel EEG amplifier. A simple responsive task performs in a drowsy environment is used to experimentally demonstrate the advantages of the proposed system. Additionally, I perform the first investigation of hybrid EEG/EOG indices for drowsiness detection. Pearson's correlation analysis reveals that hybrid EEG/EOG indices are better correlated with the Karolinska Sleepiness Scale (KSS)—the standard subjective measure—than are conventional EEG or EOG indices. My investigation could contribute to both sleep research and the development of real-time drowsiness detection in the near future.

Acknowledgements

Firstly, I would like to express my sincere gratitude to my advisor Prof. Tohru Yagi for the continuous support of my Ph.D study and related research, for his patience, motivation, and immense knowledge. His guidance helped me in all the time of research and writing of this thesis. Besides my advisor, I would like to thank the rest of my thesis committee: Prof. Norio Inou, Prof. Motomu Nakashima, Prof. Jun-ichi Imura and Prof. Seiichiro Hara, for their insightful comments and encouragement, but also for the hard question which incented me to widen my research from various perspectives. Moreover, I specially thank to Japan Society for the Promotion of Science (JSPS) for all financial supports on my research.

My sincere thanks also goes to Prof. Kenji Kansaku (Research Institute of National Rehabilitation Center for Persons with Disabilities, Japan), Dr. Sissades Tongsima (National Center for Genetic Engineering and Biotechnology, Thailand), and Dr. Erin Flynn-Evans (NASA Ames Research Center, USA), who provided me opportunities to join their team as intern. Also I thank Alex Popovici (NASA Ames Research Center, USA) and Chris Micek (The Johns Hopkins University) who are my research collaborators. I thank my fellow lab mates (Yagi Laboratory) for the stimulating discussions, and for all the fun we have had in the last three years.

In Thailand, I would like to thank Prof. Widhayakorn Asdornwised who is my former advisor at Chulalongkorn University. Also, I thank Junior Science Talent Project (JSTP), National Science and Technology Development Agency (NSTDA), Thailand for all supports. Lastly, my thoughts go also to my family, lover and friends who enriched my life with their presence. I would not be where I am without their support, care and love.

Contents

List of Figures

List of Tables

Chapter 1

Introduction

1.1 Motivation

Nowadays, information and technology plays an important role in our daily life. In engineering field, this is an era of 'big data' or 'Internet of things'. Almost everybody have own mobile devices such as smart phone, tablet and other wearable devices, and always communicate to each other across the world. To improve capabilities in using those smart devices, a development of human computer interfaces (HCIs) for both medical and non-medical purposes has became active research. HCIs are supposed to be interconnection between human body and smart device. One of the most useful option for connecting human body to smart device is making a circuit between human and devices. Therefore, knowledge on biopotentials are very important. Electromyogram (EMG), electrooculogram (EOG) and electroencephalogram (EEG) are biopotential measurement techniques which are commonly used in development of HCIs. These techniques represent non-invasive measurement of muscle, eyes and brain activities, respectively.

Electromyogram (EMG) signal is commonly measured in millivolt (mV) level, 1-10 mV [2]. Frequency range is 20-2000 Hz which is higher than EOG and EEG. Either contraction or relaxation of muscle fibers can generate EMG signal. Ag-AgCl (silver-silver chloride) or carbon, stainless steel, needle electrodes are commonly used in EMG measurement. Various applications are proposed based on EMG such as neuromuscular disorder diagnosis, prosthesis and HCI applications [2].

Electrooculogram (EOG) signal is result of eyeball movement. Structures of human eyeballs and skull create electrical dipole property. Cornea side of eyeballs represent positive pole and the retina side represent negative pole. Movement of eyeballs cause changing in direction of electrical dipole. Hence, measurement of biopotentials around

the eyeballs can predict eye gaze direction. EOG is usually measure in 10-100 microvolts (μV) [2]. DC amplifier and Ag-AgCl electrodes are commonly used in measurement of EOG. EOG is widely used in development of eye gaze interfaces.

Electroencephalogram (EEG) signal is composed of electrical signals from billions of neurons. Source of signals locate in brain which is under scalp and skull. Therefore, the signal level is extremely lower than EMG and EOG. EEG is usually measured at 1-10 microvolts (μV) [2] with bandwidth 0.5-40 Hz. To get high signal to noise ratio EEG, skin preparation is very important. Moreover, multiple electrodes are usually used to increase EEG resolution. Gold plate and Ag-AgCl electrodes are commonly used in measurement. Well-known clinical application using EEG is diagnosis of seizure. Furthermore, EEG is the most practical technique in brain-computer interface (BCI) technologies.

Originally biopotentials based HCIs, especially BCIs, were focusing on applications for rehabilitation engineering so that most system had been designed for handicapped people. Due to low signal-to-noise ratio and complexity of measurement system, applying conventional BCIs into non-medical applications still be challenging issues. These issues motivate me to do research and develop BCIs based applications toward general purposes. In this study, I develop two types of interfaces which are based on background of BCIs and hybrid BCIs.

1.2 Brain-Computer Interfaces (BCIs)

Non-muscular communication channels or brain-computer interfaces (BCIs) have been developed over the past two decades to allow for direct control of external processes by brain signals [3] (see Figure 1.1). Early BCI researchers concentrate on clinical applications for patients with severe neurodegenerative disorders such as amyotrophic lateral sclerosis (ALS). Using BCIs, patients can send commands to a computer using endogenous brain signals evoked by specific stimulus patterns as measured invasively or non-invasively by various techniques.

1.2.1 Measurement Techiques for BCIs

In typical BCI technologies, brain activity is acquired through electrophysiological activity. Three techniques named electroencephalography (EEG), electrocorticography (ECoG) and magnetoencephalography (MEG) are commonly used to record of electrophysiological signals.

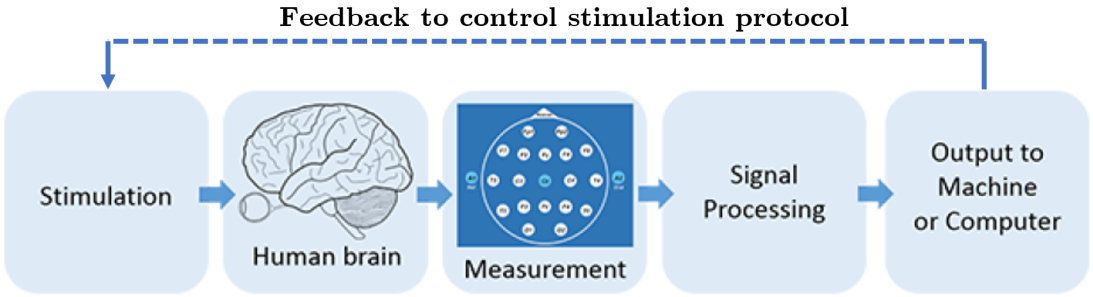

FIGURE 1.1: Overall architecture of BCIs.

Electroencephalography (EEG) is used to measure potential variation across scalp over time. Major drawback of EEG is distortion of signal within skull and scalp. Hence, quality of signal in terms of signal-to-noise ratio is very low. In measurement setup, EEG requires at least three electrodes for recording point, reference point and ground point. Temporal and spatial resolution is about 0.05 seconds (s) and 10 millimeter (mm) respectively [4]. This is the lowest spatial resolution compared to ECoG and MEG signal. However, there are several advantages of this technique. The first advantage is that EEG is an non-invasive measurement, and therefore there is no risk. The other advantage is that various portable devices are available in the market.

Electrocorticography (ECoG) is an invasive brain measurement technique. Electrode arrays are implanted directly to the brain under the skull. Hence, ECoG signal is stronger signal than the others. Due to invasive measurement, ECoG is the highest risk measurement system. Therefore, ECoG is usually studied with animals such as monkey. Only a few research groups implanted it to human. Temporal and spatial resolution is about 0.003 s and 1 mm respectively [4]. Furthermore, ECoG performs extremely higher temporal and spatial resolution than both EEG and MEG.

Magnetoencephalography (MEG) is used to measure brain activity through induced magnetic field. The neurophysiological processes that generate MEG signal are the same processes as in EEG; however, magnetic field is measured instead of electric filed. The advantage of magnetic field over electric field is that magnetic field will not be distorted by skull and scalp. Temporal and spatial resolution is about 0.05 s and 5 mm respectively [4]. Although MEG signal has higher spatial resolution than EEG, the system is more complex and not portable.

By comparison of EEG, ECoG and MEG in Table 1.1, EEG is the most suitable choice for a study and development of practical BCI applications. Even if EEG signal

TABLE 1.1: Summary of measurement techniques for BCIs

Measurement technique	Activity measured	Temporal resolution	Spatial resolution	Risk	Portability
EEG	Electrical	∼0.05 s	∼10 mm	Non-invasive	Portable
ECoG	Electrical	∼0.003 s	∼1 mm	Invasive	Non-portable
MEG	Magnetic	∼0.05 s	∼5 mm	Non-invasive	Portable

is very low magnitude and poor quality of signal, EEG-based BCIs still be the most practical BCI technologies. Therefore, I continue focusing on EEG-based BCIs in this study.

1.2.2 EEG-Based BCIs

Event related potential (ERP) technique is widely used in EEG-based BCIs. Principle concept of ERP technique is an ensemble averaging of brain responses from specific stimulus. Visual, auditory and tactile stimuli are generally used to stimulate human brain. Synchronization of stimulus protocols and ERPs allows human to send commands to the computer at specific time. Therefore, EEG-based BCIs can be classified into three modalities (visual, auditory and tactile stimulation-based BCI) based on types of stimulations.

Visual stimulation-based BCI is widely used in communication applications. To induce brain responses, visual stimulation is used in this modality. In typical applications, the stimulation works as a flicker light. The response will be analyzed in frequency domain in case that system generates steady frequency of flickering. Detection of responses in frequency domain is known as steady state evoked potentials (SSVEPs)-based BCI. On the other hand, if stimulation is randomly flickered, responses will be considered in time domain. Detection of responses in time domain is known as P300-based BCI. P300 represent the highest peak component of ERPs.

Auditory stimulation-based BCI uses auditory stimulation instead of visual stimulation. Analysis and technique to detect brain responses is similar to visual stimulation-based BCIs. The advantage of this modality is that blind person can use the system. However, several research groups reported that auditory stimulation-based BCI had lower accuracy than the other modalities [5].

Tatile stimulation-based BCI is novel solution. Small vibrators are used to be simulator by placing on human body. One research group tested tactile-based BCI application by placing vibrator units on locked-in state patient's arm, and the results revealed higher accuracy than visual and auditory stimulation-based BCI application [5]. However, it is difficult to memorize positions of targets in case that many vibrator units

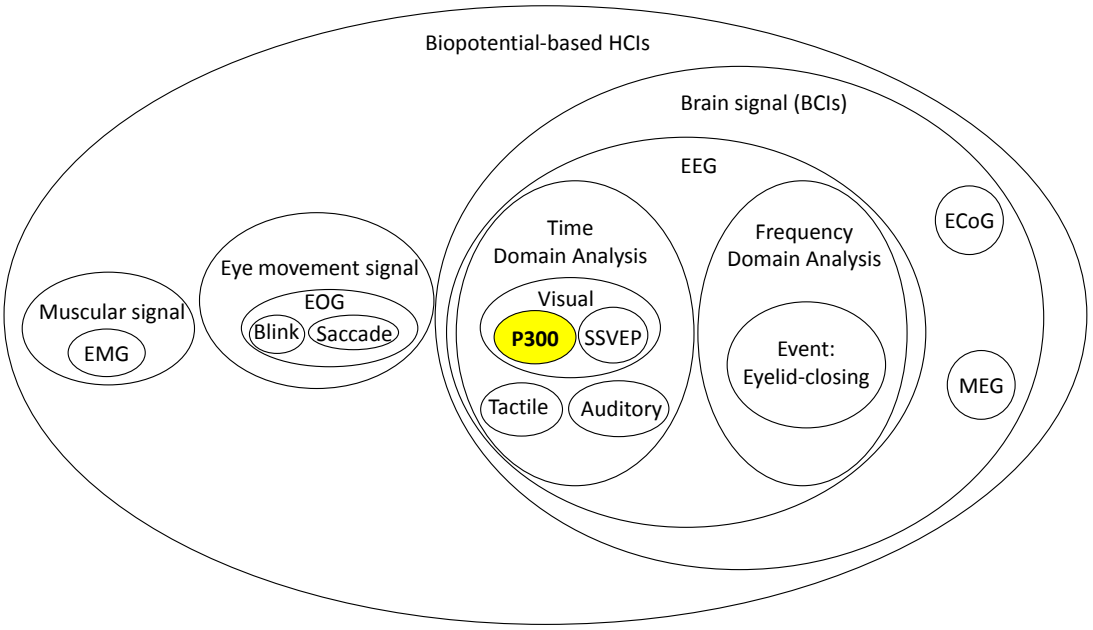

FIGURE 1.2: Biopotential-based HCI related research. P300 states position of P300-based BCIs.

are placed on human body. Furthermore, there is no report about optimal positions for placing vibrator units. Hence, development of BCI applications based on tactile modality has to concern a lot of external factors which can effect to the system.

In conclusion, all related research on biopotentials towards HCIs are summarized as the diagram in Figure 1.2. To achieve the goal towards practical BCI applications for general purposes such as HCI applications, I mainly focus on an improvement of P300-based BCIs using visual stimulation in this research. The major ERP component used for this purpose is P300, a reliable positive voltage peak occurring about 300 ms after onset of a target stimulus. The P300 is usually elicited using the visual oddball paradigm in which a subject detects a rare target among more non-target stimuli [6]. The P300-Speller, which uses the P300 to indicate choice of letter (target) as the alphabet is flashed on a computer screen, was among the first P300-based BCI systems [7] (see Figure 1.3)

Recently, BCI research has continuously expanded to encompass not only medical applications but also general engineering applications. Some applications are aimed at monitoring mental states, such as attention level, workload, and music perception. BCI has also been used for entertainment, for instance, in computer games and toys. Due to the low signal-to-noise ratio (SNR) of EEG-measured P300, BCI is not as practical as other HCI technologies for healthy people.

To improve performance of BCI technologies, most researchers focus on algorithm, signal processing or multi-modal BCIs. Few researchers investigate novel visual stimulus

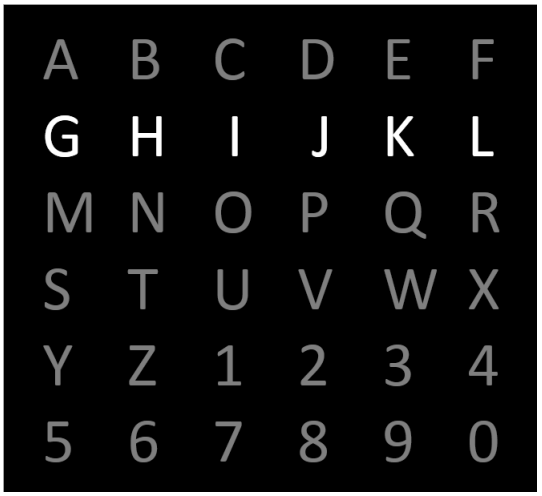

FIGURE 1.3: Illustration of the conventional P300-Speller capture screen.

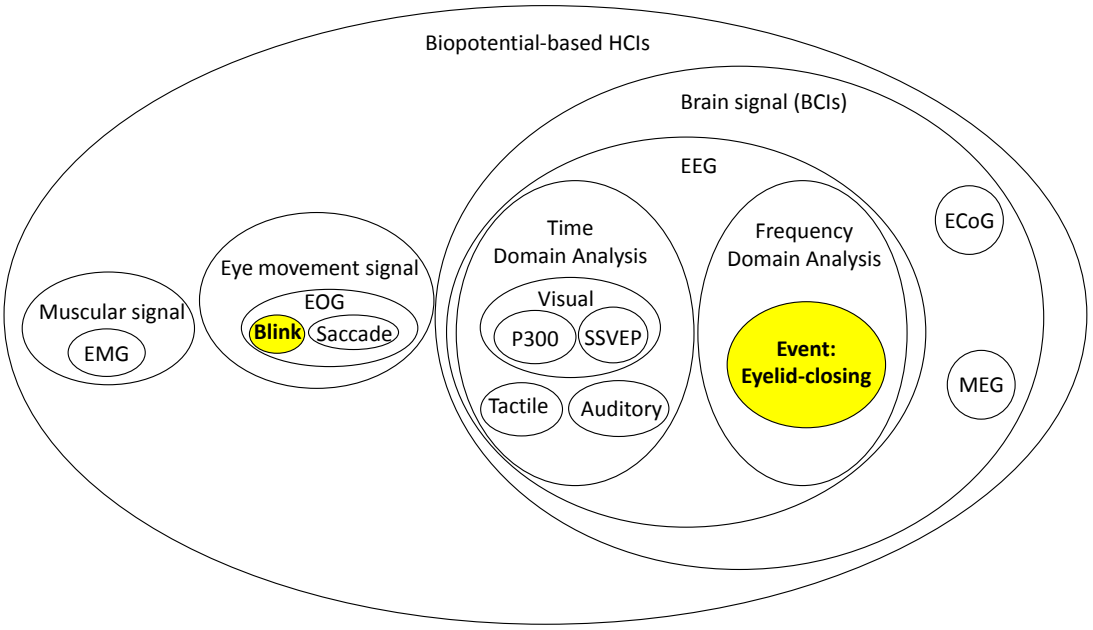

FIGURE 1.4: Biopotential-based HCI related research. Eyelid-closing and blink state position of proposed hybrid BCI in this thesis.

paradigms. However, their stimulus designs are not based on human visual factors. On the other hand, I study various visual factors, and demonstrate feasibility in an improvement of BCI toward control applications.

1.2.3 Hybrid Brain-Computer Interfaces (Hybrid BCIs)

Recently, researchers have developed hybrid BCIs in two different directions. First, hybrid BCIs for individuals who have residual motor abilities, such as controlling muscles related to eye movement [8]. Hybrid is referred to combination between EEG and EOG/EMG in this case [9, 10]. Second direction, hybrid is referred to simultaneously obtain two different kinds of brain responses using EEG, such as SSVEP and P300 [11–15]. Compared with conventional BCIs, hybrid BCIs achieve higher accuracy and information transfer rate. In this research, I propose novel hybrid BCI named hybrid Brain/Blink interface. Proposed system targets on EEG signal while eyelid-closing and blink signal from EOG. Figure 1.4 presents position of proposed hybrid system inside HCI related research areas.

1.3 Goal and Challenge Issues

The objective of my research is to investigate novel techniques for development of EEG-based BCIs/hybrid BCIs. Developed BCIs are aimed at high reliability and user-friendly interfaces. To demonstrate advantages of proposed BCIs, I invent personal identification number (PIN) application to serve as a test-bed application. Finally, feasibility study of drowsiness detection using hybrid BCIs perform the future of BCIs beyond typical control applications.

Issue I: Complexity of Conventional Recording System: Due to non-invasive measurement, EEG is not persistent to noisy environment. BCI users are always required to wear multiple channels of recording electrodes (multiple channels-EEG). Attaching electrodes is not user-friendly and time consuming works, so typical BCI is not useful HCI for healthy people. To make BCI more simply, I come up with two approaches. The first one is that we have to increase brain potential magnitudes so that brain responses can be easily detected by sparse electrodes. The other alternative is that we have to increase features of input signals by integration of other bio-signals such as EOG, EMG and Blinking.

Issue II: Side Project for Future Works: Beyond Control Applications: Original BCI is supposed to be non-muscular communication pathway between motor disabled person and computer. Thus, most researchers focus on development of control related applications. This point motivates me to invent other BCI-based technologies. At the end of this study, I start to introduce drowsiness detection using proposed hybrid BCIs.

1.4 Overview of my Approaches

I deal with the above mentioned issues through the following approaches. Approach I and II deal with Issue I, and Approach II deals with Issue II.

Approach I: Single Channel Electroencephalography (EEG) Amplifier Based BCIs': Here, experimental study and development are based on single channel EEG. I first improve conventional P300-BCIs by development of visual stimulation for an increasing brain evoked potentials. To design visual stimulation, I conduct basic experiments for studying of several human visual factors. By combination of two visual factors which are ***Motion-Modulated Stimulus*** and ***Orientation-Modulated Stimulus***, BCI can record higher P300 response in terms of amplitude than typical visual stimulus. And P300 amplitude can be inferred to accuracy of BCI in my study. To demonstrate usefulness of proposed BCIs, I develop a BCI-based personal identification number (PIN) application to serve as a test-bed application. Nowadays, users typically use keypads to input PINs. A major drawback of keypads is that PINs can be visually or optically observed when they are entered or recovered afterward by thermal camera-based attacks. Various approaches based on biometrics and biosignals have been proposed in order to solve this problem. Fingerprints are widely used in biometric system. However, fingerprints can be duplicated by various techniques. Recently, one research group proposed gaze-based password entry, but gaze tracking requires a long time for calibration. Hence, we proposed a PIN application using a BCI as an alternative modality. There are three advantages of the proposed PIN application over the above-mentioned techniques. The first is that no calibration is required before using the application. The second is that the user can avoid the problem of the PIN being observed during entry, as is possible with keypads. The third is that BCIs allow for non-touch input, so no heat signal or fingerprint is left behind after use.

Approach II Hybrid Brain/Blink-Computer Interface: Experimental study and development are also based on single channel EEG. To make practical and reliable system, I switch to work on hybrid BCI. I target on two obvious signals which are ***Alpha Wave*** from EEG and ***Hard Blink*** from EOG. The proposed hybrid BCI is called ***Hybrid Brain/Blink-Computer Interface***. PIN application which mentioned in Approach I of Issue I is used to be test-bed application for this approach as well.

Approach III: Drowsiness Detection: To demonstrate advantage of proposed hybrid BCI for non-control related application, I conduct feasibility study to use it for drowsiness detection. By comparison of EEG drowsy index, EOG drowsy index and hybrid EEG/EOG drowsy index, preliminary results perform that hybrid index has highly significant correlated to standard subjective measure for sleepiness. Moreover,

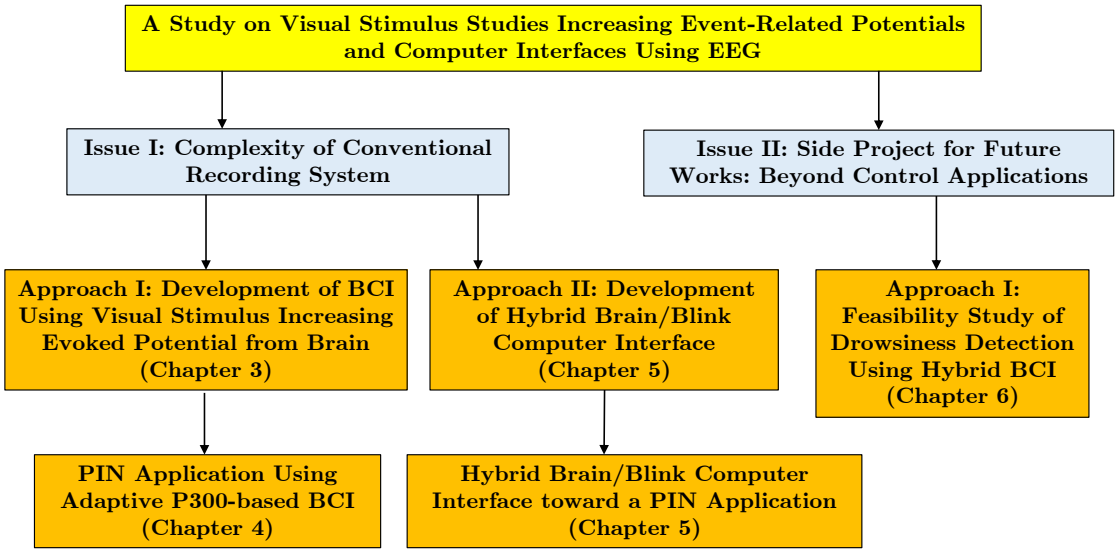

FIGURE 1.5: Organization of this thesis.

my on-going BCI research regardless to control application is introduced in the section for future works.

1.5 Thesis Organization

This thesis consists of seven chapters. The organization as shown in Figure 1.5.

Chapter 2 covers a survey of the research related to P300-based BCIs using visual stimulation, hybrid BCIs and BCI applications. Finally, I emphasize my research position towards BCI research fields.

Chapter 3 presents visual stimulus studies. Here, I focus on characteristics of P300 responses from several visual factors. Experimental results can be implemented as fundamental visual stimulus design knowledge for P300-based BCIs.

In Chapter 4, I incorporate research findings from Chapter 3 into PIN application. Moreover, novel algorithm for P300 detection is reported in this Chapter. Finally,

performance evaluation of PIN application using proposed P300-based BCI has been performed.

Hybrid Brain/Blink is introduced in Chapter 5. To extract and classify feature signals from brain waves and blinks, novel technique and experimental study are demonstrated in this Chapter. Proposed hybrid interface is applied to PIN application. Evaluation of the proposed hybrid interface is performed through two modalities of PIN application (visual and sound navigated systems).

In Chapter 6, the same recording system as Chapter 5 is used for feasibility study of drowsiness detection. Preliminary results have been promising for future studies.

Chapter 7 discusses the contributions of this thesis and remaining issues for future works. Final conclusion is summarized in this Chapter.

Chapter 2

Literature Review

According to Chapter 1, challenge issues are classified into three research areas which are development of visual stimulation for P300-based BCIs, hybrid BCIs and current BCI applications and future trends. Thus, literature review of each area is done separately. Finally, I also point out the position of my studies towards mentioned research areas.

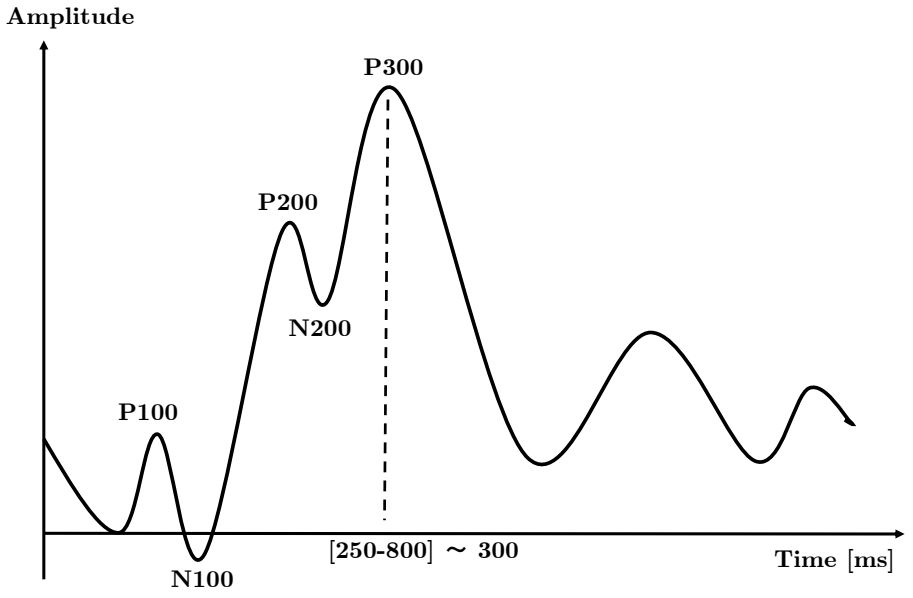

FIGURE 2.1: Illustration of P300 wave. P and N are referred to Positive and Negative peaks respectively. 100, 200 and 300 present averaged latencies in milliseconds

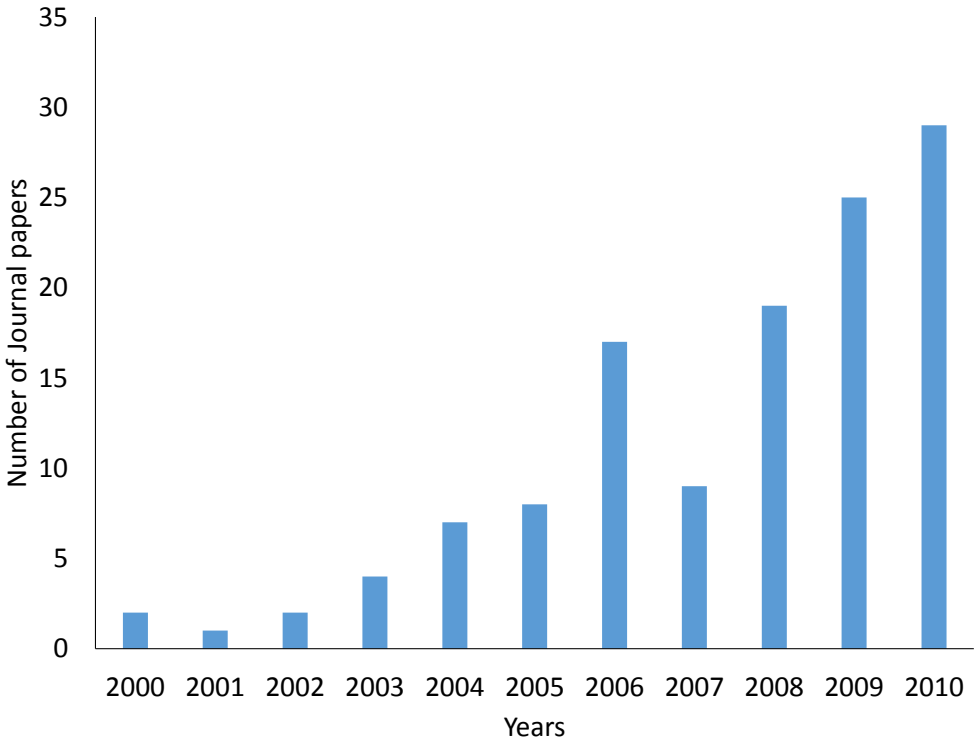

FIGURE 2.2: Number of published journal papers in PubMed from 2000 to 2010 which are related to "(P300 or P3) and (BCI or Brain Computer Interface)" [1]

2.1 Development of visual stimulation for P300-based BCIs

Brain–computer interfaces (BCIs) have been actively researched for over two decades. One of the primary goals is to create a non-muscular communication channel for locked-in patients [3]. Event related potential (ERP) technique is widely used in EEG-based BCIs. Principle concept of ERP technique is an ensemble averaging of brain responses from specific stimulus. Visual, auditory and tactile stimuli are generally used to stimulate human brain. Synchronization of stimulus protocols and ERPs allows human to send commands to the computer at specific time. The major ERP component used for P300-based BCIs is P300, a reliable positive voltage peak occurring about 300 ms after onset of a target stimulus, as illustrated in Figure 2.1. The P300 is usually elicited using the visual oddball paradigm in which a subject detects a rare target among more non-target stimuli [6]. The P300-Speller, which uses the P300 to indicate choice of letter (target) as the alphabet is flashed on a computer screen, is state-of-the-art BCI application, see Figure 1.3 [7]. Even though BCIs have a long history, their performance is still limited by the low signal-to noise ratio of EEG. After 20th century, the number of research related to BCI and P300 are dramatically increased as shown in Figure 2.2. In this Section, I begin with introduction to visual stimulation in original P300 speller.

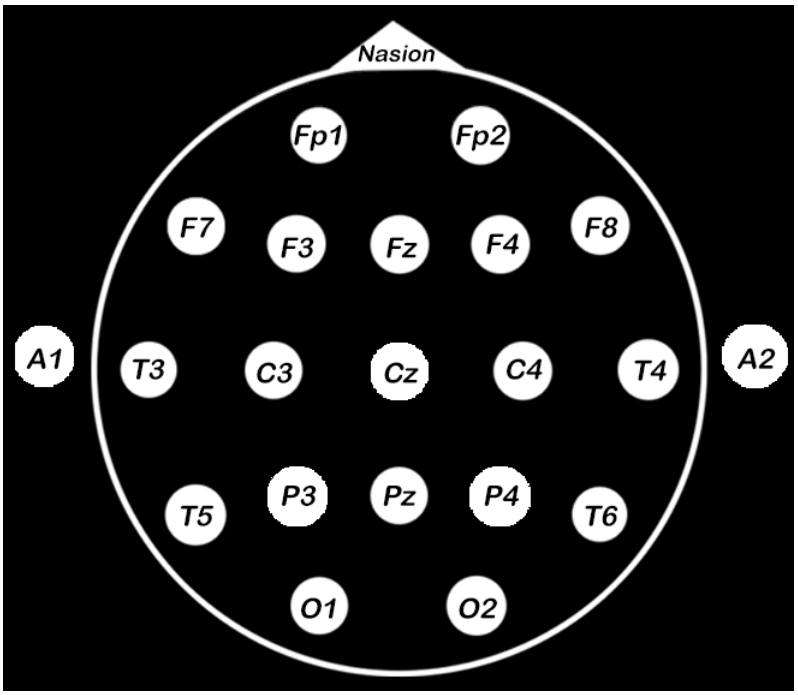

FIGURE 2.3: 10/20 international standard system for EEG measurement

Then, I review research studies on an improvement of P300 speller by designing novel visual stimulus paradigms. Finally, the position of my research towards development of visual stimulus paradigm for P300-based BCIs is explained.

2.1.1 Conventional P300 speller

Original P300 speller uses 6x6 white/gray flicker alphabet matrix for visual stimulation [7]. EEG with Ag-AgCl electrode is used to record brain signal. Single electrode is placed at Pz position (10/20 international standard system, see Figure 2.3). Skin preparation gel and conductive paste are typically used in electrode placement. To detect attended or target signal, typical algorithm is stepwise linear discriminant analysis (SWDA). Although original P300 speller can operate accurately at 12 bits/min (averaged from four subjects, N=4), researcher try to improve both accuracy and transmission rate by proposing new visual stimulation paradigm.

2.1.2 Row and column paradigms (RC)

In the first decade of their existence, the most common visual presentation format for P300 BCI was the row/column (RC) white/gray flicker matrix [1]. Alphabet characters

FIGURE 2.4: The P300 speller with row/column green/blue flickering matrix

are randomly flashed in row and column. Recently, one medical research group proposes that green/blue flickering RC matrices are more accurate than the conventional gray/white matrix (see Figure 2.4) [16]. Two major sources of error for RC format are signal overlap from temporally adjacent ERPs (especially when same row or column is flashed twice in succession) and interference flashes from adjacent characters [17, 18].

2.1.3 Single character paradigms (SC)

Single character paradigm (SC) presents same alphabet matrix as RC (see Figure 2.5). However, single character is randomly flashed during stimulation. Therefore, SC requires stimulation period longer than RC. One research group compared RC and SC speller, and reported that RC reached 85.3% of mean accuracy and SC reached 77.9% of mean accuracy (N=19) [19].

2.1.4 Region-based paradigms (RB)

Region-based paradigm (RB) is grouping of alphabet into several groups in order to decrease interference flashes from adjacent characters and signal overlap from temporally adjacent ERPs [20]. To select target character, user has to select target group and then

FIGURE 2.5: Single character paradigm (SC)

target character (see Figure 2.6). Comparison of RC, SC and RB with same set of subjects performed mean accuracy at 85%, 72.2% and 90.6%, respectively.

2.1.5 Checker board paradigms (CB)

The checkerboard (CB) paradigm is designed to overcome two major sources of error in RC paradigm [21]. The 72 items are separated into two flash groups, black and white as shown in Figure 2.7(a) (not seen by viewers). In each time of flickering, computer randomly selects six items from one group, and then flashes on the screen (Figure 2.7(b)). The computer repeats flash until completion of all possible characters. Same flash group are prohibited from twice flashing in succession. Therefore, same character flashes twice in succession has never been happened in CB paradigm. Moreover, interference flashes from adjacent characters are avoided by the segregation of adjacent items into separate flash groups.

2.1.6 RC with human face stimulus paradigm

One research group combine human face stimulus into conventional RC white/gray flicker matrix [22]. Character is changed to human face stimulus during flashing period, and

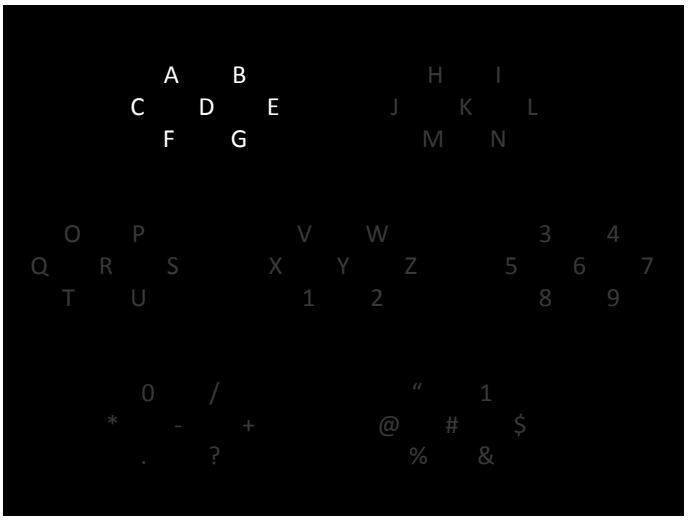

(a) Target group selection

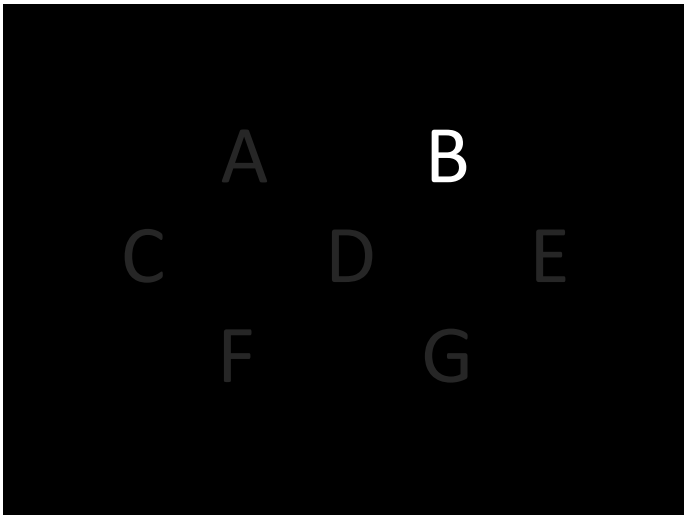

(b) Target character selection

FIGURE 2.6: Region-based paradigm (RB)

then returned to character again in non-flashing period. Comparison of RC with human face stimulus and conventional RC performs that human face can enhance P300 amplitude and improve accuracy of BCI system. RC with human face stimulus reached more than mean accuracy of 90% while conventional RC reached about mean accuracy of 75% at same set of subjects (N=10). Furthermore, they tried to improve performance of their stimulation by modulation of facial motion and emotion. However, they could not achieve their goal.

2.1.7 Non-flicker paradigms

Recently, a motion-onset paradigm for BCI application has been proposed, in which an empty rectangular button is presented on the screen (see Figure 2.8). In the stimulus

A	B	C	D	E	F	G	H
I	J	K	L	M	N	O	P
Q	R	S	T	U	V	W	X
Y	Z	Sp	1	2	3	4	5
6	7	8	9	0	.	Ret	Bs
?	,	;	\	/	+	-	Alt
Ctrl	=	Del	Home	UpAw	End	PgUp	Shift
Save	‘	F2	LfAw	DnAw	RtAw	PgDn	Pause
Caps	F5	Tap	EC	ESC	email	!	Sleep

(a) Assignment of possible target into two flashing goups (not seen by viewers)

(b) Example of target flashing in CB paradigm

FIGURE 2.7: Checker board paradigms (CB)

state, a red vertical line appeared on the right side of the rectangle that moved leftward until it disappeared. This stimulus induced a motion-onset VEP (mVEP) with major N2 and P2 components. In that study, it was reported that an mVEP-based BCI performed with up to 98% accuracy using 10 trials [23]. There was no flickering or flashing in this paradigm. Moreover, they implemented mVEP based stimulus into Google search task application. Finally, Google search application using single electrode reached averaged information transfer rate at 42.2 bits/min with a mean accuracy of 83% (N= 12) [24].

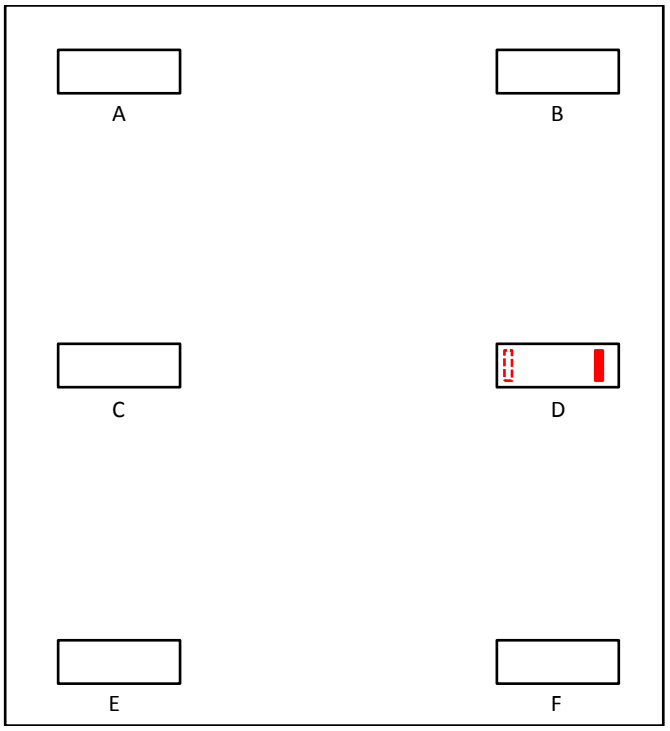

FIGURE 2.8: Non-flicker paradigms

2.1.8 Position of my research towards an improvement of P300-BCI applications

To improve performance of BCI technologies, most researchers focus on algorithm, signal processing or multi-modal BCIs. Few researchers investigated novel paradigms as mentioned in previous section. However, their paradigm designs were not based on human visual factors. On the other hand, I conduct basic research to investigate human visual factors which are related to P300. Color effect, motion-modulated attention (modulated by saccade-ERP), complexity-modulated attention and orientation-modulated effects for a design of visual-based BCIs are first introduced by my research. I demonstrate that introduced visual factors do enhance the P300 responses and suggest their feasibility in the practical use of BCI system. Based on my findings, the P300 wave is strongly related to human visual system. My experiments indicate that motion-modulated attention, complexity-modulated attention and orientation-modulated effects significantly increase peak P300 amplitude. In the near future, I plan to combine various visual factors such as color contrast, motion, depth and frequency into one stimulus. My ultimate goal is to simplify existing BCI technologies for both medical and non-medical. I expect that well-designed visual stimuli will facilitate single channel BCIs. More information on these studies can be seen on Chapter 3.

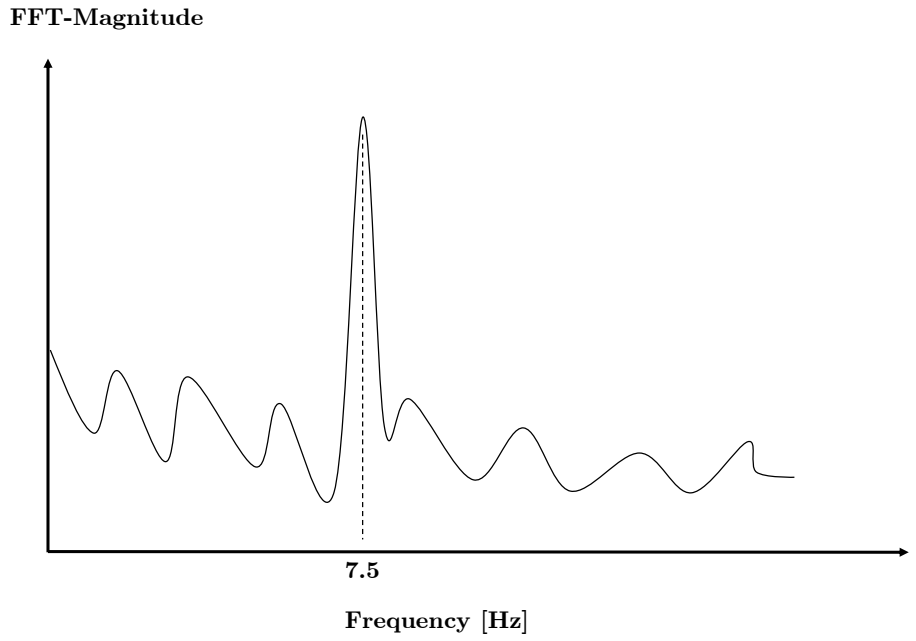

FIGURE 2.9: Drawing of 7.5 Hz-SSVEP response

2.2 Development of hybrid BCIs

According to Chapter 1, hybrid BCIs has been classified into two major groups.

- In first group, hybrid refers to combination between two feature signals from brain such as P300, steady-state visual evoked potential (SSVEP) and event-related desynchronization/synchronization (ERD/ERS). P300 response had been introduced in previous Section, and illustration of P300 wave can be seen in Figure 2.1. SSVEP is steady state of brain wave which is responding to steady frequency-flickering stimulus. Figure 2.9 is a drawing to represent 7.5 Hz-SSVEP response in frequency domain. FFT or Fast Fourier Transform is conventional method to obtain SSVEP. ERD/ERS is typical target responses from motor-imagery tasks.
- In second group, hybrid refers to combination between different types of bio-potentials such as EEG, EOG and EMG. (More information on EEG, EOG and EMG can bee seen in Chapter 1.)

According to review article on existing hybrid BCI research [8], several different systems can be summarized as in Table 2.1.

TABLE 2.1: Comparison of existing hybrid BCI systems

Reference #	**Feature signals**	**System**	**Contributions**	**Classification technique**
[11]	ERD, SSVEP	Simultaneous	Accuracy significantly improved compared to ERD and slightly better than SSVEP	LDA
[12]	ERD, SSVEP	Sequential	False positive rate was reduced	FLDA
[13]	ERD, SSVEP	Simultaneous	Feedbacks were added to the work done in [11]	LDA
[14]	P300, SSVEP	Sequential	Improved information transfer rate (bit rate)	FLDA and BLDA
[25]	P300, ERD	Sequential	Expand control functions in virtual environment	SVM and FLDA
[26]	P300, ERD	Simultaneous	Increase reliability	FLDA
[10]	EEG, EMG	Simultaneous	Improvement in performance	Frequency analysis and Gaussian classifier
[27]	ERD, EOG	Sequential	Improvement in performance	LDA

Existing systems can be classified in to simultaneous and sequential systems. Simultaneous system can recognize two feature signals at the same time. On the other hand, sequential system can only recognize one by one feature signal. Most algorithms for identifying of feature signals are based on linear discriminant analysis (LDA). Moreover, contributions of previous research towards development of hybrid BCIs are also reported in Table 2.1. (FLDA := Fischer's LDA, BLDA := Bayesian LDA, SVM := Support Vector Machine)

2.2.1 Position of my research towards development of hybrid BCIs

I propose novel hybrid BCI based on EEG and Blink signals. Both signals can simultaneously record using single channel EEG amplifier. Researchers usually analyze EEG signal in four frequency bands, δ(0.5-4 Hz) θ(4-8 Hz) α(8-13 Hz) β(13-30 Hz) [28]. Alpha wave is the only one band that human can partly control by eyelid closing [29]. Thus dominating of Alpha wave has been selected to be a feature signal for proposed interface. I define Hard Blink signal to be another feature signal, and LDA is used as an classification algorithm. Proposed hybrid BCI has three majors advantages over the others. First, single channel recording is more user-friendly. Second, feature signals are easy to generate by eyelid closing and Hard Blink. Third, system works simultaneously in classifying of incoming feature signals. Furthermore, proposed interface suggests me to add more feature signals such as EOG signals from eye-movements in future. More details on proposed hybrid BCI can be found on Chapter 5.

2.3 Current and emerging applications

Since initial period of BCIs, researchers mainly focus on control applications. Most applications allow user to send command to control machines or computers. This Section begins with a review of BCI-based control applications. Then my proposed BCI applications have been explained at the end of Section.

2.3.1 Applications related to control

According to Section 2.1, the P300 speller is state of the art BCI interface which allows human directly select items such as alphabets on a monitor screen. It might conclude that the P300 speller is a discrete input paradigm. On the other hand, In last century, several research groups proposed analog input paradigms such as moving cursors among four directions [30, 31]. Moreover, basic knowledge on P300-based BCI has been applied

into various fields. In robotics, It is performed feasibility in control of partially autonomous humanoid robots [32]. In assistive technologies, It has been widely proposed to use with wheelchair such as in [33]. P300-BCIs are also incorporated to entertainment applications such as painting [34], gaming [35] and virtual reality [36].

2.3.2 Position of my research towards development of BCI based applications

Based on basic knowledge of P300-based BCI and control applications, I propose personal identification number (PIN) application. There are two version of PIN applications. The first version is incorporated to my developed P300-based BCI, and the second one is incorporated to my proposed hybrid BCI. Performance of the applications are evaluated together with proposed interfaces. On development of PIN applications and outcomes are explained in Chapter 4 and 5. Moreover, I demonstrate advantage of proposed hybrid BCI towards non-control application as drowsiness detection, in Chapter 6.

Chapter 3

Development of BCI Using Visual Stimulus Increasing Evoked Potential from Brain

The event-related potential (ERP) P300 is an electroencephalographic correlate of target recognition in decision-making tasks. The P300 is used in several brain-computer interfaces (BCIs) as a non-motor signal of decisions, such as letter choice in the P300-Speller utility. Accuracy in choice specification depends on the difference in P300 amplitude evoked by target versus non-target stimuli. In this Chapter, I study human visual factors, Color, Complexity, Motion and Orientation, related to P300 amplitude. Based on research findings, I propose novel P300 stimulus paradigms for an increasing of P300 amplitude. Stimulus arrays incorporating these stimulus paradigms may be used for the design of improved P300-based BCIs with greater choice accuracy and speed.

3.1 Visual factor I: Color

The conventional P300 speller is based on a white/gray flicker matrix on a black background. Recently, the use of different color combinations in a flicker matrix was studied, and a comparison of white/gray and green/blue flicker matrices was proposed, in which a P300 speller based on a green/blue flicker matrix gave better results than the conventional flicker matrix [16]. Subsequently, the effect of the green/blue flicker matrix was studied using both EEG and MRI [37], and it was found that the amplitude of the P300 response in the case of the green/blue flicker matrix was always higher than that for the white/gray flicker matrix.

Thus, the use of green/blue flicker matrices for practical BCI applications was proposed. Moreover, clinical research has also reported that green/blue flickering is the least provocative type of stimulus, whereas red/blue or Pokemon flickering are the most provocative types of stimuli [38]. There is also incident that Pokemon flickering caused seizure in many children [39]. Despite the fact that color combination has an effect on P300, there was no clear explanation as to what causes this phenomenon.

In my research, I developed a human color vision-based visual stimulation protocol for studying various characteristics of the P300 based on the effects of color. The structure of the retina plays an important role in color sensitivity [39]. Human color receptors called cone cells are located in the retina. The human eye contains three types of cone cells, namely S-cones (short wavelengths), M-cones (medium wavelengths) and L-cones (long wavelengths). The numbers and distributions of these three types of cone cells are not equal. According to the physiology of human color perception, I hypothesized that the different color of stimuli cause different characteristics of P300. In the experiments, I investigated the characteristics of P300 from primary color stimuli (red, green and blue).

3.1.1 Materials and Methods

Experiments were conducted in an electromagnetically shielded dark room. Participants were seated 90 cm away from a monitor (Acer G235H LCD Monitor, 23 in), and each subject was requested to conduct the experiment only once. (The experiments followed Helsinki Declaration of 1975, as revised in 2000)

- **Participants**

  Eleven healthy volunteers participated in the experiments. All participants were males aged 23–27. Although none of the participants had a history of color vision disorders, such as color blindness, they were tested for color blindness by using the Ishihara test.

- **Stimulation**

  I prepared RGB-based color target stimuli placed on a black background on a screen with a resolution of 1920 × 1080 px (see 3.1(a)). Fifteen sets of three dots with the same color were presented on the screen, where each dot had a diameter of 2.3 cm. The size of each set was aligned to be within 5° from the center of each participant's retina (area with a high density of cone cells). The color targets were made to flicker by changing their luminance. Here, I defined two states of flickering, namely inter-stimulus or no flashing (see 3.1(a)(a)) and intensification or flashing

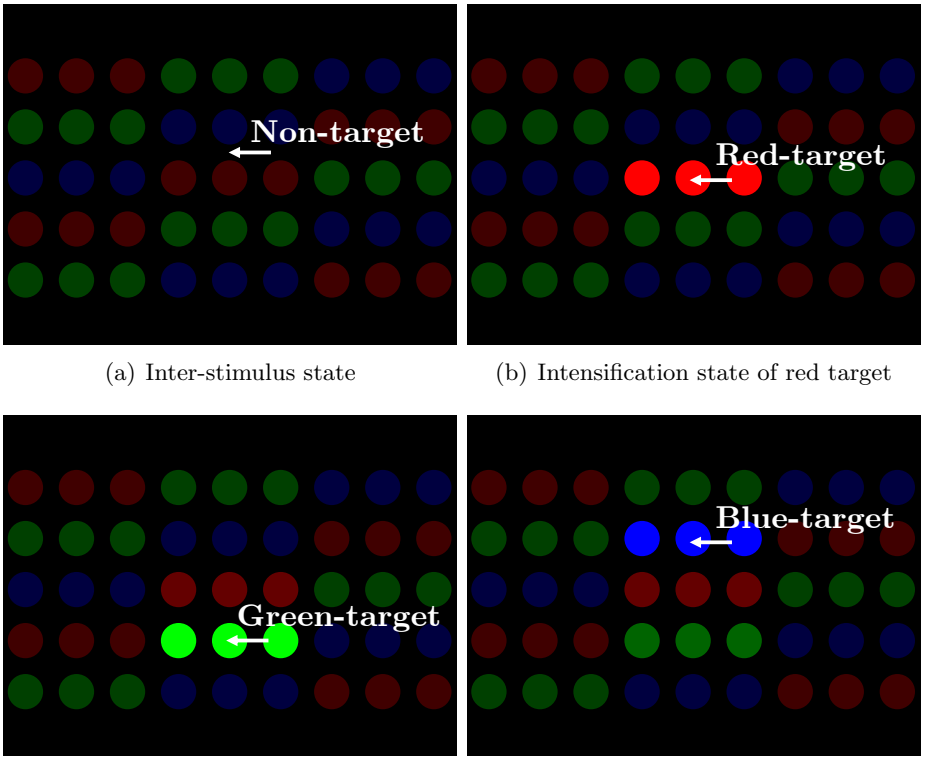

(a) Inter-stimulus state (b) Intensification state of red target

(c) Intensification state of green target (d) Intensification state of blue target

FIGURE 3.1: (a) Target color (red, green and blue) and non-target color (black background). (b) Intensification of red target. (c) Intensification of green target. (d) Intensification of blue target.

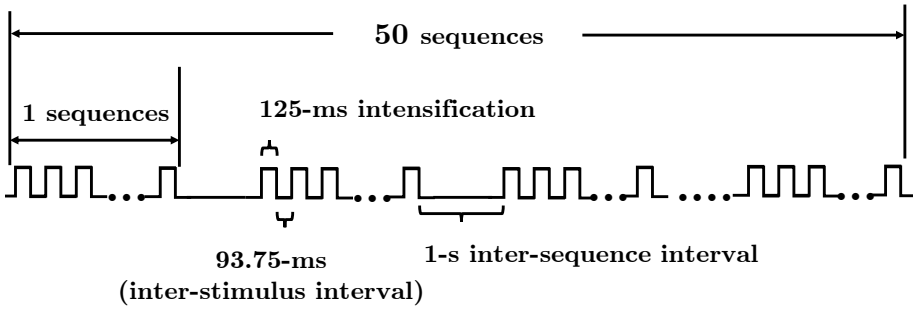

FIGURE 3.2: Color target stimulation protocol.

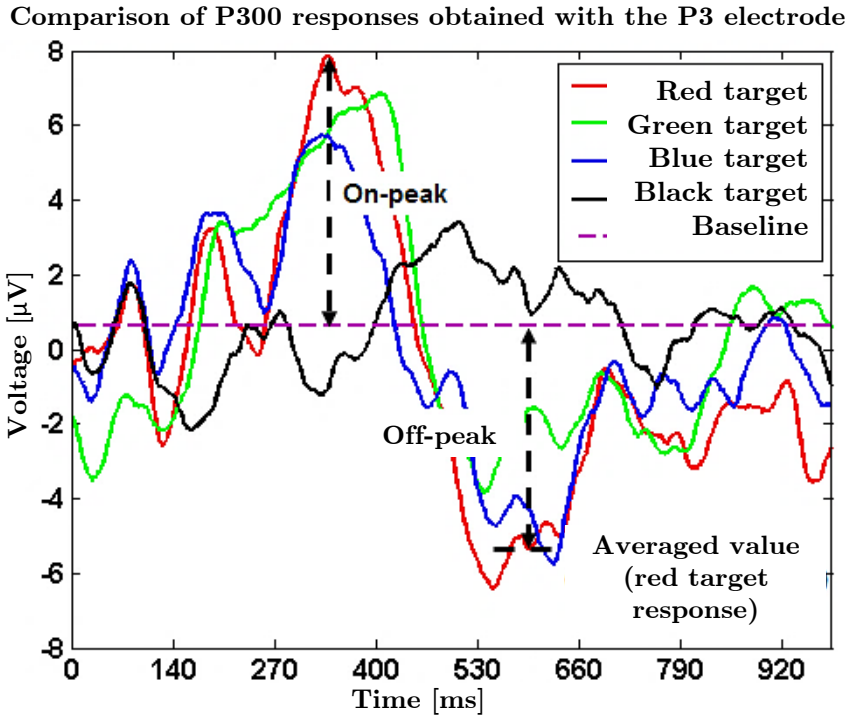

FIGURE 3.3: Example of P300 response to different color stimuli and definition of on-peak and off-peak indices.

(see 3.1(a)(b)-(d)). Three colors in the same state had the same luminance in the CIE XYZ color space, where the color luminance in the inter-stimulus state was 12.5% of the color luminance in the intensification state.

The color target stimulation followed the protocol illustrated in Figure 3.2. Participants were asked to look at one target color located in the center of the screen. Fifteen sets of three dots were presented in a random sequence. The intensification of each set was 125 ms, and the inter-stimulus interval was 93.75 ms. Participants were instructed to look at the target color for the duration of 50 sequences or trials, where the inter-sequence interval was 1 s. In total, participants looked at 4 sets of 50 sequences for three different target colors and the non-target color (the black space between two colors). The target color sequences were randomized, and the stimulation was paused for 30 s before changing the target color.

3.1.2 Data acquisition and analysis

The 10-20 international standard-based EEG system was used, and the signals from the Cz, P3 and P4 electrodes were recorded (QPET-EEG, BrainQuiry Co., Ltd.). It has been previously reported that strong P300 signals have been observed in the case of P3

and P4 based on a green/blue flicker matrix [37]. Reference and ground electrodes were placed on the left and right mastoids, and the sampling rate was 750 Hz/channel.

In the analysis, first I applied a band pass filter (0.5–13 Hz) to the raw data. Then I took ensemble averages using the first 40 trials from the recorded data. Finally, I obtained the P300 response for all three target colors as well as a small ripple response for the non-target color (see Figure 3.3). In the interpretation based on Figure 3.3, I considered the P300 response over a period of 1 s after the stimulation (stimulation started at time = 0 ms) and calculated the mean value of the non-target response as a normalized factor or a baseline. Moreover, I empirically defined the following two significant measures based on the P300 characteristics in order to compare the response from different target colors:

- On-peak: maximum magnitude of the response in the range of 270–400 ms after stimulation compared to the baseline.
- Off-peak: average magnitude of the response in the range of 540–670 ms after stimulation compared to the baseline (absolute value).

For instance, the on-peak and off-peak values for the red target are shown in Figure 3.3. In the case of the off-peak value, responses always had a high variance, so I used the averaged value instead of the minimum value. Calculation results from two measures were subjected to statistical analysis. I performed one-way repeated measures analysis of variance (ANOVA) based on assumption of sphericity. Correction was used when data set violated the sphericity assumption. I selected type of correction based on Greenhouse-Geisser estimate of sphericity (ϵ). Greenhouse-Geisser correction was used in case of $\epsilon < 0.75$ and the Huynh-Feldt correction was used when $\epsilon > 0.75$. In post hoc analysis, I performed Bonferroni correction and pairwise comparisons (paired t-test). In previous research, this method has also been used to analyze alpha wave response from color stimulation [40].

3.1.3 Results

On-peak and off-peak values were calculated for the eleven participants (n = 11) and separately averaged in Cz, P3 and P4, as shown in Figure 3.4 and Figure 3.5. The ANOVA results showed significant difference for the on-peak values at Cz ($F(2,20) = 5.273$, $p = 0.014$) and P4 ($F(2,20) = 3.716$, $p = 0.042$). In the post hoc analysis, pairwise comparison based on the Bonferroni correction showed that the on-peak value for the red target was higher than that for the green target at Cz ($p = 0.047$) and P4 ($p =$

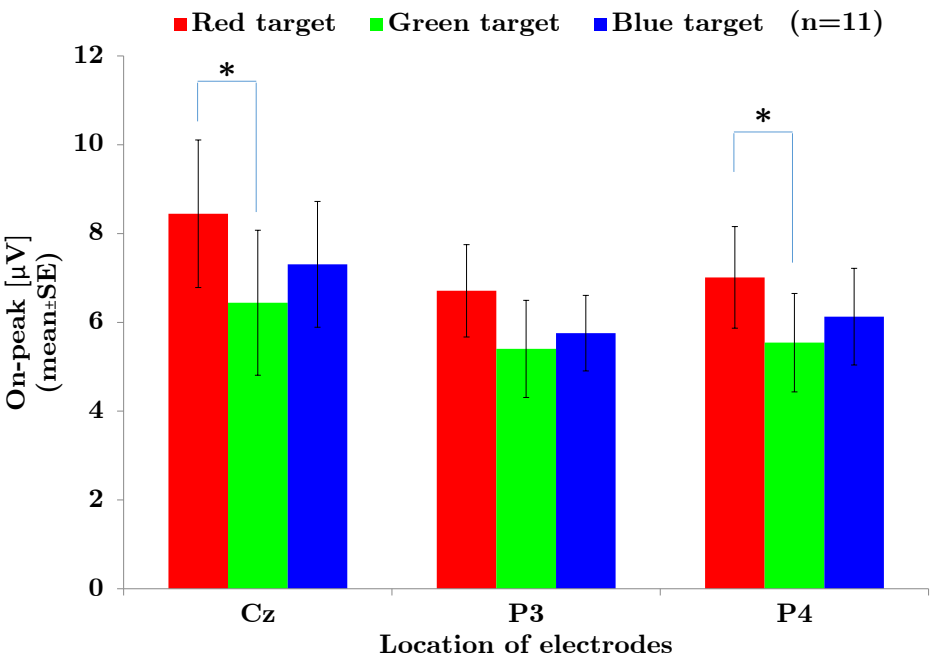

FIGURE 3.4: Comparison of on-peak values for three different color stimuli among three electrodes. (* $p < 0.05$, ** $p < 0.01$)

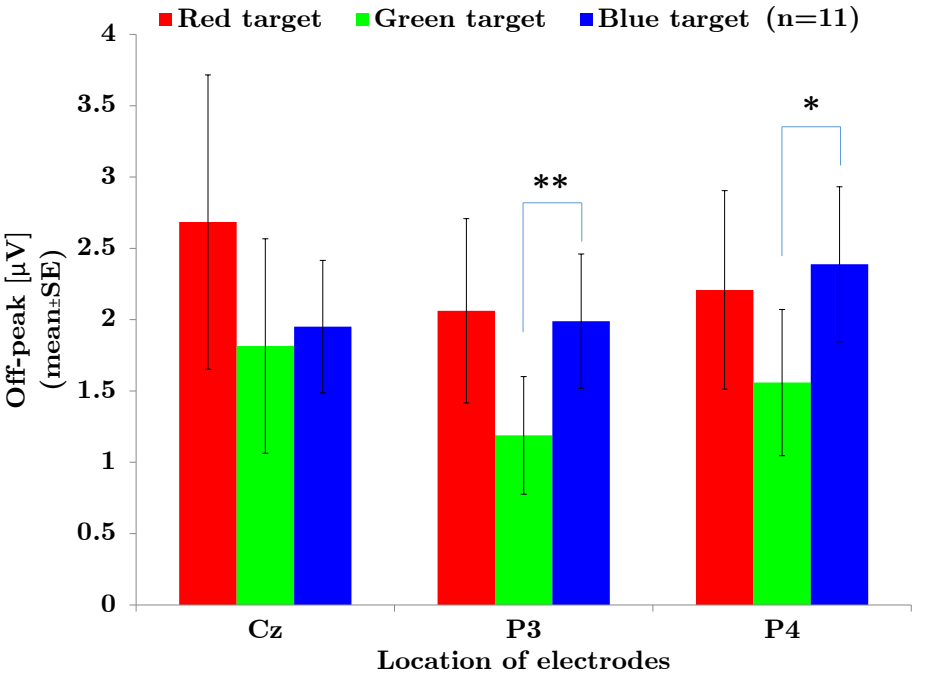

FIGURE 3.5: Comparison of off-peak values for three different color stimuli among three electrodes. (* $p < 0.05$, ** $p < 0.01$)

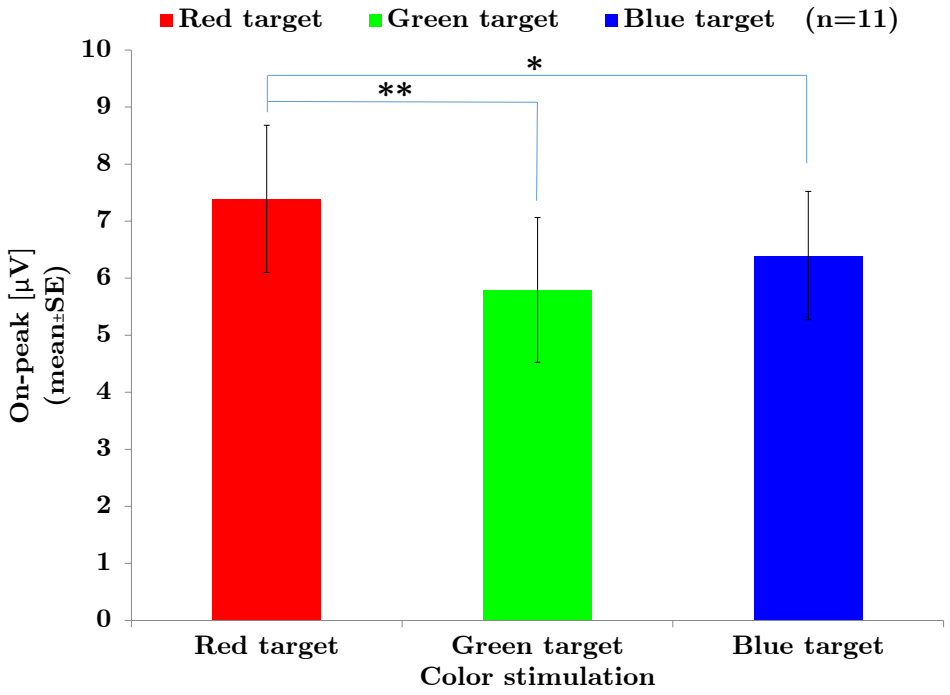

FIGURE 3.6: Averaged on-peak values from three electrodes for each target color. (* $p < 0.05$, ** $p < 0.01$)

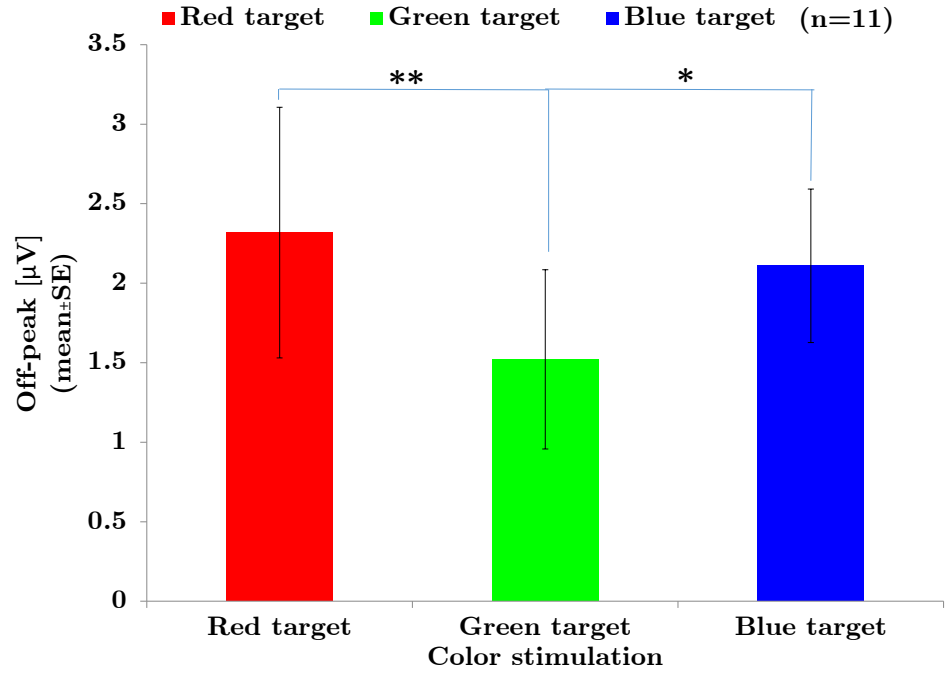

FIGURE 3.7: Averaged off-peak values from three electrodes for each target color. (* $p < 0.05$, ** $p < 0.01$)

0.043). Significant difference was found in the off-peak response in P3 (F(1.842,18.422) = 6.403, $p = 0.009$) and P4 (F(2,20) = 5.627, $p = 0.012$). The post hoc analysis showed that the off-peak value was lower for the green target compared to the blue target at P3 ($p = 0.006$) and P4 ($p = 0.038$).

Moreover, the averaged values from three electrodes are also shown in Figure 3.6 and Figure 3.7. ANOVA results showed a significant difference among the three color in both the on-peak (F(2,64) = 13.055, $p < 0.00005$) and off-peak (F(1.492,47.736) = 7.728, $p = 0.003$) values. The post-hoc analysis showed that the red target induced higher on-peak values compared to the green ($p < 0.00005$) and blue ($p = 0.015$) targets. In contrast, the green target induced a weaker off-peak value compared to the red ($p < 0.0001$) and blue ($p = 0.014$) targets.

Furthermore, the results showed a high standard error (SE) because the magnitude of the P300 response of one participant was considerably about two times higher than that of the other participants. However, the tendencies in the results were not changed by removing the outlier participant from the analysis.

3.1.4 Discussion

My experimental results demonstrate the validity of the hypothesis that the P300 response is affected by color. Furthermore, the results of the previous research that studied the color-based oddball paradigm, where it was reported that red targets yielded the highest peaks of P300 [41], also support the findings of present experiment. However, the off-peak measure was not mentioned in that research. Based on my statistical analysis, red and green stimuli yielded the most significant difference in the on-peak and off-peak values in averaged data. Thus, I conjecture that the analysis of averaged data from all electrodes may have yielded more consistent results compared to sparse or independent analysis. I plan to continue this line of investigation with a larger number of electrodes. Moreover, in this study, I found that P300 responses to green and red targets might be classified more easily compared to those to red and blue targets or blue and green targets. This fundamental result can be used in the development of future applications.

My investigation is expected to contribute to various existing and future biomedical applications. In BCI communication and control, the results may be of use in the design of more effective P300 spellers or other graphical user interfaces based on human color vision. Various characteristics of the P300 response from different color stimulations can be used to improve the performance of such applications in terms of speed and accuracy. In clinical applications, I may be able to develop P300-based system for the identification of color blindness or cone cell dysfunction syndrome. My ideas are supported by clinical

research on color blindness diagnosis based on visually evoked potential (VEP) [42], where experiments were conducted using a checkerboard pattern with flickering green and red squares as a stimulus. Moreover, electroretinography (ERG) and color VEP in cone cell diagnosis have also been reported [43], where the results showed that color VEP is more suitable for identifying cone dysfunction syndrome in children. Furthermore, my research not only contributes to biomedical applications, but also contributes to human lifestyle innovation. In the future, I may be able to develop color vision-based password generators based on P300 color response classification.

3.2 Visual factor II and III: Motion-modulated and Complexity-modulated attention effects

In the first decade of their existence, the most common visual presentation format for P300 BCI was the row/column (RC) white/gray flicker matrix [1]. Alphabet matrices were shown on the screen, and then randomly flickered in each row and column. During EEG processing, the system attempted to find the highest P300 amplitude as an indicator of target choice. One group proposed that green/blue flickering RC matrices were more accurate than the conventional gray/white matrix [16]. A major source of error for this stimulus presentation format is signal overlap from temporally adjacent ERPs and interference flashes from adjacent characters [17], [18]. Several novel presentation formats have been proposed to improve the accuracy of the conventional RC format. A single character speller [19] and a region-based speller [20] were developed to reduce errors from adjacent non-target characters, while a checkerboard presentation format was developed to further improve RC presentation [21]. However, these presentation formats might decrease accuracy in display screen applications with small number of targets.

Recently, I conducted several basic sensory ERP experiments to develop visual stimuli that can signal higher cognitive functions for P300-based BCIs. I hypothesized that a visual stimulus presentation format that could enhance the P300 waveform amplitude would improve resolution of target-associated from non-target-associated signals. In my previous study [44], I investigated P300 variation to the primary colors (red, green, and blue) and found higher P300 amplitudes using red stimuli and highly significant differences in P300 response amplitudes between red and green stimuli. I implemented these findings in a modified red/green visual presentation format for a preliminary study of visual attention [45]. In addition, I developed two novel visual attention stimuli, termed *motion-modulated* and *complexity-modulated*. The motion-modulated stimulus is a moving subtarget that randomly appears between two positions inside the main target (Figure 3.8, middle panel). The complexity-modulated stimulus consists of a checkered pattern of variable spatial frequency (low or high) (Figure 3.8, right panel). Preliminary results showed that modulation of motion and complexity can be used to increase P300 amplitude. In a subsequent study, I further improved the motion-modulated stimulus and demonstrated a statistically significant increase in target-associated P300 [46]. In this paper, I describe a new version of the complexity-modulated stimulus presentation format and conducted experiments with the motion-modulated stimulus presentation format. I found strong motion- and complexity-modulated attention effects on P300 as measured by a single electrode (Cz). These newly designed visual stimuli may help improve BCI systems for more general user applications.

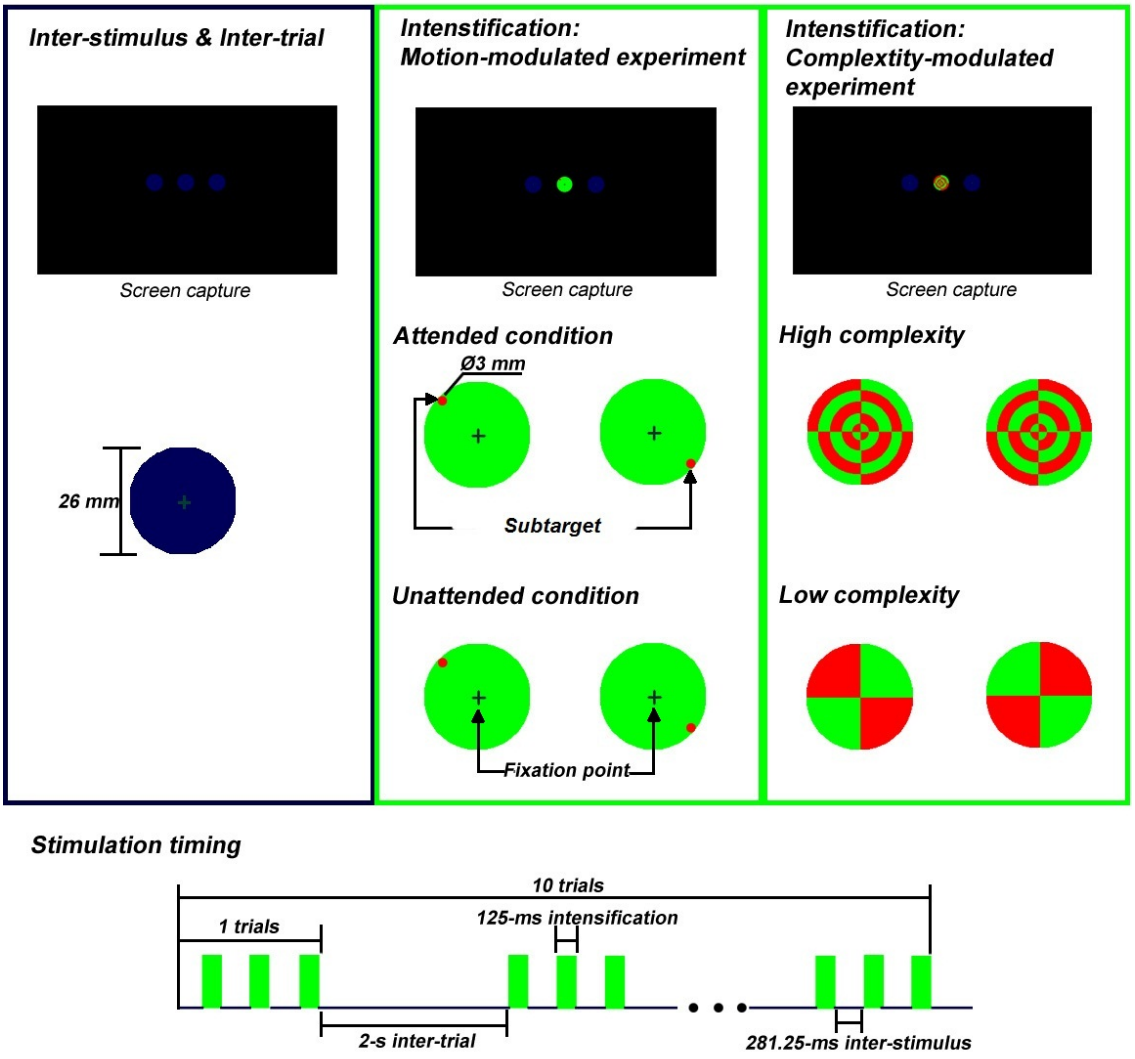

FIGURE 3.8: Visual stimuli and presentation protocols used to investigate motion-modulated and complexity-modulated attention effects on the P300 visual evoked potential

3.2.1 Materials and Methods

Experiments were conducted in a normally lit room without electromagnetic shielding. A participant sat at a viewing distance of 60 cm from a monitor (23 in. diagonal, V236HL LCD Monitor, Acer). The experiments were performed in accordance with the Declaration of Helsinki of 1975 as revised in 2000.

- **Participants**

  Eight healthy male volunteers aged 23-27 years participated in the experiments. None of the participants had a history of color vision disorders, such as color blindness, as confirmed by the Ishihara test.

- **Stimulation design and experimental protocol**

  The basic stimulus format consisted of a 1×3 matrix of flickering discs on a black background viewed on a screen with resolution of 1920×1080 pixels (see Figure 3.8, left panel). Each disc had a diameter of 2.6 cm. Here, I defined two states of flicker, intensification and inter-stimulus. The color luminance in the inter-stimulus state was 25% of that in the intensification state. To study motion-modulated and complexity-modulated attention effects, I conducted two experiments with different stimuli in the intensification state.

  To study motion-modulated attention effect, I used the stimuli proposed in my previous research [46]. Green/blue flicker was implemented in my stimuli. The fixation point and a red spot (subtarget) were shown within a disc. Each spot was 0.3 cm in diameter. The spot color was decided based on my previous finding that among red, green and blue, the combination of red and green produced the largest difference in P300 response amplitude [44]. Thus, a red spot should be easy to distinguish from a green disc by human color vision. I defined two experimental conditions: 'Attended' (Att.) and 'Unattended' (Un-att.). In the Att. condition, participants were asked to pay attention to a red spot that was randomly shown at one of two positions within the green disc. In the Un-att. case, participants were instructed to keep looking at the central fixation point (+). The stimuli were presented temporally as shown in Figure 4.1 (bottom). Discs were intensified in a random sequence in each trial. The intensification interval for each disc was 125 ms, and the inter-stimulus interval was 281.25 ms. Each participant was instructed to look at the target disc for the entire trial duration for 10 trials, where the inter-trial interval was 2 s. Participants were tested under the two conditions with an approximately 1-min relaxation break between conditions. Moreover, participants were asked to avoid blinking during the tasks in the experiments.

  To study complextity-modulated attention effect, a red-green checkered pattern was presented with either 'High complexity' (HC) or 'Low complexity' (LC) (see Figure 3.8, right panel). The HC condition had higher spatial frequency than the LC condition. Stimulation timing and the experimental protocol were exactly same as in the motion-modulated experiment. In both HC and LC conditions, participants were instructed to look at the center of the target disc.

- **Data acquisition**

  The international 10-20 EEG system was used for recording. The signal from the electrode Cz was recorded using a QPET-EEG system (BrainQuiry Co., Ltd.). Reference and ground electrodes were placed on the left and right mastoids, respectively, and the sampling rate was 1 kHz.

3.2.2 Data analysis

Before analysis, the raw data were band-pass filtered (0.01-4 Hz). This frequency range is appropriate for ERPs elicited by visual stimuli [47]. The study comprised four experimental conditions (Att., Un-att., HC, and LC) and I recorded EEG data during both target flashing and non-target flashing. The recorded data in each condition could be divided into three data sets according to the trigger signals from the three disc positions: left (non-target 1), center (target), and right (non-target2). Each data set had 10 trials. In each trial, I analyzed the 700-ms period after the start of the intensification state. To compare VEPs acquired in response to target and non-target stimuli, I measured peak P300 amplitude, defined empirically as the maximum voltage reached within the period from 100 ms to 600 ms after stimulus onset. P300 amplitudes were compared between conditions (Att. vs. Un-att. or HC vs. LC) by one way repeated measures analysis variance (ANOVA) with Bonferroni correction (post hoc test). Moreover, data normality and sphericity were concerned before analysis.

3.2.3 Results

Ensemble averages were acquired after t = 4, 6, 8, and 10 trials to obtain visual evoked potentials (VEPs) of a target data set and two non-target data sets for each experimental condition (see Figure 3.9 and Figure 3.10). In the motion-modulated experiment, the Att. condition evoked higher amplitude P300 responses than the Un-att. condition in 6 out of 8 subjects, while in the complexity-modulated experiment, the HC condition evoked higher amplitude P300 responses than the LC condition in 7 out of 8 subjects. In the motion-modulated experiment, I found a highly significant difference in target-evoked versus non-target-evoked peak P300 in the Att. condition whether average P300 waveforms were derived from 4, 6, 8, or 10 trials (see and Figure 3.11). In contrast, there were no significant differences in target-evoked and non-target-evoked P300 amplitudes in the Un-att. condition whether derived from 4, 6, or 8 trials. Only for the 10-trial average was there a significant difference in P300 amplitude. For HC complexity-modulated stimuli, I found highly significant differences in target-evoked versus non-target-evoked P300 amplitudes for averages of 4, 6, 8 or 10 trials (see and Figure 3.10). In the LC condition, there was no significant difference between target-evoked and non-target-evoked P300 amplitude for the 4-trial average. The effects of motion- and complexity-modulation on peak P300 and the number of trials required to obtain a significant difference are displayed in . The HC condition yielded the highest peak P300 waveforms for all averages. The second highest peak P300 waveforms were obtained in the motion-modulated Att. condition. Although the peak P300 in the

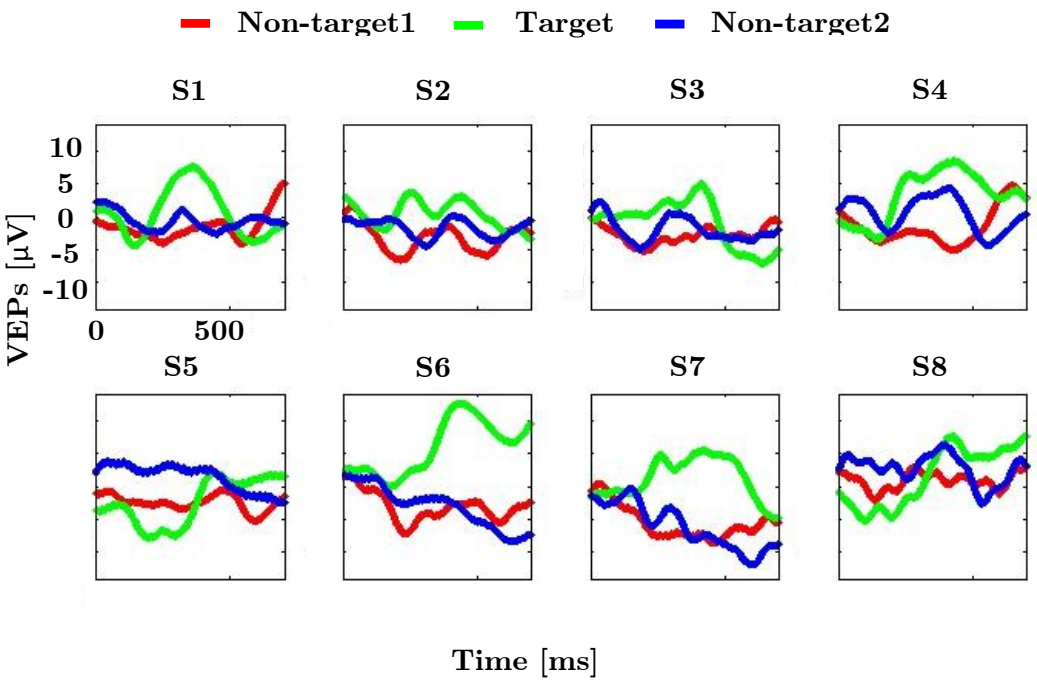

(a) Att.

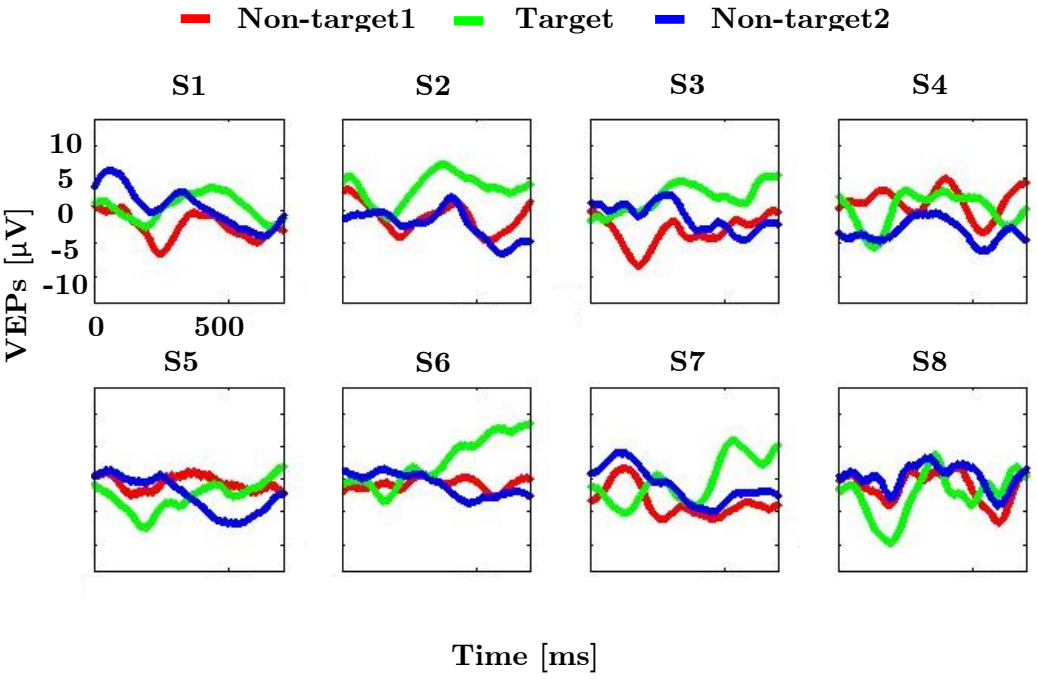

(b) Un-att.

FIGURE 3.9: VEP waveforms acquired from electrode Cz in response to motion-modulated stimuli from one subject. Attended condition (a). The unattended condition (b). All waveforms are the average of 10 trials.

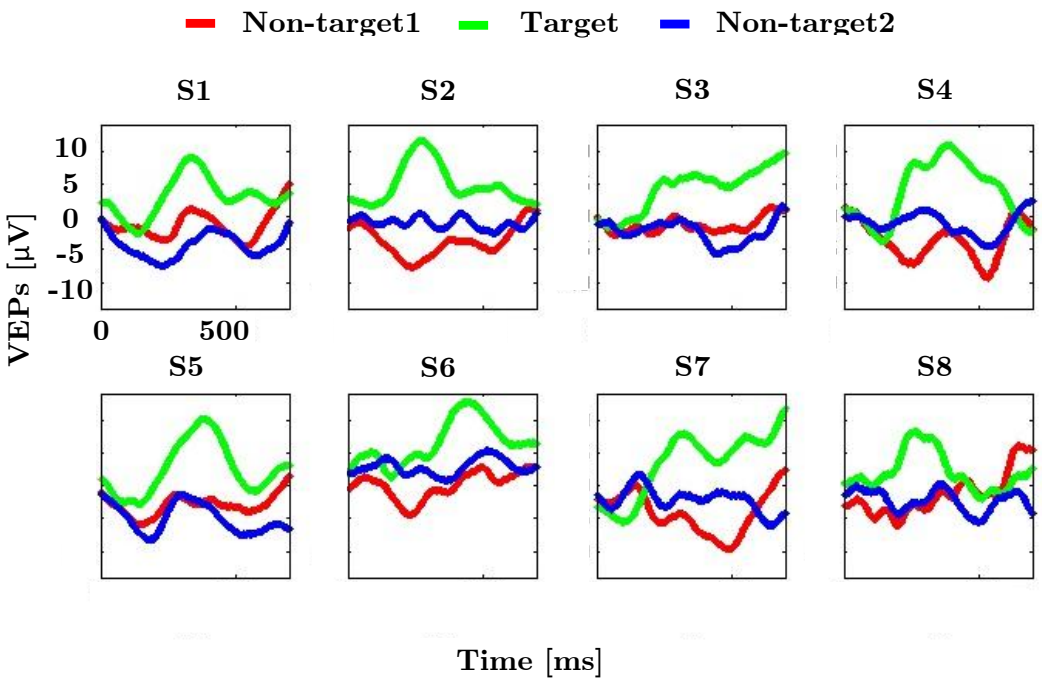

(a) HC

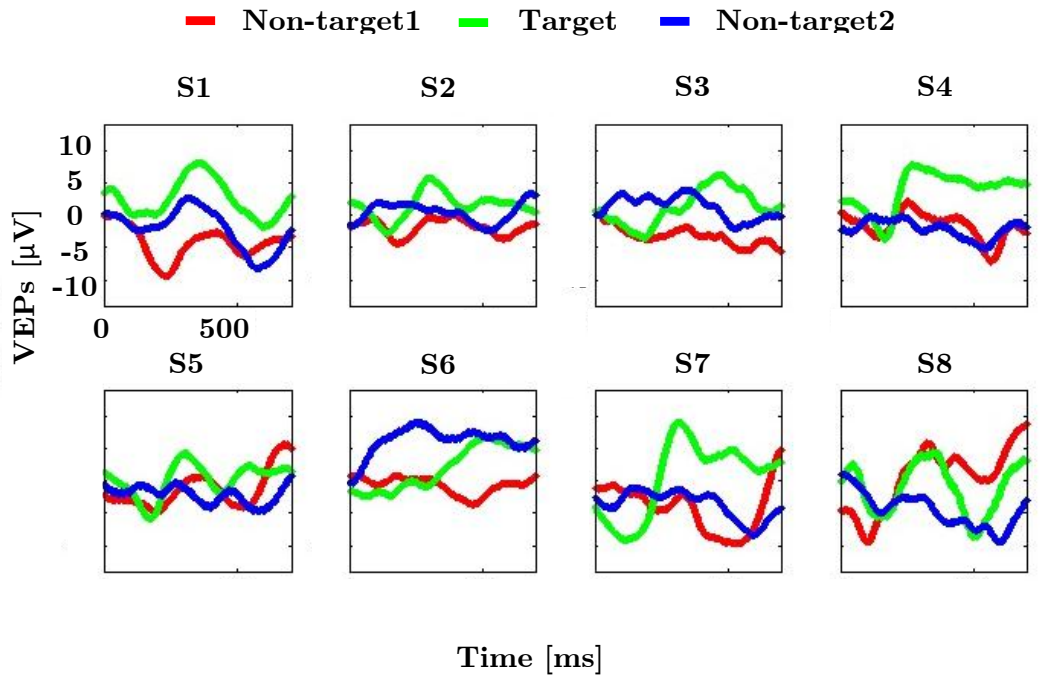

(b) LC

FIGURE 3.10: VEP waveforms acquired from electrode Cz in response to complexity-modulated stimuli from one subject. High complexity condition (a). Low complexity condition (b). All waveforms are the average of 10 trials.

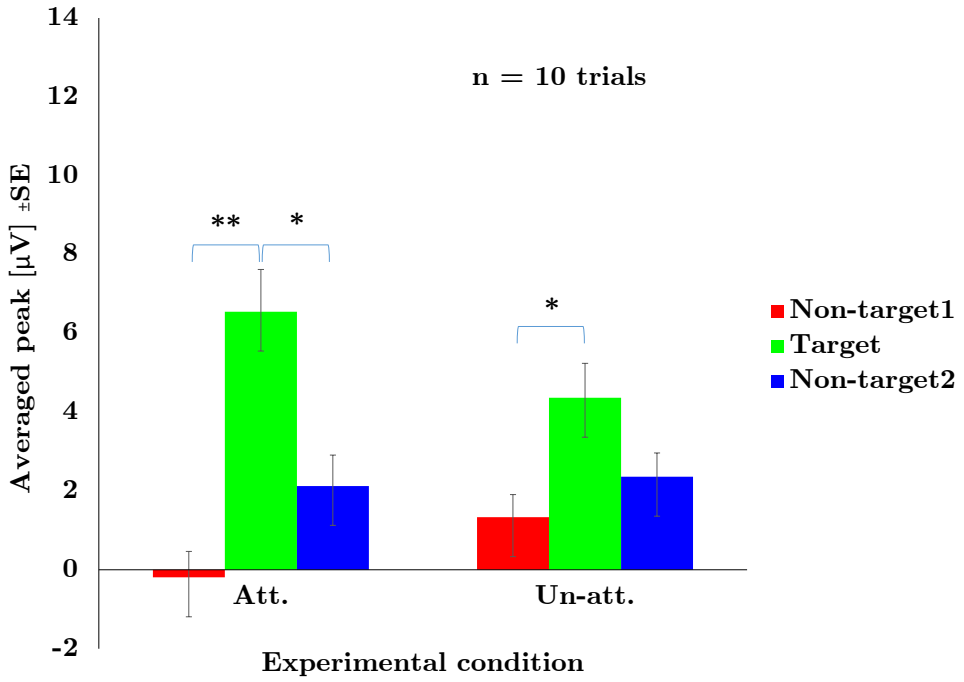

(a) 10 trials

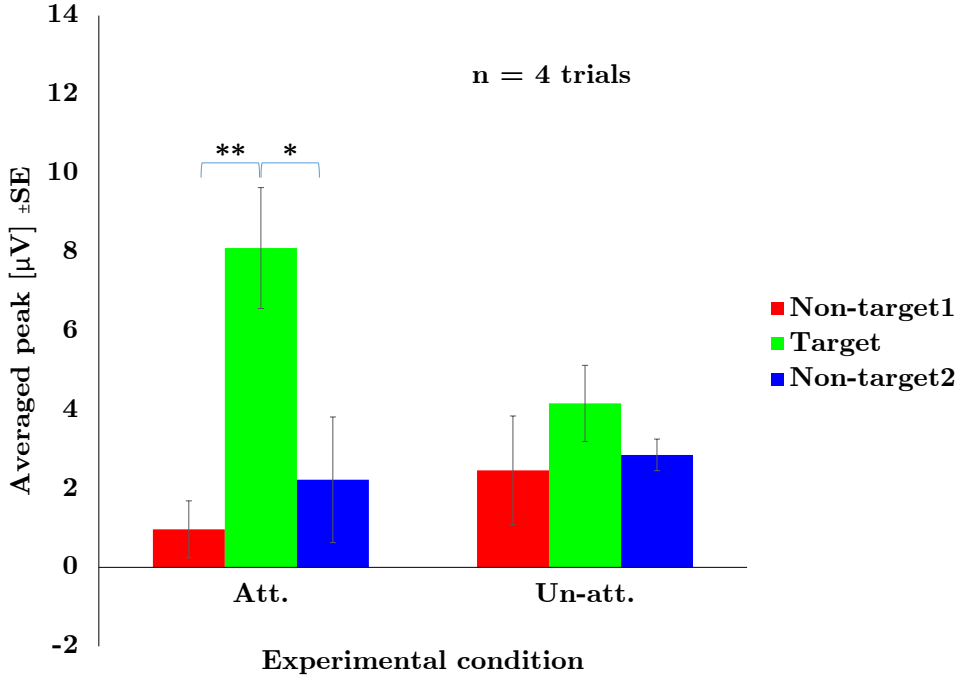

(b) 4 trials

FIGURE 3.11: Comparison of P300 peak amplitudes under Att. and Un-att. conditions. (a) 10-trial averages and (b) 4-trial averages. Error bars indicate ±standard error (SE). (* $p < 0.05$, ** $p < 0.01$)

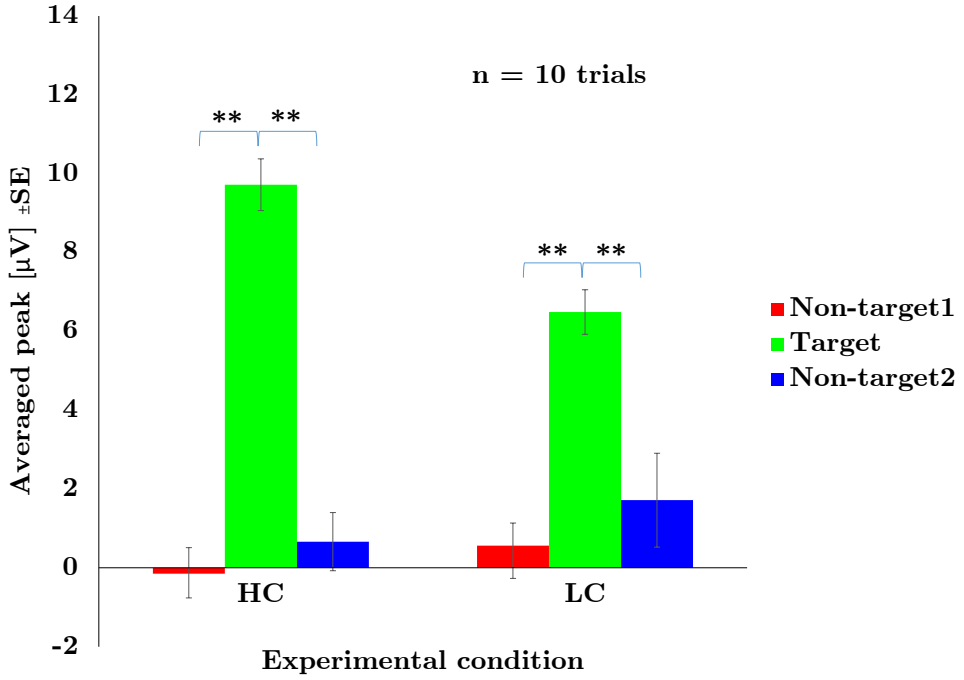

(a) 10 trials

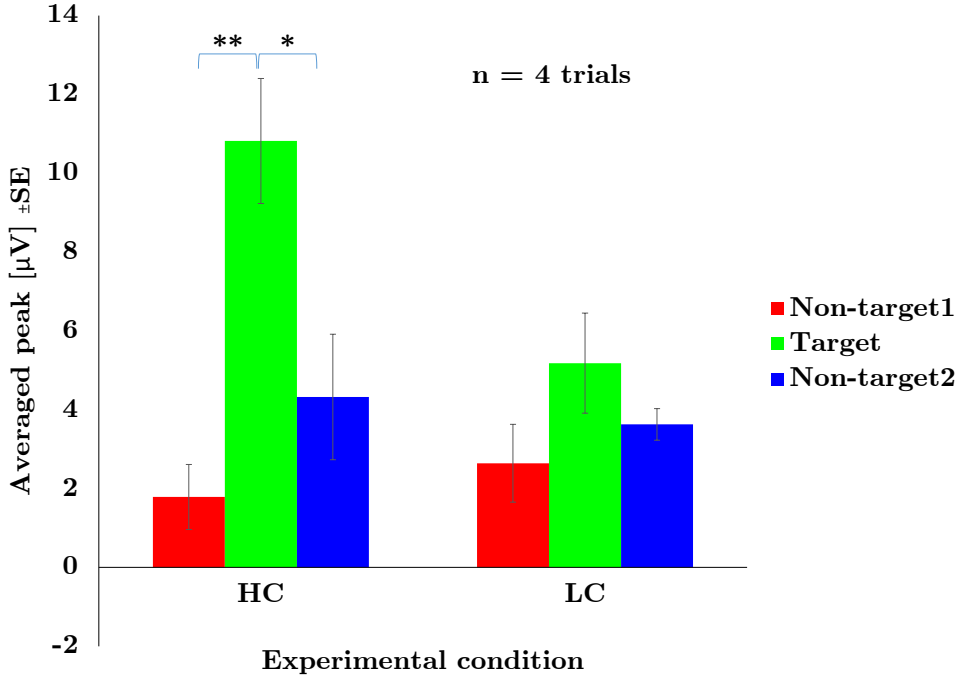

(b) 4 trials

FIGURE 3.12: Comparison of P300 peak amplitudes under HC and LC conditions. (a) 10-trial averages and (b) 4-trial averages. Error bars indicate ±SE. (* $p < 0.05$, ** $p < 0.01$)

TABLE 3.1: Comparison of non-target-evoked (N1 and N2) and target-evoked (T) P300 amplitudes under Att. and Un-att. conditions for n = 4, 6, 8 and 10 trials.

Number of trials (n)	ANOVA			Post hoc test	
	Condition	F	p	Comparison	p
n=4	Att.	F(2,14)=11.70	**<0.005**	T-N1	**<0.001**
				T-N2	**<0.05**
	Un-att.	F(2,14)=0.47	0.635		
n=6	Att.	F(2,14)=12.44	**<0.005**	T-N1	**<0.0005**
				T-N2	**<0.05**
	Un-att.	F(2,14)=1.90	0.186		
n=8	Att.	F(2,14)=18.32	**<0.0005**	T-N1	**<0.0005**
				T-N2	**<0.01**
	Un-att.	F(2,14)=2.33	0.134		
n=10	Att.	F(1.06,7.43)=22.77	**<0.005**	T-N1	**<0.0005**
				T-N2	**<0.05**
	Un-att.	F(2,14)=3.93	**<0.05**	T-N1	**<0.05**
				T-N2	0.087

complexity-modulated LC condition was similar to that of the motion-modulated Att. condition for t = 10 trials, a significant difference in target-evoked versus non-target evoked P300 waves was not detected for a smaller number of trials. P300 waveforms were smallest for the motion-modulated Un-att. condition.

3.2.4 Discussion

In this study, I demonstrate motion-modulated attention effects and complexity-modulated attention effects on the P300 visual evoked potential. I found significant differences between target-evoked and non-target-evoked P300 responses in the Att. and HC conditions, even for relatively small numbers of trials (4-trial averages). In contrast, significant differences in peak P300 were not obtained in the Un-att. and LC conditions until the waveforms were the averages of 10 trials and 6 trials, respectively. Thus, the Att. motion-modulated condition and the HC complexity-modulated condition evoked large P300 responses that were distinguishable from non-target response even in as few as four trials (see and , Figure 3.11 and Figure 3.12).

- **Motion-modulated attention effect** In conventional P300-based BCI, subjects were asked to maintain their visual fixation on the target stimuli, similar to the Un-att. condition of my experiments. On the other hand, in the Att. condition, the subtarget evoked small saccadic eye movements within the target stimulus (disc). I hypothesize that these small saccades may have potentiated the ERP P300 component. Indeed, several previous studies reported an effect of saccade on

TABLE 3.2: Comparison of non-target-evoked (N1 and N2) and target-evoked (T) P300 amplitudes under HC and LC conditions for n = 4, 6, 8 and 10 trials.

Number of trials (n)	ANOVA			Post hoc test	
	Condition	F	p	Comparison	p
n=4	HC	F(2,14)=11.40	**<0.005**	T-N1	**<0.001**
				T-N2	**<0.05**
	LC	F(2,14)=1.11	0.357		
n=6	HC	F(2,14)=35.19	**<0.000005**	T-N1	**<0.00005**
				T-N2	**<0.001**
	LC	F(2,14)=4.63	**<0.05**	T-N1	**<0.05**
				T-N2	**<0.05**
n=8	HC	F(2,14)=60.84	**<0.0000005**	T-N1	**<0.00005**
				T-N2	**<0.00005**
	LC	F(2,14)=5.55	**<0.05**	T-N1	**<0.05**
				T-N2	**<0.05**
n=10	HC	F(2,14)=87.13	**<0.00000005**	T-N1	**<0.00005**
				T-N2	**<0.000005**
	LC	F(2,14)=8.80	**<0.005**	T-N1	**<0.01**
				T-N2	**<0.01**

visual ERPs, especially P300, compared to the fixation condition. In one study [48], ERPs (Oz) were modulated by microsaccades (fixation) and small saccade (1.5° and 4.5°) and larger saccades resulted in higher ERP amplitudes. With my visual stimuli, the maximum saccade within the target green disc was 2.5°. Another study found that P300 responses (Fz, Pz, Cz, and Oz) were enhanced by 10° saccades compared to P300 responses under fixation conditions [49]. Furthermore, a motion-onset paradigm for BCI application has been proposed [23], in which an empty rectangular button is presented on the screen. In the stimulus state, a red vertical line appeared on the right side of the rectangle that moved leftward until it disappeared. This stimulus induced a motion-onset VEP (mVEP) with major N2 and P2 components. In that study, it was reported that an mVEP-based BCI performed with up to 98% accuracy using 10 trials. Thus, the motion-modulated attention effects in my study are consistent with previous results.

- **Complexity-modulated attention effect** Higher complexity was conferred by a higher spatial frequency of colored alternating green and red rings within the target disc. To demonstrate a complexity-modulated effect, I compared this HC stimulus to a lower spatial frequency or LC stimulus with the same color ratio and intensity. The HC stimuli evoked higher amplitude P300 responses. In an early P300 study, Picton (1992) reported a "difficulty effect" on P300 responses; the P300 wave became smaller as the difficulty discriminating target from non-target stimuli increased. I suggest that the high spatial frequency difference between target and background in the HC condition allowed for easier discrimination than in the LC condition.

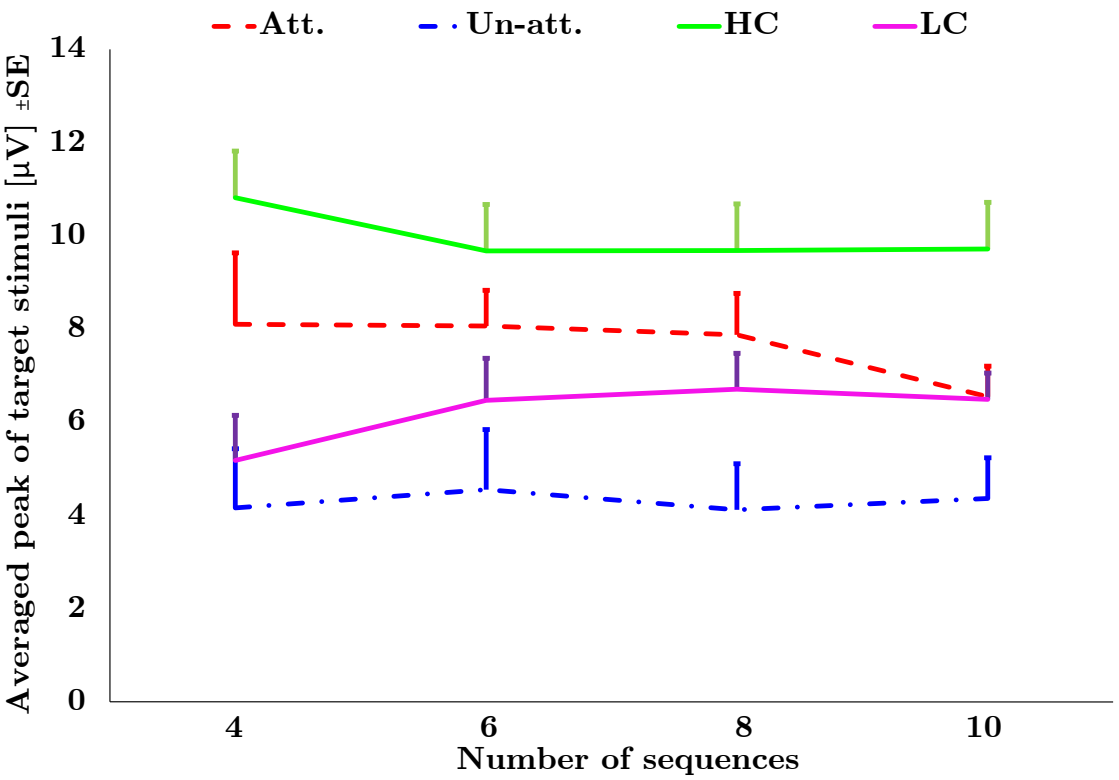

FIGURE 3.13: Summary of peak P300 amplitudes for all conditions as a function of number of trials averaged. Error bars indicate +SE.

- **Comparison of motion-modulated and complexity-modulated attention effects** The peak P300 amplitude was generally larger in the HC condition than in the Att. condition. While P300 responses in the Att. condition were no larger than those in the LC condition, fewer trials were required to reach a significant difference in amplitude between target-evoked and non-target-evoked responses (see Figure 3.13). Alternatively, the smallest peak P300 responses were evoked by the Un-att. condition. The Un-att. condition was similar to the conventional stimulation presentation format in that subjects were asked to fix their eyes on the center of flashing targets. One reason for the larger P300 in the HC condition compared to the Att. condition may be the effect of color, as red stimuli evoke larger responses than blue or green stimuli [44] and the complexity-modulated visual stimuli contained a larger red area than the motion-modulated stimuli. A stimulus presentation format based on red/green contrast may be highly efficacious for BCI applications.

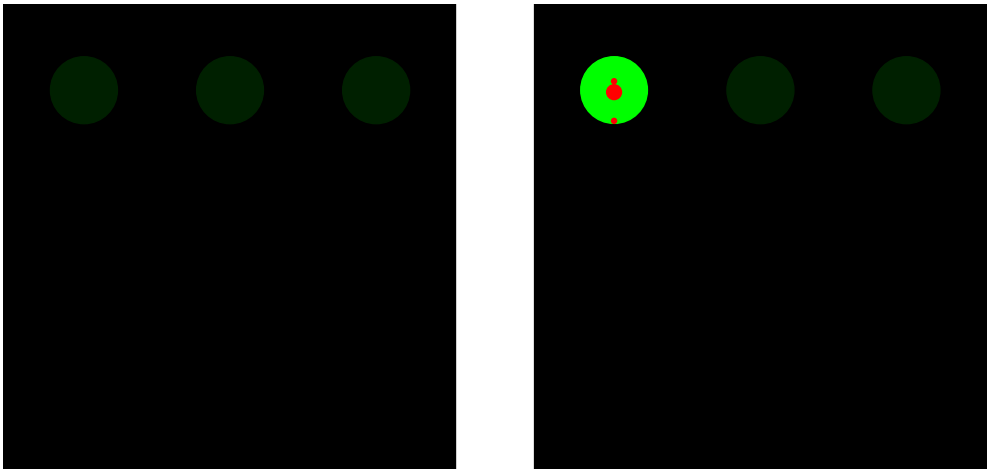

FIGURE 3.14: Stimulation screen.

3.3 Visual factor IV: Orientation-modulated attention effects

In this study, I investigated the *orientation-modulated attention effect* on VEP. Furthermore, I modulated orientation effects into motion-modulated stimulus, which I call *combinational stimulus*.

3.3.1 Materials and Methods

Experiments were conducted in a normally lit room without electromagnetic shielding. In the test, a participant sat at a viewing distance of 45–50 cm from a monitor (23 in. diagonal, V236HL LCD Monitor, Acer). The experiments were performed in accordance with the Declaration of Helsinki of 1975 as revised in 2000.

- **Participants**

  Seven healthy male participants aged 23–27 years participated in the experiments. None of the participants had a history of color vision disorders, including color blindness, as confirmed by the Ishihara test.

- **Stimulation design and experimental protocol** *combinational stimulus.*

  Three flicker discs (diameter: 2.6 cm) were placed on a black background (750 × 750 px), Figure 3.14. Here, I defined the state of flickering as being one of intensification and inter-stimulus. The luminance in the inter-stimulus state was 12.5% of that in the intensification state. Stimulation timing is illustrated in Figure 3.15. All experiments showed dark green discs in the inter-stimulus state. Each disc had a gray fixation point in the center. However, intensification state

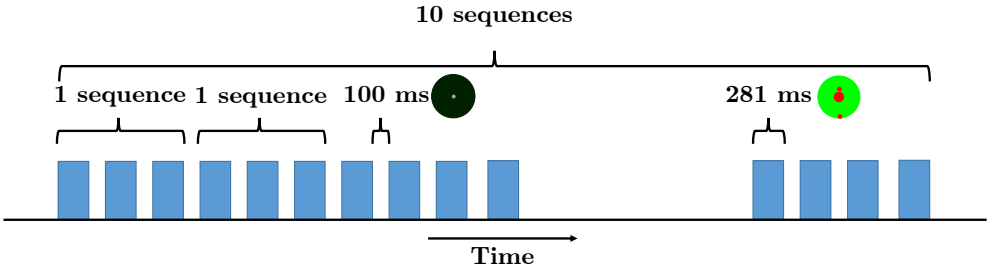

FIGURE 3.15: Stimulation timing.

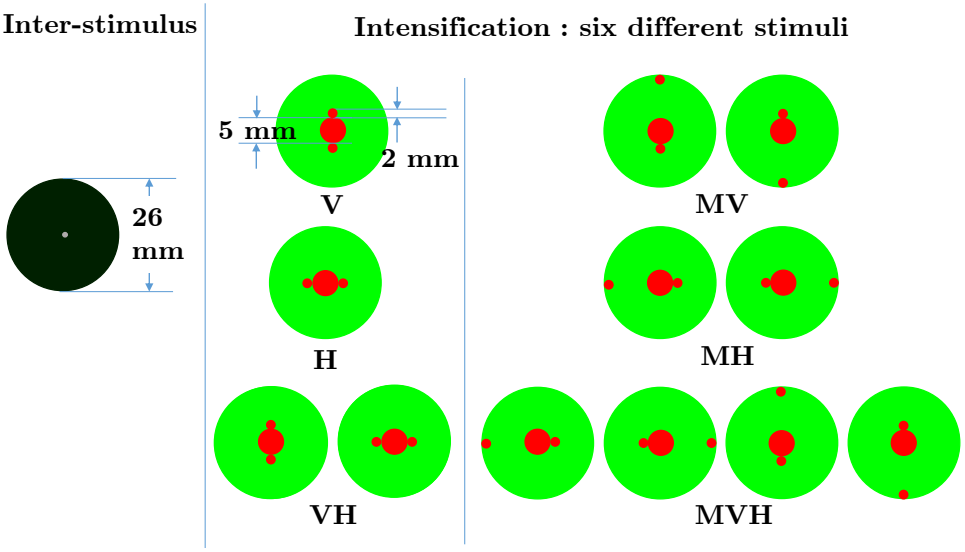

FIGURE 3.16: Six stimuli for different experimental conditions.

stimuli were varied among different conditions as presented in Figure 3.16. Discs were intensified in a random sequence. The intensification duration of each disc was 281 ms, and the inter-stimulus interval was 100 ms.

To study visual stimulation, I defined six experimental conditions, each with different visual stimuli Figure 3.16: 'Vertical' (V), 'Horizontal' (H), 'orientation' (VH), 'Motion-modulated stimulus in vertical direction' (MV), 'Motion-modulated stimulus in horizontal direction' (MH), and 'Combinational stimulus' (MVH). V and H stimuli had three red discs (sub-targets) aligned on the vertical and horizontal diameters, respectively, of a green disc (main target). Small sub-targets had 2 mm diameters, and a big sub-target had a 5 mm diameter. VH was composed of randomly shown V and H stimuli in intensification state. MV and MH had sub-targets that moved randomly along the vertical and horizontal diameters,

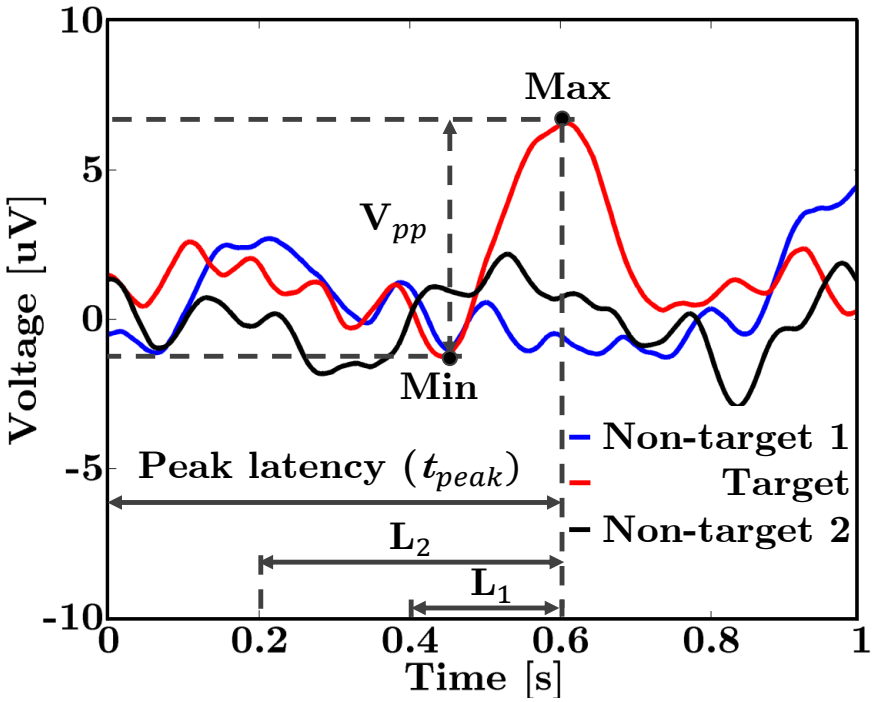

FIGURE 3.17: Definition of measure used in data analysis

respectively, of the main target. MVH had sub-targets that moved randomly along both vertical and horizontal diameters.

Participants were tested under each of the six conditions with an approximately 1-min relaxation break between trials. In each experimental condition, participants were asked to look at the center disc on the screen (target) until ten stimulus trials or sequences had been seen. They were asked to look at the fixation point during stimulation in V, H, and VH conditions. For MV, MH, and MVH conditions, they were requested to target on a moving sub-target. Moreover, participants were asked to avoid blinking during the tasks in the experiments.

- **Data acquisition**

  For EEG, the internationally standard 10–20 system was used, and the signal from the Cz electrode was recorded (OpenBCI 8-bit Board Kit; Arduino-compatible). Reference and ground electrodes were placed on the left and right mastoids, and the sampling rate was 250 Hz

3.3.2 Data acquisition analysis

In the analysis, a bandpass filter (0.4–5 Hz) was applied to the raw data. The frequency range of the filter is appropriate for VEPs [47]. After filtering, the recorded data were ensemble-averaged using stimulus-sequence lengths of 4, 6, 8, and 10. Finally, I obtained

the VEP responses for targets and non-targets. I considered the VEP response over a period of 600 ms after every stimulation onset. The response was normalized by a baseline, which was taken as the averaged magnitude of the signal over the 80 ms before each stimulation onset. To compare VEPs acquired in response to target and non-target stimuli, I measured peak-to-peak VEP (V_{pp}), defined empirically as the difference between the maximum voltage within 400 ms to 600 ms after stimulus onset (L1) and minimum voltage within 200 ms after stimulus onset to the time of maximum voltage (L2) (Figure 3.17).

3.3.3 Results and Discussions

Statistical testing was performed to identify significant differences between V_{pp} of the target and V_{pp} of non-targets in the VH, MV, MH, and MVH conditions, as shown in Figure 3.18. As a result, both VH and MVH showed a highly significant ($p < 0.01$) difference from the other types, especially for sequence lengths of 6, 8, and 10.

In a visual stimulation study, I investigated the orientation-modulated attention effect by comparing among V, H, and VH stimuli. There were no significant differences between V_{pp} of the targets and non-targets when sub-targets were aligned in certain directions during stimulus presentation (Figure 3.17(a)–(b)). In contrast, I found strongly significant differences when the orientations of sub-targets were randomly chosen during stimulus presentation (Figure 3.17(c)). It is widely known that specific cells in the visual cortex respond to specific line orientations [50]. In my experiments, I hypothesized that showing both horizontal and vertical alignments of sub-targets (the VH stimulus type) would induce stronger brain activity in terms of VEP than with the V and H stimulus types. Moreover, I modulated the orientation effect to obtain a motion-modulated stimulus, the MVH stimulus. A comparison of V_{pp} from targets and non-targets under the MV (Figure 3.17(d)), MH (Figure 3.17(e)), and MVH (Figure 3.17(f)) conditions showed that MVH, the combinational stimulus type, resulted in significantly higher response than MV and MH did. This might be a consequence of changing the movement direction of sub-targets during the stimulation period and thereby inducing a high VEP amplitude.

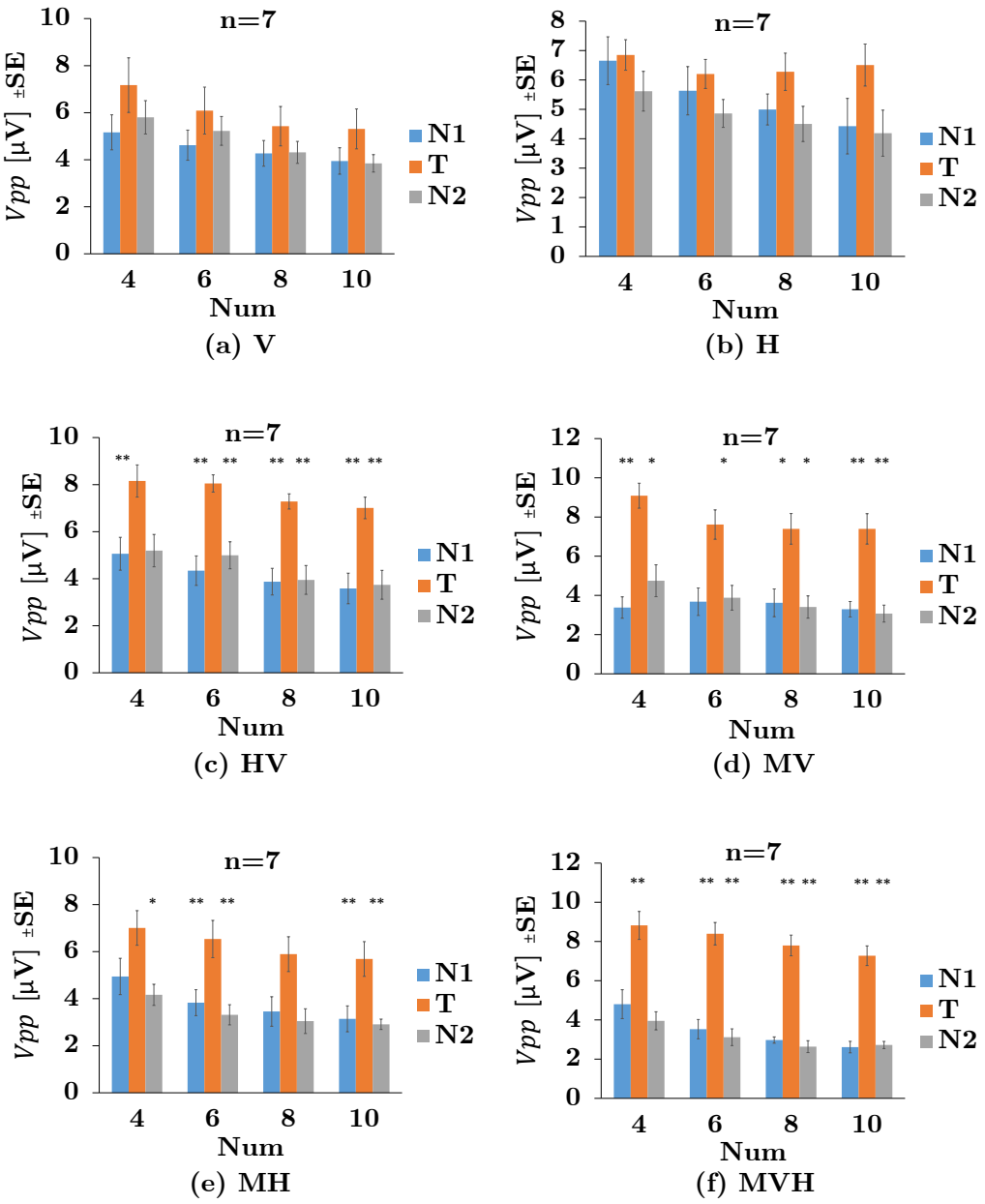

FIGURE 3.18: Comparison of V_{pp} among targets and non-targets in each condition at various sequence lengths (Num). Standard errors and statistical results are shown in the figures (* $p < 0.05$, ** $p < 0.01$). (a) 'Vertical' (V), (b) 'Horizontal' (H), (c) 'orientation' (VH), (d) 'Motion-modulated stimulus in vertical direction' (MV), (e) 'Motion-modulated stimulus in horizontal direction' (MH), and (f) 'Combinational stimulus' (MVH).

3.4 Summary

Results of the studies in this Chapter have been summarized into three categories of visual factors.

3.4.1 Color

By comparison of P300 responses from three color stimuli, red, green and blue, red stimulus induces the highest P300 magnitude, in terms of on-peak. Averaged on-peak voltage from eleven participants with red stimulus was about 15.6% and 27.6% higher than that with blue and green stimulus respectively. However, using single red or red/blue combination as visual stimulus might cause human anger as mentioned in Section 3.1. Thus, red/green combination would be the best alternative.

3.4.2 Motion-modulated and Complexity-modulated attention effects

The P300 wave is strongly related to visual attention. My experiments indicate that motion-modulated attention and complexity-modulated attention effects significantly increased P300 amplitude up to 100.0%, with complexity-modulated attention effects yielding the largest P300 responses and requiring the fewest trials to reach a significant difference between target-evoked and non-target-evoked ERPs. This finding suggests that spatially complex visual stimuli may be useful for P300-based BCIs. In the near future, I plan to combine various visual parameters such as color contrast, motion, and frequency into one stimulus.

3.4.3 Orientation-modulated attention effects

Experimental results from seven participants perform that P300 amplitude using combination of two different orientation stimuli was about 14.2% higher than that using single orientation stimulus. Furthermore, P300 amplitude was enhanced by incorporating both motion- and orientation-modulated attention effects into the visual stimulation. To evaluate performance of proposed stimulus, MVH is further compared to conventional stimulus, and then implement into PIN application in the next chapter.

Chapter 4

Personal Identification Number Application Using Adaptive P300 Brain–Computer Interface

4.1 Introduction

To demonstrate performance of my proposed stimuli *motion-modulated stimulus* (MMS) (MMS is MVH in Chapter 3), I started to develop a BCI-based personal identification number (PIN) application to serve as a test-bed application [51]. PIN technology for access-control equipment was invented in 1966 and granted a US patent in 1975. Nowadays, users typically use keypads to input PINs. A major drawback of keypads is that PINs can be visually or optically observed when they are entered or recovered afterward by thermal camera-based attacks [52]. Various approaches based on biometrics and biosignals have been proposed in order to solve this problem. Fingerprints are widely used in biometric system. However, fingerprints can be duplicated by various techniques [53]. One research group proposes gaze-based password entry [54], but gaze tracking requires a long time for calibration.

Recently, researchers first introduce BCI-based PIN application as alternative modality [55]. There are two advantages of BCI-based PIN application over the above-mentioned techniques. The first is that the user can avoid the problem of the PIN being observed during entry, as is possible with keypads. The second is that BCIs allow for non-touch input, so no heat signal or fingerprint is left behind after use. However,

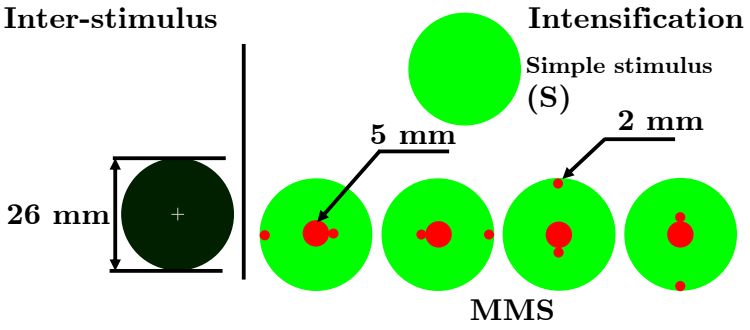

FIGURE 4.1: Motion-modulated stimulus (MMS) and simple stimulus (S)

time-consuming for training session and multiple electrodes are drawbacks of their system. To overcome the drawbacks of original BCI-based PIN application, I propose novel visual stimulus paradigm and decoding algorithm in this paper.

In this study, I further investigated an improvement of my MMS by the *orientation-modulated attention effect*, which was introduced in my previous work [56]. I then incorporated my visual stimulation format into my PIN application. Moreover, I propose *'adaptive P300 BCI'* to improve the information transfer rate (ITR) of the PIN application. The advantage of the adaptive BCI over a conventional BCI is that visual stimulation can be stopped automatically whenever the P300 signal is accurate enough for target determination. Finally, I experimentally investigated whether the adaptive P300 BCI could improve the ITR while maintaining acceptable accuracy, and I focused on single-channel EEG with a computationally inexpensive algorithm.

The rest of the Chapter is organized as follows. In Section 4.2, I describe the design and study of visual stimuli. Section 4.3 introduces the PIN application using adaptive BCI. In Section 4.4, the experimental results are presented and the contributions of this research are discussed. Finally, conclusions are given in Section 4.5.

4.2 Experiment I: Development of visual stimulation

In this section, I review the principal concept of motion-modulated stimulus. Then, I report an experiment comparing the MSS with a simple stimulus (S) in a BCI application.

4.2.1 Review of motion-modulated stimuli

Flickering or flashing stimuli are commonly used in BCIs. The target stimulus flickers between two states: inter-stimulus and intensification (Figure 4.1). In this study, the

luminance in the inter-stimulus state was 12.5% of that in the intensification state. In conventional visual stimulation using a simple stimulus, the user typically looks at the center of the target stimulus during both inter-stimulus and intensification. In contrast, the MMS induces a small saccade during intensification. In the inter-stimulus state, the user looks at the fixation point, which is represented by a plus sign (+) in Figure 4.1. Then, the user makes a small saccade to the red subtarget (single dot, 2 mm), which randomly appears at one of four positions during the intensification state. The dimensions shown in Figure 4.1 were used in my previous work. Recently, I reported the advantage of MMS over conventional methods in terms of P300 amplitude [46][56]. Several research groups have also demonstrated that saccade ERP enhances the P300 wave. One group compared P300 amplitudes that were modulated by microsaccades (fixation) and small saccades (1.5° and 4.5°) [48]. It was found that larger saccades resulted in higher P300 amplitudes. Another study found that P300 responses were enhanced by 10° saccades in comparison with P300 responses under fixation conditions [49].

4.2.2 Comparison between motion-modulated and simple stimuli

Here, I examined the performance of the MMS relative to that of the simple stimulus.

- **Experimental setup**

  I conducted experiments in a normally lit room without electromagnetic shielding. Participants were 7 healthy men aged 23–27 years with no history of color vision disorders. In the experiments, a participant sat at a viewing distance of 40–50 cm from a monitor (23 in. diagonal, V236HL LCD Monitor, Acer). The visual presentation format was a 1×3 matrix of flickering disks (left, center, and right positions) on a black background (Figure 4.3(a)). Each disk had a diameter of 2.6 cm. Disks were intensified in a random sequence. The intensification duration of each disk was 281 ms, and the inter-stimulus interval was 100 ms. The stimulation timing is illustrated in Figure 4.3(b). This study was conducted in accordance with the Declaration of Helsinki of 1975 as revised in 2000. (Note: Experiment I and II shared the same stimulation framework. However, the number matrices were not included in the first experiment).

  Participants were tested under the two conditions, namely, the simple stimulus and the MMS, with an approximately 1-min rest between conditions. Three trials were done for each condition. In each trial, the participant was instructed to attend at the center disk (target) during the entire trial for 10 sequences. Left and right disks were represented non-target stimuli in both experimental conditions.

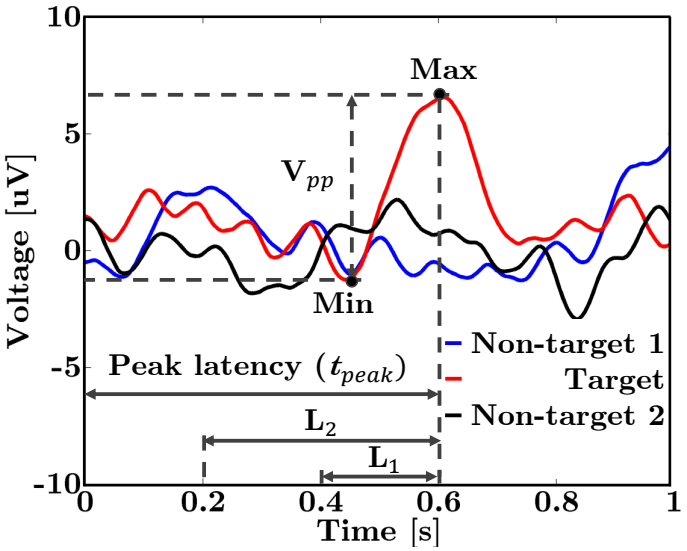

FIGURE 4.2: Definition of peak-to-peak P300 amplitude (V_{pp})

In simple stimulus, the participants were asked to keep looking at fixation point on the center of disk. In MMS, the participants were asked to move their eyes to the small subtargets that randomly appeared within the main target, which would produce small saccades. Participants were asked to avoid blinking during the experiment tasks.

- **Data acquisition and analysis**

  The international 10-20 EEG system was used for recording. The signal from the Cz electrode was recorded using a OpenBCI device (8-bit Board Kit; Arduino-compatible). Reference and ground electrodes were placed on the left and right mastoids, respectively, and the sampling rate was 250 Hz. Before offline analysis, raw data were band-pass filtered (0.5–4 Hz). This frequency range is appropriate for visual ERPs [47]. The recorded data in each condition could be divided into three data sets according to the trigger signals from the three disk positions: left (non-target1), center (target), and right (non-target2). I denote the number of sequences in a data set by Num. (Here, $Num = 10$.) Note that in my statistical analysis both non-target 1 and non-target 2 were considered as a single non-target group.

  In each trial, I analyzed the 600-ms period after the start of the intensification state (stimulation onset). To compare recorded potentials acquired in response to the target and non-target stimuli, I measured peak-to-peak P300 amplitude (V_{pp}). I empirically defined V_{pp} as the difference between the maximum voltage within 400 ms to 600 ms after stimulus onset (L_1) and the minimum voltage within 200 ms after stimulus onset to the time of maximum voltage (L_2) (Figure 4.2). P300

amplitude elicited by the target (V_{ppt}) stimulus is usually higher than that elicited by a non-target (V_{ppn}) stimulus, so that I could distinguish the target stimulus from the non-target stimuli in this experiment. Robustness of elicited P300 Target detection accuracy was used to evaluate the performance of the simple stimulus and MMS.

4.3 Experiment II: Personal identification number application

I implemented the MMS stimulus which was studied in Experiment I to a PIN application (Figure 4.3). Moreover, I introduced 'adaptive BCI' for P300 detection. Adaptive BCI is aimed at increasing the ITR of the PIN application while maintaining high accuracy.

4.3.1 PIN application

Figure 4.3 shows screen captures and the stimulation timing of the PIN application. The user could select nine possible target numbers $(1, 2, 3, \cdots, 9)$ by selecting two target columns from two matrices that contained the target number. Figure 4.3(a) shows how to select '4'. Once the first stimulus matrix appears on the monitor screen, stimulation starts. The user first looks at the stimulus disk located above the column containing the desired number, '4' (left disk in this figure) until completion of stimulation. Then, the matrix is transposed. Next, the user again selects the stimulus disk located above the column containing '4' (center disk). Finally, the application detects the target number.

4.3.2 P300 detection for PIN application

- **Original P300 BCI**

  In my experiments, V_{ppt} from the target stimulus was usually higher than V_{ppn} from non-target stimuli. Experimental results in the previous section suggest that the peak-to-peak value (V_{pp}) might be practical and consistent enough for distinguishing a target stimulus from non-target stimuli. Therefore, I propose the simple P300 detection algorithm as shown below:

$$T = \arg\max\{V_{pp}(x), x = 1, 2, 3\}. \tag{4.1}$$

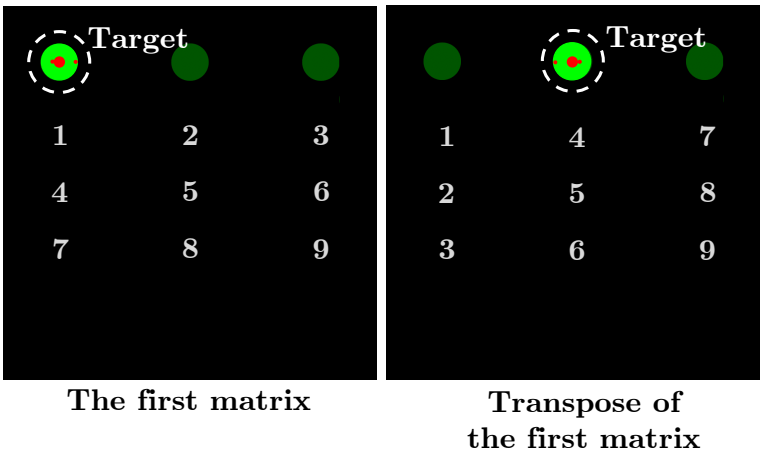

(a) PIN application

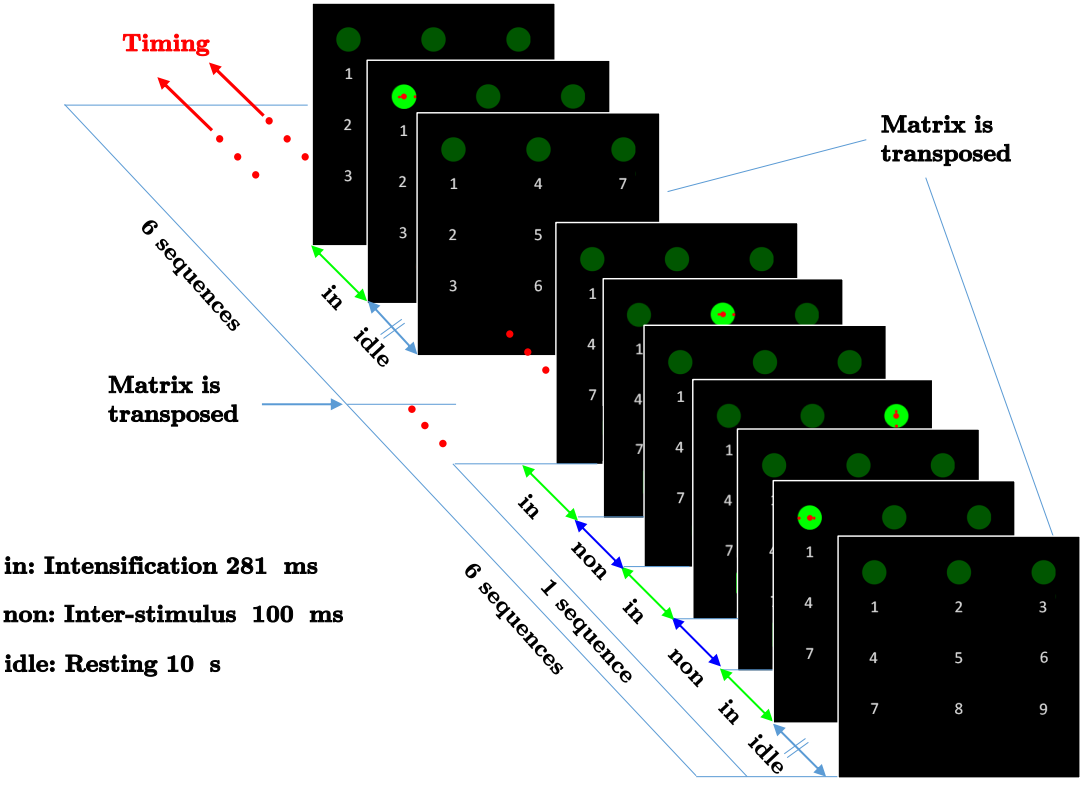

(b) Stimulation timing

FIGURE 4.3: Screen captures of the PIN application. (a) shows how to select '4'. (b) shows the stimulation timing used in this research.

Here, T is the position of the target stimulus and $V_{pp}(x)$ is V_{pp} at position x. I have three stimulus disks or three possible positions $x = 1, 2, 3$. The stimulus disk that gives the maximum V_{pp} is taken to be the target stimulus.

- **Adaptive P300 BCI**

  The number of sequences (Num) of visual stimulation for a typical P300 BCI is fixed at certain number. In fact, the optimal Num (n_{opt}) for optimal accuracy varies among individuals. Here, I proposed adaptive BCI to optimize n_{opt}. Here, both V_{pp} and peak latency (t_{peak}) were used in P300 detection. An illustration of t_{peak} is shown in Fig. 3. The P300 detection algorithm is based on (4.2) and (4.3). We used (4.2), to measure variance of t_{peak}, as a constraint equation, and (4.3) to measure V_{pp}. The stimulation and algorithm terminated to increase Num whenever (4.3) gave the solution (T= x) which was matched constraint equation, (4.2).

$$\sum_{Num=2}^{n_{opt}} C_{x,Num} \geqslant a_2,$$

$$C_{x,Num} = \begin{cases} 1 & \text{if } |t_{peak}(x, Num) - t_{peak}(x, Num-1)| < a_1, \\ 0 & \text{otherwise.} \end{cases} \tag{4.2}$$

$$T = \arg\max\{V_{pp}(x), x = 1, 2, 3\}. \tag{4.3}$$

  In this study, a_1 and a_2 were arbitrary constants that were empirically set to 200 ms and 2, respectively.

- **Experimental setup**

  I conducted experiments using the stimulation timing shown in Figure 4.3(b). Ten healthy participants ($n = 10$) participated in this experiment. They were asked to freely select four target numbers (two participants did five numbers). To select a target, they were asked to look at one of the target disks until the completion of 6 stimulus sequences in each matrix ($Num = 6$). All experiments used the same experimental environment and setup as described in Section 4.2.

- **Offline performance evaluation**

  To demonstrate the advantage of the adaptive P300 BCI over the original P300 BCI for the PIN application, I analyzed the data as in both the adaptive and original versions. I evaluated the performance of the PIN application in terms of decoding accuracy and ITR. BCI researchers commonly use the following definition of bit rate per trial (B) for computing ITR [3]:

$$B = \log_2 N + P \log_2 P + (1 - P) \log_2 \left(\frac{1 - P}{N - 1} \right). \tag{4.4}$$

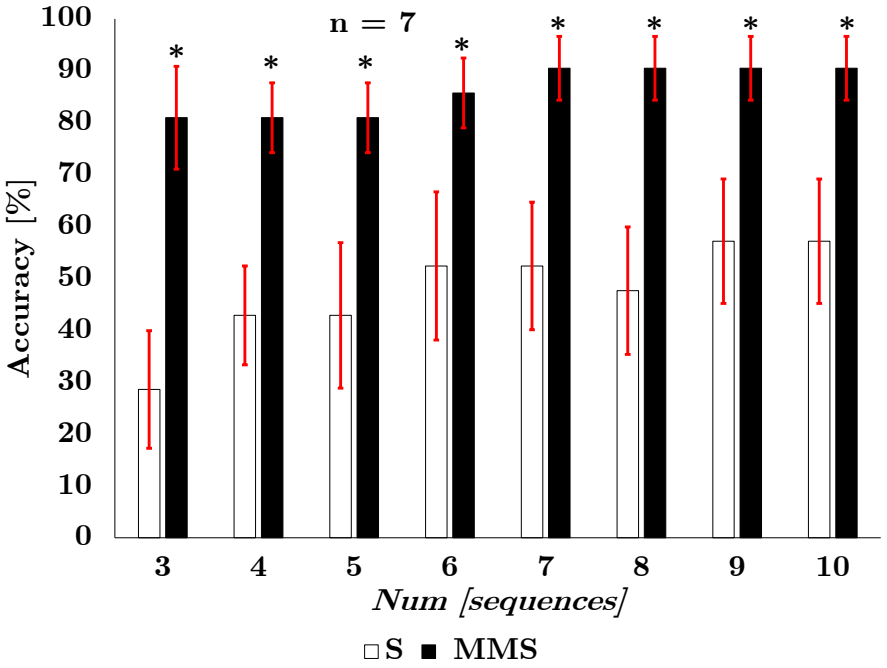

FIGURE 4.4: Accuracy of P300 detection using V_{pp} from the simple stimulus (S) and motion-modulated stimulus (MMS). Results are shown as the average from seven participants ($n = 7$). Errors bars show the SE. * $p < 0.05$

Here, N is the number of possible targets and P is the probability that the target is accurately classified. ITR (bits/min) is calculated by dividing B by the sequence duration (min). When $P = 1$, the equation became $B = \log_2 N$. Here, I calculated ITR using $N = 9$ possible targets. The sequence durations can be calculated from Figure 4.3(b). For the calculation, I omit the rest period and the time to switch matrices because these periods had no stimulation.

4.4 Results and discussion

I first present a comparison of the performance of my proposed stimulus (MMS) against the simple stimulus in Section 4.4.1. I then show the results of experiments on the proposed PIN application in Section 4.4.2. Finally, I conclude by noting the novelty of this work and its contribution to BCI research in Section 4.4.3.

4.4.1 Experiment I: Development of visual stimulation

As shown in Figure 4.4, the standard t-test assuming unequal variances revealed that there were significant differences in mean accuracy between the two stimulus conditions for all Num. The MMS reached 90.5% mean accuracy at $Num = 7$ while the simple

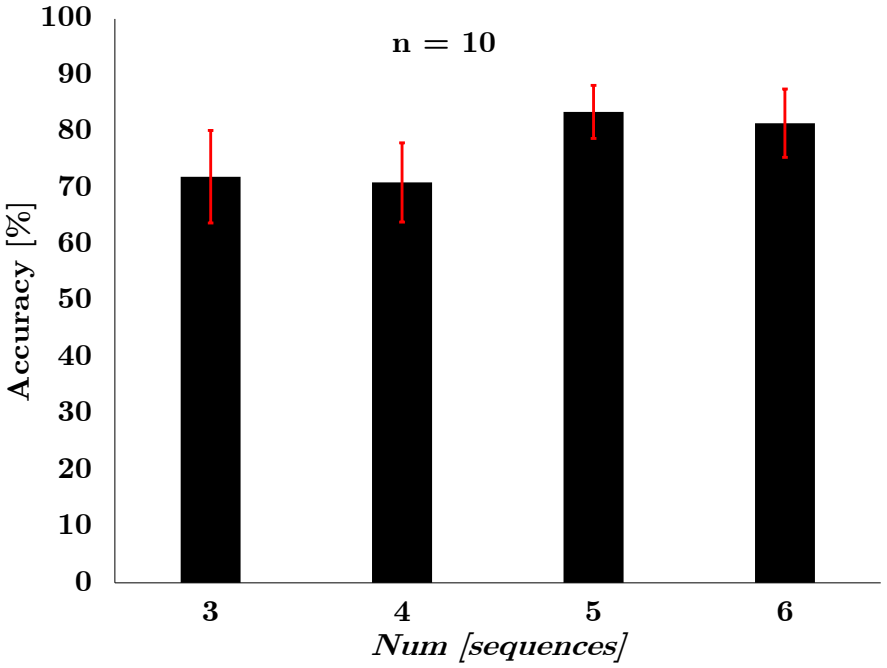

FIGURE 4.5: Accuracy of the PIN application using the original P300 BCI. Results are shown as the average from 10 participants ($n = 10$). Errors bars show the SE.

stimulus reached 57.14% mean accuracy at $Num = 9$. These results indicate that the MMS had higher performance than the simple stimulus did. Hence, I incorporated the MMS into the PIN application.

4.4.2 Experiment II: Personal identification number application

The mean accuracy of the PIN application using the original P300 BCI was shown in Figure 4.5. Time-ensemble averaging for $Num = 5$ sequences gave the highest accuracy with the lowest standard error (SE). To compare the results of the original P300 BCI with those of the adaptive P300 BCI, I calculated the accuracy and ITR at $Num = 5$ for each participant as shown in Table 4.1. Table 4.2 presents the results for the PIN application using the adaptive P300 BCI. The optimal Num (n_{opt}) was less than 4 sequences for each participant. In this experiment, n_{opt} was never less than 3 sequences because of the setting of the arbitrary constant $a_2 = 2$ in the adaptive P300 BCI algorithm. By comparing Table 4.1 and Table 4.2, I can see that the adaptive BCI achieved higher accuracy at higher ITR than the original BCI did. Moreover, the standard t-test assuming unequal variances revealed that mean ITR from adaptive P300 BCI (18.63* bits/min) was significantly higer than that from original BCI (11.40 bits/min), ($t(15) = 2.51$,* $p < 0.05$). Hence, I concluded that the proposed adaptive P300 BCI improved ITR while maintaining acceptable accuracy in the PIN application.

TABLE 4.1: Accuracy and ITR of the PIN application using the original P300 BCI.

Participant	n_{opt} **[seq.]**	**Accuracy [%]**	**ITR [bits/min]**
s1	5	75.0	8.4
s2	5	75.0	8.4
s3	5	60.0	5.2
s4	5	100.0	16.6
s5	5	100.0	16.6
s6	5	100.0	16.6
s7	5	75.0	8.4
s8	5	75.0	8.4
s9	5	100.0	16.6
s10	5	75.0	8.4
mean	**5**	**83.5**	**11.4**

TABLE 4.2: Accuracy and ITR of the PIN application using the adaptive P300 BCI.

Participant	n_{opt} **[seq.]**	**Accuracy [%]**	**ITR [bits/min]**
s1	3.3	100.0	25.6
s2	3.0	100.0	27.7
s3	3.7	80.0	13.1
s4	3.5	80.0	13.9
s5	3.1	100.0	26.6
s6	3.5	75.0	12.1
s7	3.3	50.0	5.4
s8	3.1	75.0	13.6
s9	3.3	100.0	25.0
s10	3.7	100.0	23.4
mean	**3.4**	**86.0**	**18.6***

4.4.3 Novelty and contribution to BCIs

To improve the performance of BCI technologies, especially for medical uses, most researchers have focused on algorithm development, signal processing, or multi-modal BCIs. A few researchers have investigated novel paradigms. However, their paradigm designs were not based on human visual factors. My research group focuses on both medical and non-medical applications. In this paper, I proposed a novel stimulus design based on human visual factors. I modulated a small saccade task during stimulation. The results show that the proposed stimulus enhanced P300 amplitude. My findings suggest that current BCI technologies for general purposes can be improved through understanding of more visual factors related to visual stimulation.

4.5 Summary

In this research, I proposed novel a stimulus for BCIs, and then demonstrated its advantages over a conventional stimulus. P300 responses from the proposed stimulus were clearly observed among participants by single-channel EEG. Even if a small number of sequences were used in ensemble averaging, P300 amplitude was high enough for further signal processing in a BCI. As results of ten participants, the proposed stimulus named MMS reached 90.5% mean accuracy at seven sequences ($Num = 7$) while the simple or conventional stimulus reached 57.1% mean accuracy at nine sequences ($Num = 9$). These results indicate that the MMS had higher performance than the simple stimulus did. Furthermore, I implemented the proposed stimulus in a PIN application using a BCI. The PIN application was based on single-channel EEG and used a computationally inexpensive algorithm. This application did not require training sessions or calibration. Moreover, an adaptive P300 BCI was proposed to optimize the number of sequences used in ensemble averaging. As results of ten participants, the PIN application achieved a mean accuracy of 86.0% and a mean ITR of 18.6 bits/min. In conventional system, 3x3 RC matrix based P300-BCI, five participants reached a mean accuracy of 85.0% and a mean ITR of 3.3 bits/min [57]. Thus, proposed system was outperform standard P300-BCI at same scale of possible input targets (nine characters).

Chapter 5

Hybrid Brain/Blink Computer Interface toward a Personal Identification Number Application

5.1 Introduction

Brain-computer interfaces (BCIs) were originally invented for people with motor disabilities and establish direct communication pathways between the brain and machines such as computers and robots [3]. The ultimate goal is for people to control the machine directly by using their brain activity and no motor functions such as hand movement. Electroencephalography (EEG) is the most useful non-invasive technique for measuring brain activity in BCI systems. Recently, researchers have introduced hybrid BCIs for individuals who have residual motor abilities, such as controlling muscles related to eye movement [8]. In addition, biopotential measurement techniques for eye movement (electrooculography, EOG), and for muscle activity (electromyography, EMG) have been included in hybrid BCI systems. Compared with conventional BCIs, hybrid BCIs achieve higher accuracy and a higher information transfer rate.

Recently, my research group has focused on EOG- and EEG-based interfaces. I began development of an eye-gaze interface using EOG [58], and I introduced a visual stimulus paradigm for EEG-based BCIs [51]. Based on my experience with biopotential

recording for a human-computer interface, here I propose a hybrid brain/blink computer interface. The proposed interface can simultaneously record EEG and blink signals. Moreover, proposed hybrid BCI can detect blinks less intrusively than optical eye-tracking. In optical eye-tracking, users have to carry optical sensors in front of their eyes. To evaluate the performance of the interface, I incorporated it into a personal identification number (PIN) application. My study demonstrates the feasibility and use of the interface for people with and without motor disabilities.

PIN technology for access-control equipment was invented in 1966 and granted a US patent in 1975. Typically, touch-based methods, such as keypads and fingerprints, are used to input PINs. A major drawback of touch-based method is that PINs can be visually or optically observed when they are entered, or recovered with a thermal camera [52]. PIN applications using BCI have been developed to solve this problem; however, the recording setup, such as skin preparation, is too complicated for practical situations [56, 59]. In this work, I proposed a PIN application using my hybrid computer interface. The PIN application has two modes: visual and auditory. In visual mode, the monitor screen is required for presenting target numbers. In contrast, the monitor screen is not required in auditory mode. In auditory mode, the user can input target numbers by following navigation sounds from headphones (The auditory mode can also be interface platform for blind people). My PIN application has two advantages over conventional touch-based methods. First, it allows for non-touch input, so no heat signal or fingerprints are left behind. Second, the PIN cannot be observed by shoulder surfing during entry in auditory mode.

The remainder of this paper is organized as follows. The hybrid brain/blink computer interface is introduced in Section 5.2. Section 5.3 discusses PIN applications using my hybrid computer interface. The experimental results and discussion of my research are presented in Section 5.4. Finally, the conclusions are given in Section 5.5.

5.2 Experiment I: offline analysis

In this section, I introduce the hybrid brain/blink computer interface. The procedures and analyses required before use of the online application are explained. Five healthy people aged 23-27 years participated in the experiments.

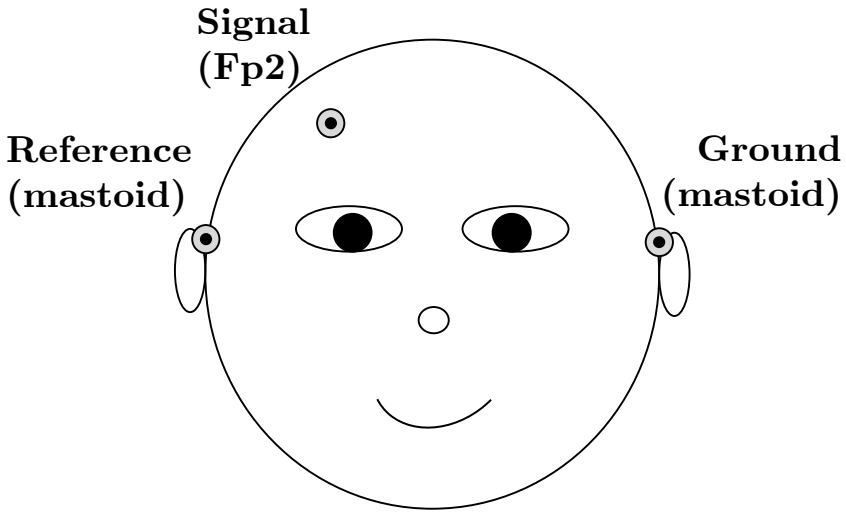

FIGURE 5.1: Recording setup of hybrid brain/blink computer interface.

5.2.1 Recording system

I used an Arduino-compatible EEG amplifier (8-bit Board Kit, OpenBCI) at a sampling rate of 250 Hz. The signal electrode was placed at the Fp2 position of the 10/20 international standard EEG measurement (Figure 5.1). The reference and ground electrodes were placed at the right and left mastoids, respectively.

5.2.2 Calibration tasks

Brain potentials elicited during eyelid closing (EC) and hard blink (HB) were used as signals to operate the interface. Figure 5.2(a) shows the characteristics of EC, HB, and involuntary blink signals. To develop the classification algorithm for online applications, I conducted calibration tasks as shown in Figure 5.2(b). Participants were trained to perform three tasks, which were HB, EC, and resting (R). They were requested to do the tasks by following trigger sounds. The trigger sound was presented 10 times per task. In HB, participants performed a hard blink after the trigger sound. In EC, they were instructed to close (C) and open (O) their eyes after each trigger sound. In R, they were asked to keep their eyes open at all times. Involuntary blinks were allowed. R represented baseline conditions, during which nothing was inputted into the interface. Complete calibration required 3 minutes. I can vary number of calibration tasks to improve performance of classification algorithm in Section 5.2.5, but I have to concern tradeoff between time consuming and accuracy.

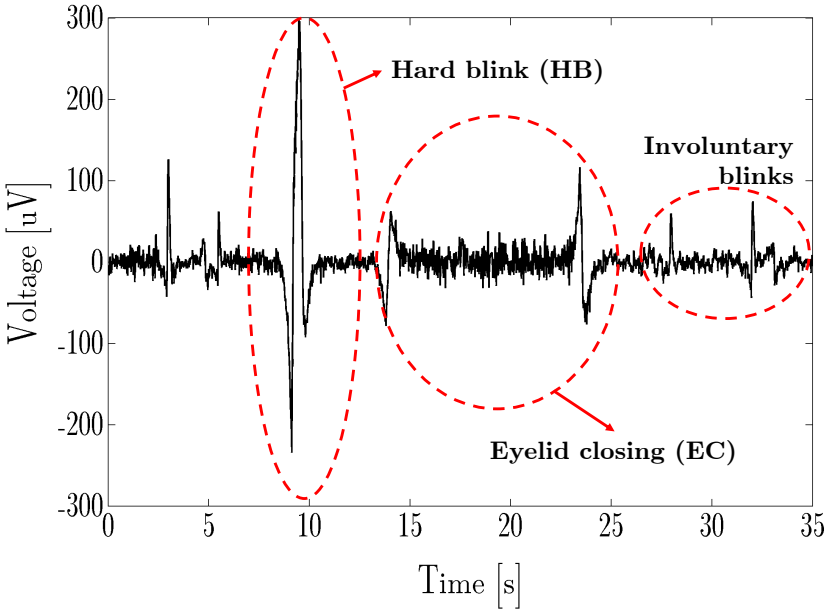

(a) Biopotential responses of calibration tasks

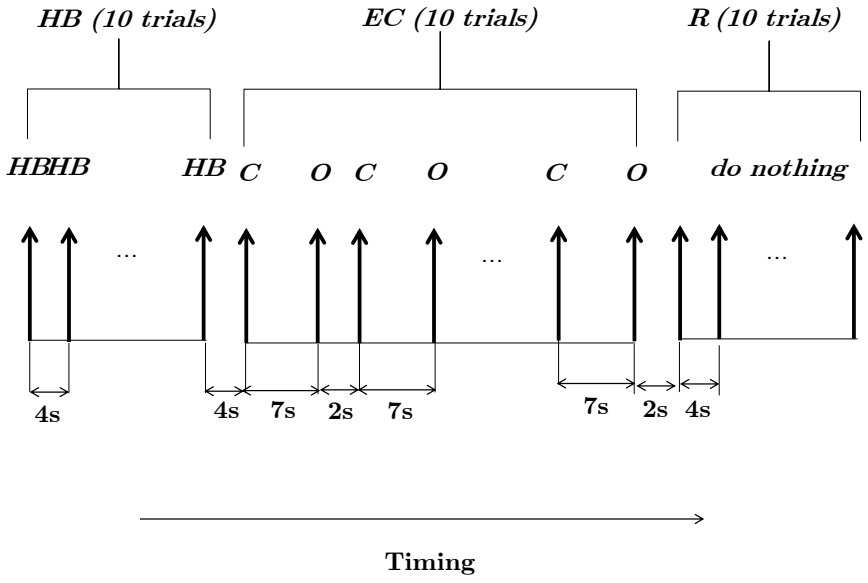

(b) Calibration protocol

FIGURE 5.2: (a) Biopotential responses of calibration tasks. (b) Timing for calibration. Participants were asked to do three tasks (HB, EC, and R) continuously. Vertical arrows represent trigger sounds.

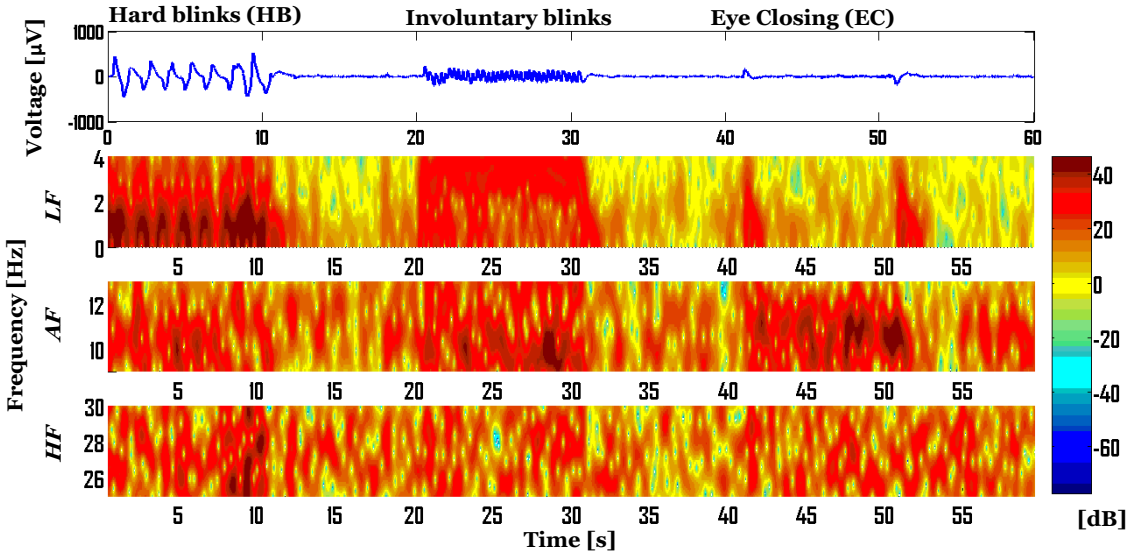

FIGURE 5.3: Illustrates representative time-frequency power spectra for HB, Involuntary blink and EC. Low frequency (LF), alpha frequency (AF), and high frequency (HF).

5.2.3 Signal segmentation

The recorded signals for the calibration tasks were filtered by a 0.5–40 Hz band-pass filter and a 50 Hz notch filter during pre-processing. During data acquisition, I took the recorded signals within 2 s after every trigger sound from HB and R. During EC, I focused on the dominant EEG response in the frequency range of 9–13 Hz. The preliminary results from 2 participants showed that the dominance of the target EEG response is clear 3–5 s after eyelid closing. Hence, I took recorded signals from 5 to 7 s after every trigger sound during EC. I obtained three data sets from the HB, EC, and R tasks. Each data set contained 10 trials, and a trial lasted 2 s.

5.2.4 Feature extraction

Fast Fourier transform (FFT) was used to transform the data sets obtained by signal segmentation. I computed the power in three frequency bands: low frequency (LF), alpha frequency (AF), and high frequency (HF). LF, AF, and HF were the sums of the magnitude (in decibels) of the FFT within the 0.5–4, 9–13, and 25–30 Hz bands, respectively. (These frequency bands could be used to recognize biopotential responses of calibration tasks as shown in Figure 5.3.) The three-dimensional feature vector ($\vec{\mathbf{F}} = [F_1, F_2, F_3]$) was constructed from LF, AF, and HF. I compared four alternative feature vectors, as shown in Table 5.1.

TABLE 5.1: Four alternative feature vectors.

Alternative $\vec{\mathbf{F}}$	F_1	F_2	F_3
A	$\frac{LF}{LF+AF+HF}$	$\frac{AF}{LF+AF+HF}$	$\frac{HF}{LF+AF+HF}$
B	LF	$\frac{AF}{LF}$	$\frac{HF}{LF}$
C	$\frac{LF}{AF}$	AF	$\frac{HF}{AF}$
D	$\frac{LF}{HF}$	$\frac{AF}{HF}$	HF

In alternative **A**, the total power in the three frequency bands ($LF + AF + HF$) was used as a normalization factor. LF, AF, and HF were used as the normalization factors in alternatives **B**, **C**, and **D**, respectively. The classification accuracies of the alternatives were compared (Section 5.2.5). According to the data sets in Section 5.2.4, I represented $\vec{\mathbf{F}}$, which was extracted from HB, EC, and R, as $\vec{\mathbf{F}}_{HB}$, $\vec{\mathbf{F}}_{EC}$, and $\vec{\mathbf{F}}_{R}$, respectively. Each data set was obtained from 10 trials, so $\vec{\mathbf{F}}_{HB}$, $\vec{\mathbf{F}}_{EC}$, and $\vec{\mathbf{F}}_{R}$ were written in the matrix forms as

$$
\begin{aligned}
\vec{\mathbf{F}}_{HB} &= \begin{bmatrix} \vec{\mathbf{F}}_{HB_1} & \vec{\mathbf{F}}_{HB_2} & \vec{\mathbf{F}}_{HB_3} \end{bmatrix} \\
&= \begin{bmatrix} F_{HB_{1,1}} & F_{HB_{1,2}} & F_{HB_{1,3}} \\ F_{HB_{2,1}} & F_{HB_{2,2}} & F_{HB_{2,3}} \\ \vdots & \vdots & \vdots \\ F_{HB_{10,1}} & F_{HB_{10,2}} & F_{HB_{10,3}} \end{bmatrix}, \\
\vec{\mathbf{F}}_{EC} &= \begin{bmatrix} \vec{\mathbf{F}}_{EC_1} & \vec{\mathbf{F}}_{EC_2} & \vec{\mathbf{F}}_{EC_3} \end{bmatrix} \\
&= \begin{bmatrix} F_{EC_{1,1}} & F_{EC_{1,2}} & F_{EC_{1,3}} \\ F_{EC_{2,1}} & F_{EC_{2,2}} & F_{EC_{2,3}} \\ \vdots & \vdots & \vdots \\ F_{EC_{10,1}} & F_{EC_{10,2}} & F_{EC_{10,3}} \end{bmatrix}, \\
\vec{\mathbf{F}}_{R} &= \begin{bmatrix} \vec{\mathbf{F}}_{R_1} & \vec{\mathbf{F}}_{R_2} & \vec{\mathbf{F}}_{R_3} \end{bmatrix} \\
&= \begin{bmatrix} F_{R_{1,1}} & F_{R_{1,2}} & F_{R_{1,3}} \\ F_{R_{2,1}} & F_{R_{2,2}} & F_{R_{2,3}} \\ \vdots & \vdots & \vdots \\ F_{R_{10,1}} & F_{R_{10,2}} & F_{R_{10,3}} \end{bmatrix}
\end{aligned}
\tag{5.1}
$$

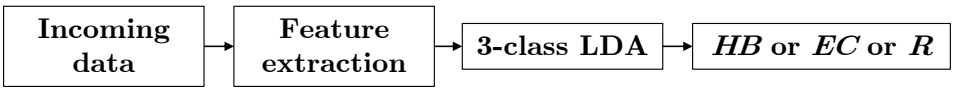

(a) 3-class LDA

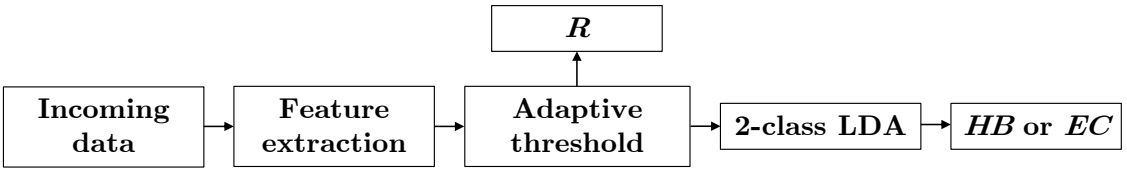

(b) 2-class LDA

FIGURE 5.4: Two alternative algorithms were compared in this experiment.

5.2.5 Classification algorithm

Two algorithms, called the three-class linear discriminant analysis (3-class LDA) and two-class linear discriminant analysis (2-class LDA), were compared (Figure 5.4). Leave-one-out cross validation was used to evaluate accuracy. The training and testing data came from feature vectors ($\vec{\mathbf{F}}_{HB}$, $\vec{\mathbf{F}}_{EC}$, $\vec{\mathbf{F}}_{R}$), which were extracted from calibration data. The algorithm with the highest accuracy was used in the online application.

- **3-class LDA**

  Figure 5.4(a) shows the overall process of 3-class LDA. This algorithm is a typical method for classifying data. After feature extraction, the feature vector of the incoming data ($\vec{\mathbf{F}} = [F_1, F_2, F_3]$) is directly used in the LDA. A linear classifier is constructed by using the training data from $\vec{\mathbf{F}}_{HB}$, $\vec{\mathbf{F}}_{EC}$, and $\vec{\mathbf{F}}_{R}$. Finally, the output is the classification result. The accuracy of the algorithm depends on the classifier.

- **2-class LDA**

  Figure 5.4(b) shows the overall process of 2-class LDA. This algorithm is expected to reduce calibration time. Only training data from $\vec{\mathbf{F}}_{HB}$ and $\vec{\mathbf{F}}_{EC}$ are used to calculate adaptive thresholds and construct the linear classifier. There are two classification steps in this algorithm. First, it is decided whether the incoming

feature vector $\vec{\mathbf{F}} = [F_1, F_2, F_3]$ is a feature vector from R by using the adaptive thresholds shown in (2)–(4) (These equations are first introduced in this research.).

$$F_1 < min\ \{\vec{\mathbf{F}}_{HB_1}\} \tag{5.2}$$

$$F_1 > max\ \{\vec{\mathbf{F}}_{EC_1}\} \tag{5.3}$$

$$F_2 < min\ \{\vec{\mathbf{F}}_{EC_2}\} \tag{5.4}$$

If (2) and either (3) or (4) hold, then the incoming data are classified as R, and the process terminates. However, if incoming data are not classified as R, then $\vec{\mathbf{F}}$ is sent for further classification using LDA. Finally, the output is estimated be either HB or EC. The accuracy of this algorithm depends on the adaptive thresholds and the classifier.

5.3 Experiment II: online PIN applications

I incorporated my interface into a PIN application. Figure 5.5 shows the application screen in visual mode. Ten numbers (0 to 9), four back buttons, and the "delete" and "enter" buttons are displayed in a 4×4 grid. The PIN application in auditory mode works the same as in visual mode, except a navigation sound is used instead of the screen. Five healthy people aged 23–27 years participated in the experiments. Although the present application allowed slight head-movement, I asked participants to minimize their head-movements.

5.3.1 Control application using HB and EC

Here, I implemented 2-class LDA. The application classified 2-s-long incoming data every 4 s. The two possible operations are moving the cursor in one direction by using HB and selecting a target by using EC. A notification sound is generated whenever EC is detected by the application because the user's eyes are closed during selection. One HB is required to start the application. There are two steps to select the target number. The user first selects the target row, and then selects the target number within the target row. To change the target row, the user needs to select the back button, which is the last button in each row. The user can delete incorrect numbers by selecting the delete button and can submit the PIN by selecting the enter button. The PIN application in auditory mode works the same as in visual mode, except the navigation is performed via sound signals, instead of displaying numbers on the screen. Figure 5.5 shows a demonstration of how the number 5 is selected. HB is performed to start the application. In visual

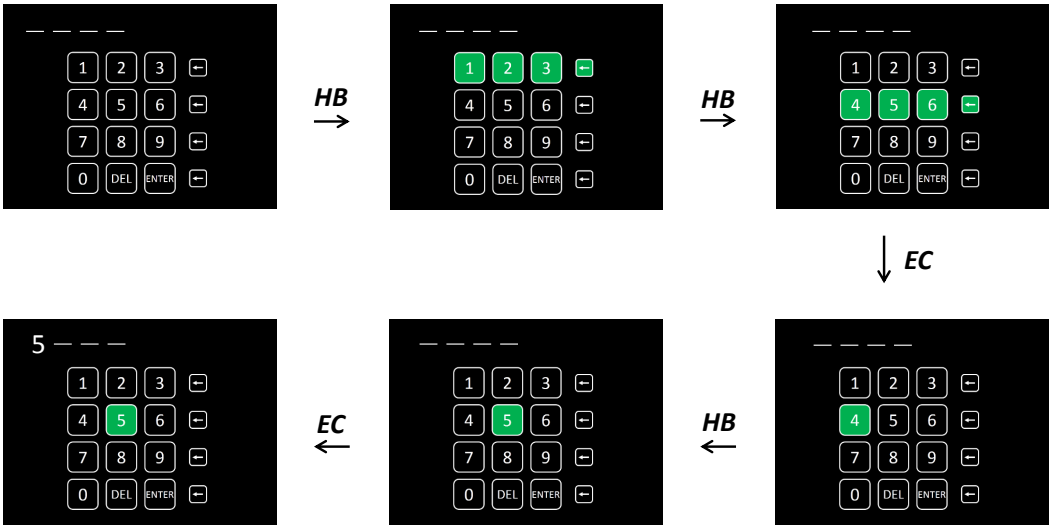

FIGURE 5.5: Demonstration of how the number 5 is selected from the start of the application. HB is performed to start the application and to advance the cursor, and EC is performed to make selections.

mode, navigate cursor is started from the first row which contains 1, 2, 3, and back button. While navigate sound "one–two–three–back" is generated. HB is performed again to advance to the second row ("four–five–six–back"), and then EC is used to select the second row (In both visual and auditory modes, notification sound "select" is generated.). One more HB is performed to move cursor to number 5 (In auditory mode, sound "five" is generated). Finally, EC is performed to select number 5.

5.3.2 Performance evaluation

I evaluated the performance of the hybrid interfaces with an online PIN application. I allowed participants to familiarize themselves with the application before the experiments, and the calibration tasks (HB and EC) took 2 min. During the experiments, participants selected four target numbers freely. They could delete numbers sequentially if an incorrect number was shown on the screen. Finally, they had to select the enter button to submit the PIN. I measured the accuracy of the participants' operation of the interface (moving the cursor and button selection). I observed the participants' faces during the experiments, so I could see their intended operation and the output operation on the application screen. If the intended operation was not same as the output operation, I counted this as an incorrect operation. In contrast, if the intended operation was same as the output operation I counted this as a correct operation. Finally, the operational accuracy was calculated. Although I did not consider the resting state or

TABLE 5.2: Overview of the results from the visual-mode PIN application (*Par.* : *Participant*, *Err.* : *Error*, *Acc.* : *Accuracy*)

Par.	***PIN***	***HB [s]***	***EC [s]***	***Operation [#]***	***Err.***	***Acc.[%]***
s1	2580	7.1	6.2	30	0	100.0
s2	4917	5.3	8.5	34	0	100.0
s3	4137	5.7	6.6	61	1	86.9
s4	3482	4.6	4.3	35	0	100.0
s5	2597	5.5	6.2	31	0	100.0
Mean		**5.6**	**6.4**			**97.4**

TABLE 5.3: Overview of the results from the auditory-mode PIN application (*Par.* : *Participant*, *Err.* : *Error*, *Acc.* : *Accuracy*)

Par.	***PIN***	***HB [s]***	***EC [s]***	***Operation [#]***	***Err.***	***Acc.[%]***
s1	2580	6.9	7.7	43	4	90.7
s2	4917	5.5	6.0	34	0	100.0
s3	4137	5.3	5.5	80	8	82.4
s4	3482	4.8	4.2	35	0	100.0
s5	2597	6.4	7.8	38	0	100.0
Mean		**5.8**	**6.2**			**94.6**

no operation, I measured the time between consecutive operations. Participants were requested to input target numbers continuously in the experiments so that I could calculate the average time per operation. The sensitivity of the interface could be obtained from the time per operation during the PIN application.

5.4 Results and discussion

In this section, I discuss the experimental results from Experiments I and II.

5.4.1 Results of Experiment I

First, I evaluated four alternative feature vectors (Table 5.1) with the 3-class LDA (see Section 5.2.5). The pooled covariance matrix of the training data was not positive definite for the alternative feature vector **A**; thus, I could not construct a linear classifier for the LDA.Figure 5.6 compares the classification accuracy of alternatives **B**, **C**, and **D**. Although I could not find any statistically significant difference among the alternatives, alternative C had the highest mean accuracy with the lowest standard error. Hence, I selected the feature vectors from alternative **C** ($[\frac{LF}{AF}, AF, \frac{AF}{HF}]$) for further comparison of the 3-class LDA and 2-class LDA. For the 3-class LDA, there were overlaps between R and EC in most participants (Figure 5.7(a)). The overlap was solved by removing

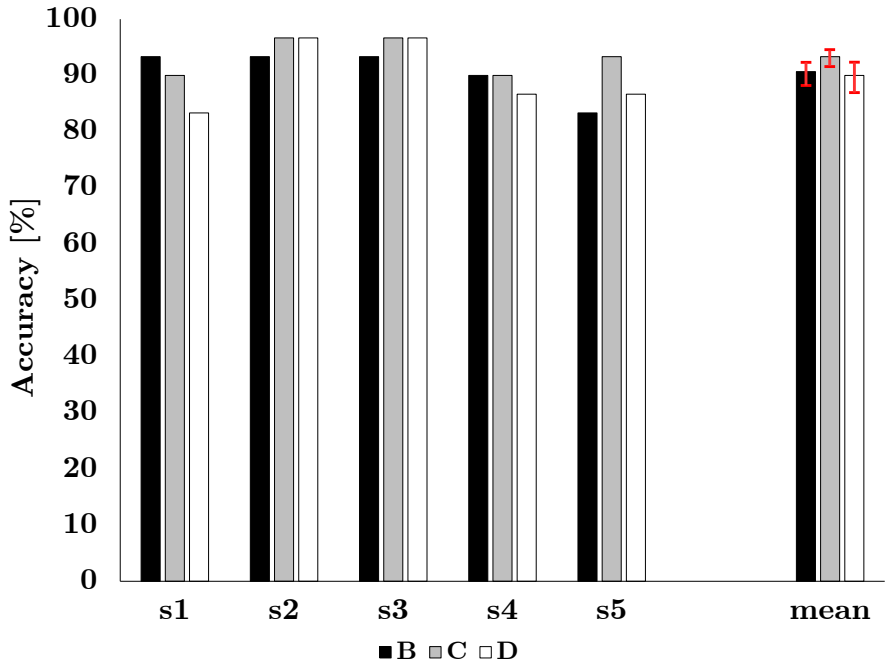

FIGURE 5.6: Comparison of the accuracy of the 3-class LDA algorithm using three alternative features among the 5 participants (s1–s5). Group means and standard errors are also shown.

R by using adaptive thresholds before classification (Figure 5.7(b)). The improvement in classification accuracy for the 2-class LDA algorithm compared with the 3-class LDA algorithm is clear in Figure 5.8. Two participants (s1 and s4) reached 100.0% accuracy, and all participants reached 97.3% accuracy. Thus, I implemented 2-class LDA with alternative **C** feature vectors in the online PIN application.

In conclusion, the highest accuracy was obtained by using the **C** feature vectors, in which data were normalized by the power in the AF band (9–13 Hz). Moreover, the 2-class LDA algorithm had a shorter calibration time and higher accuracy compared with the 3-class LDA algorithm. The calibration tasks for the 2- and 3-class LDA algorithms took 2 and 3 min, respectively.

5.4.2 Results of Experiment II

According to Table 5.2 and Table 5.3, the 5 participants showed high accuracy in using the PIN application. Four participants reached 100.0% accuracy. All participants reached 97.4% and 94.6% mean accuracy in visual and auditory mode, respectively. The mean time per operation was about 5–6.5 s in both modes. There was no significant difference between visual and auditory modes in the time per operation (Figure 5.9).

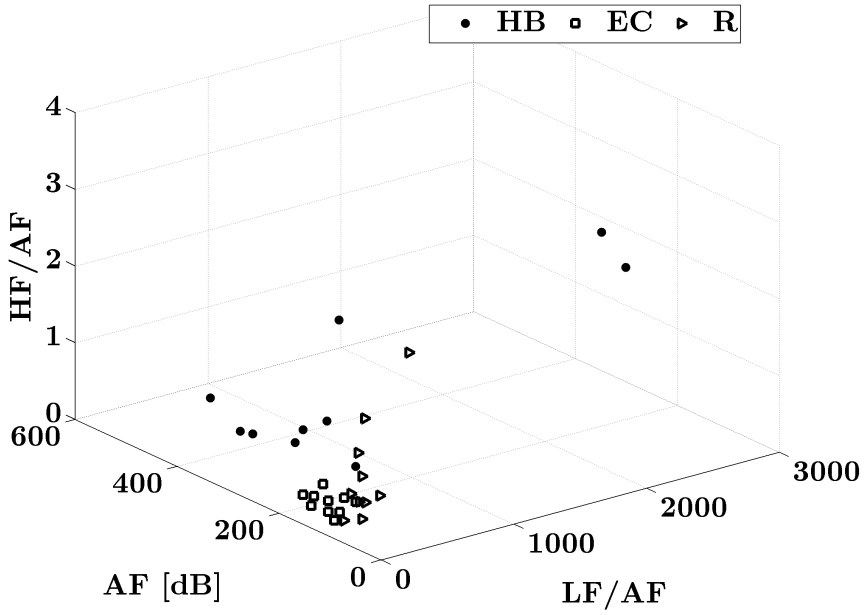

(a) 3-class LDA

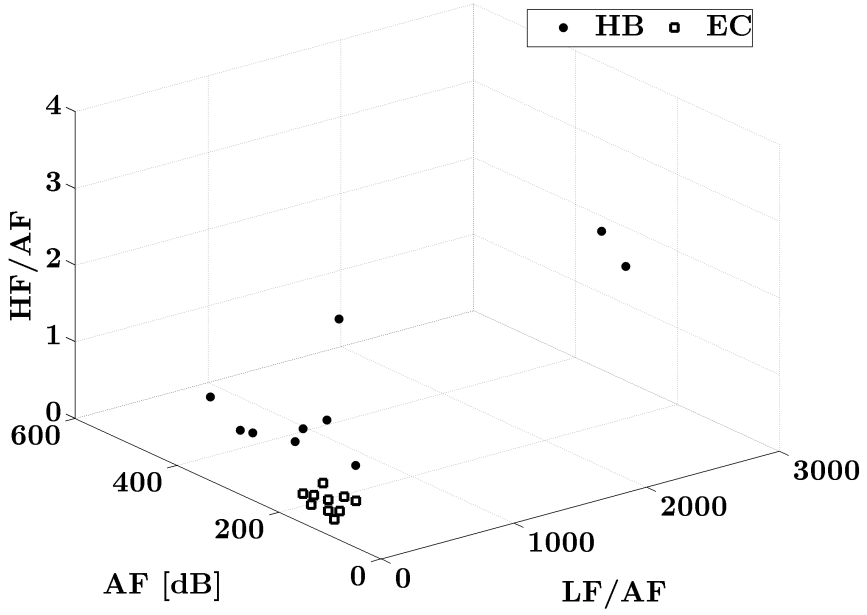

(b) 2-class LDA

FIGURE 5.7: Comparison of 3-class and 2-class LDA data on three-dimensional features (alternative **C**, participant s1).

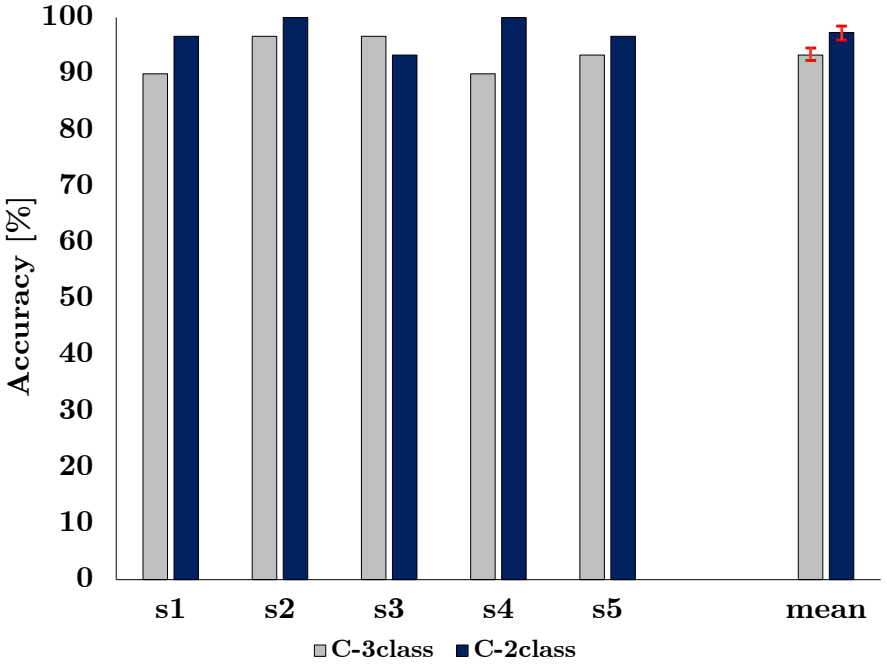

FIGURE 5.8: Comparison of the accuracy of the 3-class and 2-class LDA algorithms using alternative **C** feature vectors among the 5 participants (s1–s5). Group means and standard errors are also shown.

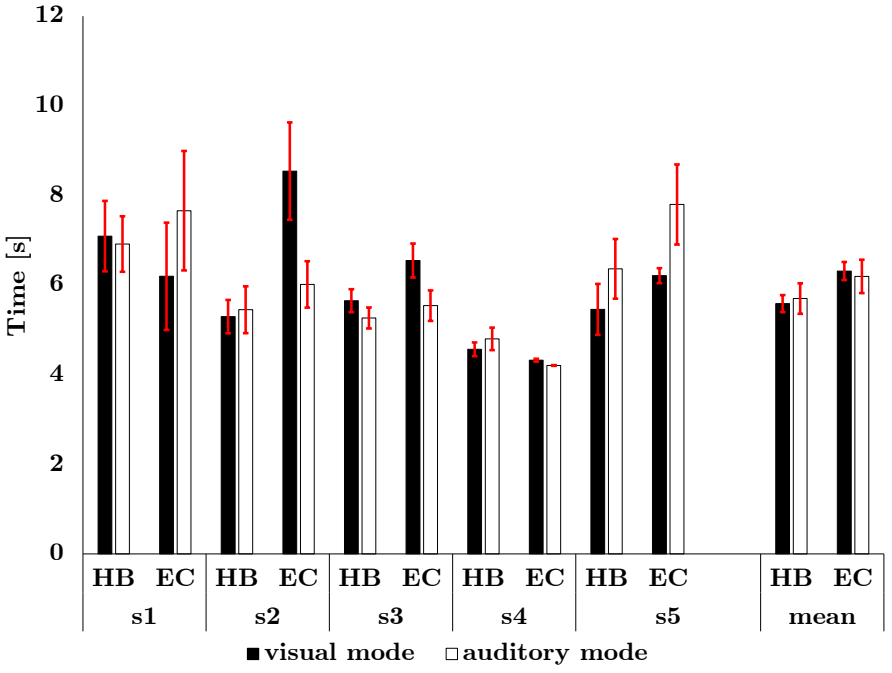

FIGURE 5.9: Comparison of time per operation for visual- and auditory-mode PIN applications among the 5 participants (s1–s5). Group means and standard errors are also shown.

Although the experimental results showed high accuracy in using the interface for a PIN application, sensitivity in terms of time per operation is still a challenge. Another point of concern is a lack of concentration in auditory-mode application, as seen in participant s5. Although s5 reached 100.0% accuracy in both visual and auditory modes, he performed a higher number of operations in auditory mode. It might be that I always use visual system more than auditory system in daily life. Thus, some subjects have difficulty to use application without monitor screen in auditory mode.

5.5 Summary

I created a hybrid computer interface using eyelid closing and hard blink, and I developed an algorithm for EEG and blink classification. I incorporated the system into a non-touch-based PIN application with visual and auditory modes. Experimental results from five participants revealed promising accuracy and feasibility of the proposed application. Four out of five participants reached 100.0% accuracy, and all participants reached mean accuray of 97.3%. The mean time per operation was about 5–6.5 seconds. The accuracy of hybrid system was about 11.0% higher than that in P300-BCI which was studied in previous Chapter. In the near future, I plan to include EOG signals in my interface to improve the information transfer rate. My proposed interface will be useful for healthy people and for people with disabilities in various machine control applications.

Even though visual evoked potential and motor imagery response from brain play important roles for conventional BCI technologies, my hybrid interface was more reliable than conventional BCI. Because it is based on not only brain signal (EEG) but also hard blink signal (EMG). However, the problems caused by motion artifacts have not been fully addressed in the present study. The resolution of motion artifact problem is important because it can potentially deteriorate user-experience of my BCI.

Chapter 6

Feasibility Study of Drowsiness Detection Using Hybrid Brain-Computer Interface

6.1 Introduction

According to the National Highway Traffic Safety Administration, drowsy driving caused about 72,000 crashes, 800 fatalities, and 44,000 injuries in 2013. Drowsiness detection methods have been actively researched for more than a decade in an effort to reduce the rate of accidents caused by drowsy driving. Subjective questionnaires, measures of driving performance (such as rates of accidents and lane changing), and physical and biopotential measures have been proposed to identify driver drowsiness [60]. These methods all have advantages and disadvantages [61]. Questionnaires cannot be used in real time, but may still be useful for validating other measures; measurement of driving performance is nonintrusive, but could be unreliable in a real driving environment; physical measures such as driver motion and pupil tracking , especially camera-based techniques, are accurate but limited by light conditions and background; and biopotential measures are quite accurate and reliable, but require intrusive measurements. In this study, I focused on two biopotential measures: electroencephalography (EEG) and electrooculography (EOG).

Feasibility studies of driver drowsiness detection using EEG were conducted almost ten years ago [62]; later, one research group did similar experiments for driver fatigue detection [63]. Both investigations focused on the ratio of EEG signals in low-frequency

TABLE 6.1: Karolinska sleepiness scale (KSS).

Score	Meaning
1	Extremely alert
2	Very alert
3	Alert
4	Rather alert
5	Neither alert nor sleepy
6	Some signs of sleepiness
7	Sleepy, no effort to stay awake
8	Sleepy, some effort to stay awake
9	Very sleepy, great effort to keep awake, fighting sleep

and high-frequency bands. Another research group validated a common subjective measure, the Karolinska Sleepiness Scale (KSS), against EEG variables [64]. Many pioneering studies have demonstrated that EEG may be a reliable and accurate measure for drowsiness detection, attracting engineers to develop more applications of this technology [65][66][67]. To improve the accuracy of drowsiness detection, a few researchers have proposed multimodal biopotential measures, including EEG and EOG [68][69]. Although such multiple-channel recording systems can reach more than 90% accuracy, they are highly intrusive for drivers.

Numerous studies on driver drowsiness have been performed over more than a decade; however, most of these were based on complicated measurement systems. Hence, the development of a practical system and application is still a challenging issue. Recently, researchers have introduced hybrid brain–computer interfaces (BCIs) for patients who have severe motor disabilities but have residual motor abilities such as eye movement [8]. Hybrid BCIs serve as a direct commutation pathway from the human brain, through computers. Here, I propose a practical system for drowsiness detection using a hybrid BCI that records EEG and EOG simultaneously. This method is less intrusive than conventional methods because the measurement system is based on single-channel EEG/EOG recording. Moreover, I investigated for the first time a hybrid EEG/EOG signal-processing algorithm for drowsiness detection.

6.2 Experiment

Six healthy people aged 22–25 years participated in the experiment. To induce drowsiness, the experiment was conducted in a dark room as shown in Figure 6.1 and was performed after participants had eaten lunch or dinner. Participants were asked to wear hearing protection headphones to avoid auditory noise. This study was conducted in accordance with the Declaration of Helsinki as revised in 2000.

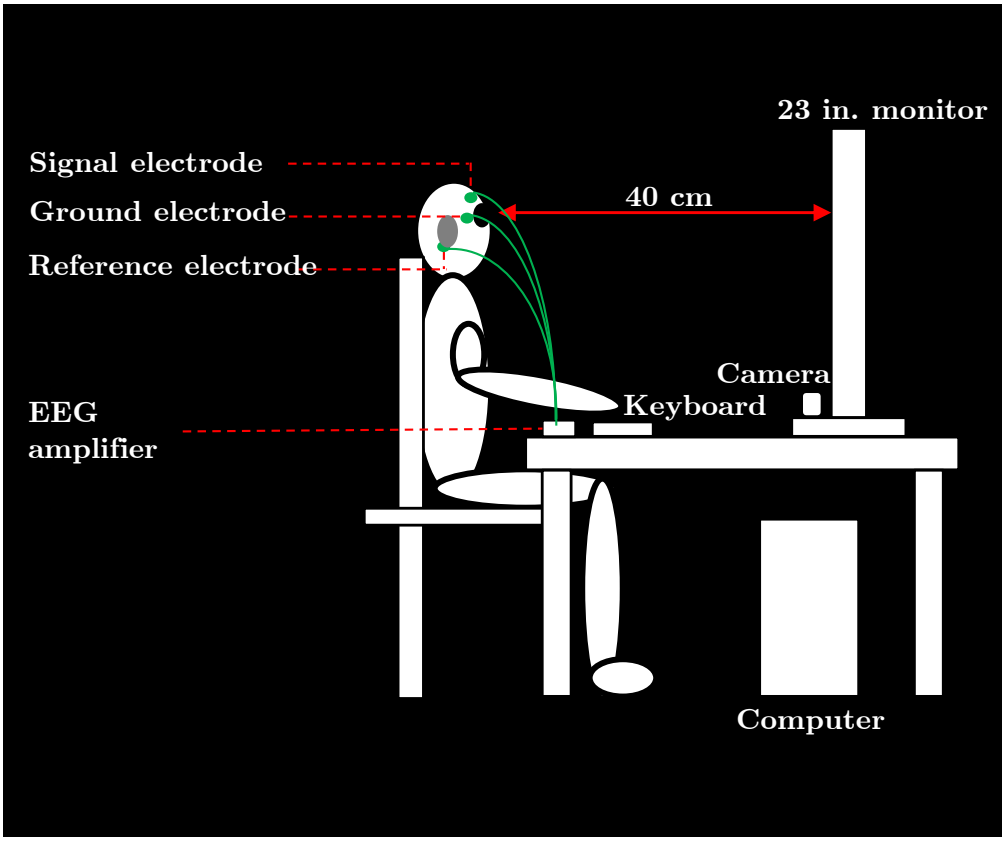

FIGURE 6.1: Illustration of the experimental setup used in this study.

6.2.1 Hybrid brain-computer interface

The hybrid BCI used single-channel EEG recording with a 250-Hz sampling frequency (OpenBCI 8-bit Board Kit, Arduino-compatible). The signal electrode was at the Fp2 position of the standard 10/20 international system for EEG measurement. The reference was placed on the right mastoid, and the ground was placed between the right eye and the right ear as shown in Figure 6.1. In my preliminary measurements, I found that EEG and EOG signals could be recorded simultaneously at this position.

6.2.2 Experimental tasks

A typical personal computer was used in my experiment. Participants were requested to do a simple response task for 25 mins as shown in Figure 6.2. At 1-s intervals, a white square randomly appeared in one of three positions on a black background. Participants were instructed to press the spacebar key as quickly as possible whenever the square appeared in the center position. Response time and error rate were recorded for further analysis. To assess drowsiness, the KSS questionnaire (Table 6.1) was performed every 5 minutes [60].

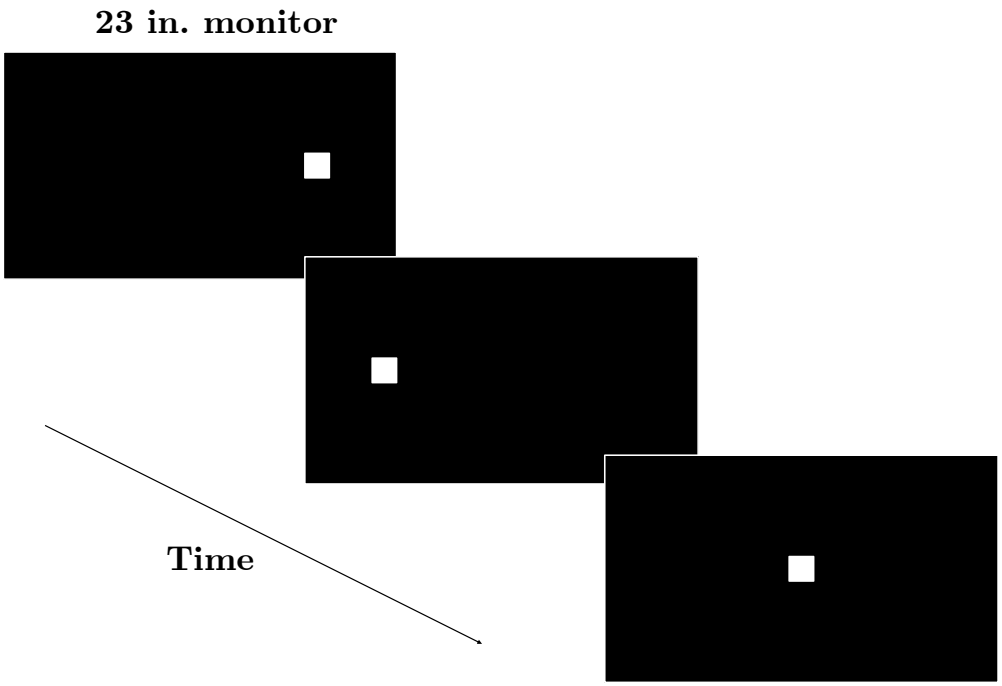

FIGURE 6.2: Depiction of the experimental task. At 1-s intervals, a white square randomly appeared in one of three positions on a black background. Participants were instructed to press the spacebar key as quickly as possible whenever the square appeared in the center position.

6.3 Data analysis

EEG and EOG signals for each participant were recorded for 25 minutes and then equally divided into five segments. After accounting for the time required for KSS assessment, each segment had a final duration of 4.5 minutes. EEG and EOG indices were extracted from the segmented data for drowsiness detection.

6.3.1 EEG index

Each data segment was preprocessed by notch filtering at 50 Hz to cut electrical noise and band-pass filtering (4–25 Hz). In this study, I targeted three frequency bands: θ (4–8 Hz), α (8–13 Hz), and β (13–25 Hz). The δ band (0.5–4 Hz) was not included in the analysis because it was usually distorted by artifacts [62]. The relative powers of the three frequency bands (θ, α, and β) and three ratios among the three frequency bands (θ/β, α/β, and $(\theta+\alpha)/\beta$) were used as EEG indices. The relative power of θ was

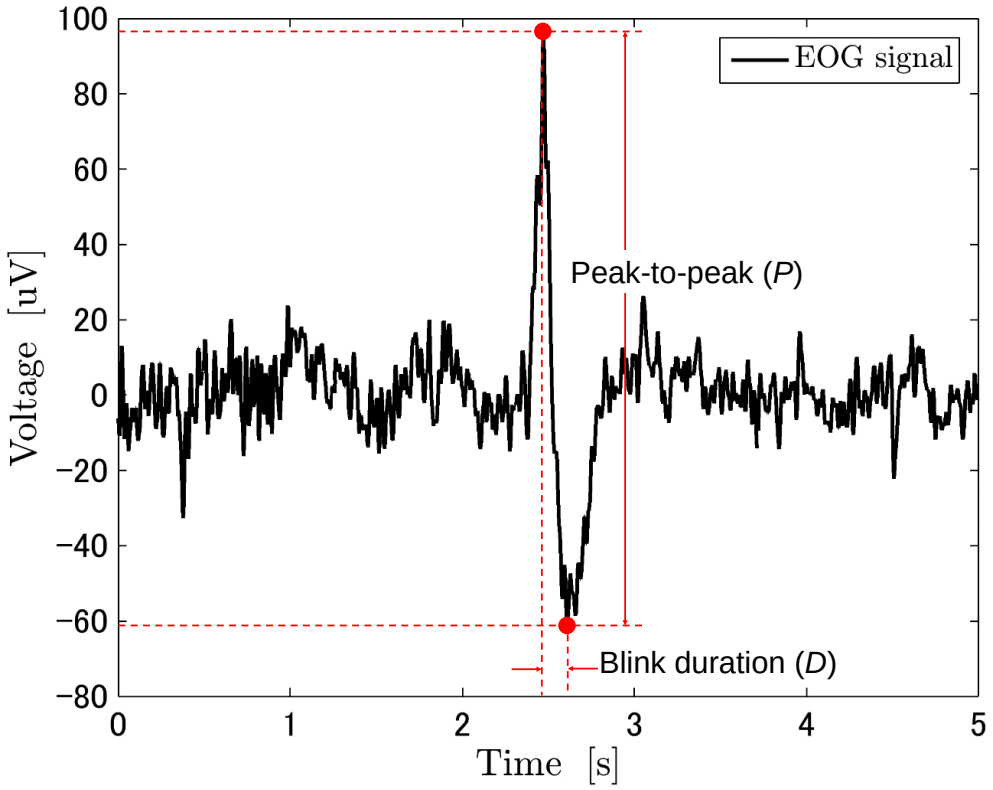

FIGURE 6.3: Demonstration of blink duration measurement.

calculated using Equation 6.1. All indices have been used in previous studies [62, 63].

$$\text{Relative power of } \theta = \frac{\text{power of } \theta}{\text{power of } \theta + \text{power of } \alpha + \text{power of } \beta} \tag{6.1}$$

For the remainder of this paper, the relative powers of the three frequency bands are denoted by θ, α, and β.

6.3.2 EOG index

To extract the EOG index, the segmented data were subjected to band-pass filtering (1–40 Hz) and notch filtering (50 Hz). Blink duration was used as an EOG index, as it has been reported to increase significantly with drowsiness [70]. I used a novel technique to detect blinking and calculate blink duration from the EOG signal. Peak-to-peak magnitude (P) and the period of time between positive and negative peaks (D) were used to determine whether the incoming signal was a blink (Figure 6.3). P was an individual threshold calculated by averaging the values of the first five blinks for each participant; the P threshold was allowed to range up to 10% less than the average value. Blinks could be confirmed by video recordings of the experiment. Whenever the incoming signal was determined to be a blink, D was recorded as the blink duration.

Average D was then calculated for each data segment. Blinking is conventionally defined as lasting for up to 1 s [71]. On the basis of my proposed technique and empirical study, however, D of more than 0.8 s was not identified as a blink signal.

6.3.3 Proposed hybrid EEG/EOG index

My preliminary studies and empirical knowledge of EEG and EOG for drowsiness detection motivated us to propose a hybrid EEG/EOG ratio index. Three hybrid indices ($\theta/(\beta\times D)$, $\alpha/(\beta\times D)$, and $(\theta+\alpha)/(\beta\times D)$) were first introduced in this research.

6.3.4 Evaluation

KSS is widely used in sleep research as the standard drowsiness measure [64, 71]. To demonstrate superiority of the proposed hybrid indices over conventional EEG and EOG indices, I calculated Pearson's linear correlations between all indices and KSS. Moreover, I validated KSS against the percentage of errors made during the experimental task.

6.4 Results and Discussion

Correlations between all indices and KSS are presented in Figure 6.5. Blink duration index (D) results were consistent with findings from previous research [70], and showed a trend toward longer duration when KSS drowsiness level was increased, especially in Participants A–D, and F. Of the EEG indices, the relative powers of θ and α were inconsistent among participants. The relative power of β had the same trend as D, and was quite consistent among participants. EEG ratio indices, which were focused on the ratio between the powers of the low- and high-frequency bands, were negatively correlated with KSS; this was particularly true for α/β. It could be concluded that an increase in high-frequency EEG power relative to low-frequency power was the result of drowsiness. Furthermore, the proposed hybrid indices ($\theta/(\beta\times D)$, $\alpha/(\beta\times D)$, and $(\theta+\alpha)/(\beta\times D)$) were better correlated with KSS than were EEG and EOG indices. In summary, $\alpha/(\beta\times D)$ had the highest significant negative correlation with KSS and performed the most consistently among participants; however, the results for Participant B were inconsistent with those of the other participants for most indices. This may have resulted from Participant B's low drowsiness level in terms of KSS, as shown in Figure 6.5 (b). One research group also has reported that EEG may be significantly different in individuals scoring 7 or higher on the KSS [72].

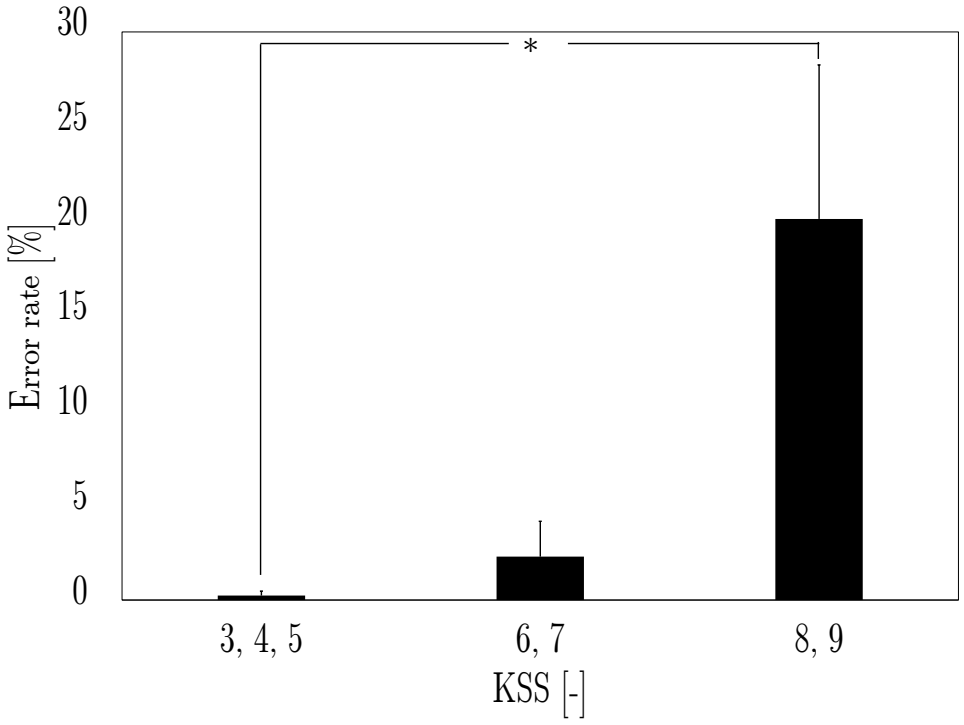

FIGURE 6.4: Validation of error rate on experimental task against KSS score. * denoted ***p<0.05***

Unfortunately, the experimental task may have been too simple in this study. Hence, I could not find significant correlations between response time and any other drowsiness indices. However, the average error rate of all participants during the experimental task was found to increase significantly with increasing KSS score, as shown in Figure 6.4. Error rates were calculated for three KSS score groups (3–5, 6–7, and 8–9) because no participant scored less than 3. Because of the small sample size, statistical testing was performed with a standard t test for unequal variance instead of the analysis of variance method. The error rate of the highest score group was significantly higher than that of the lowest score group ($t(13) = 2.44, p = 0.03$). Motivated by these results, I plan to perform studies using a more complicated experimental task, such as a driving stimulator, in the near future. In conclusion, the results of this study indicate that it is feasible to develop real-time drowsiness detection using my proposed hybrid BCI.

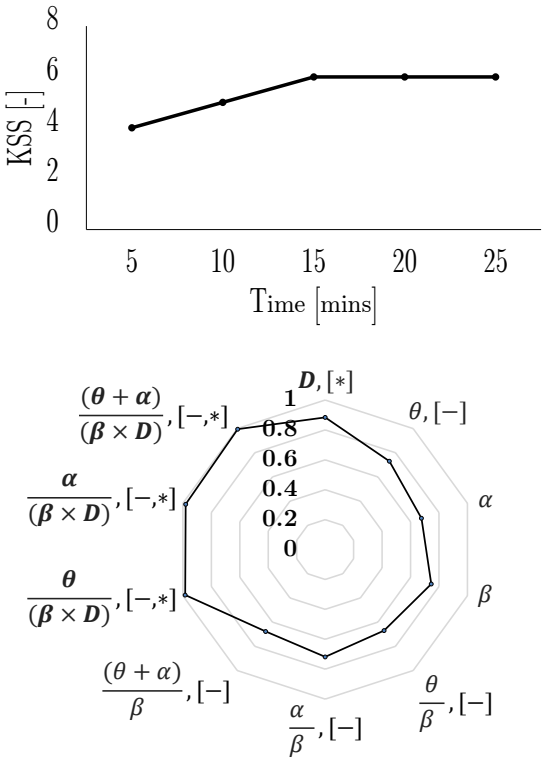

FIGURE 6.5: KSS results and comparison of Pearson's linear correlations between all drowsy indices and KSS among the six participants. [−] indicates negative correlation, and significant correlation ($p < 0.05$) is denoted by [∗].

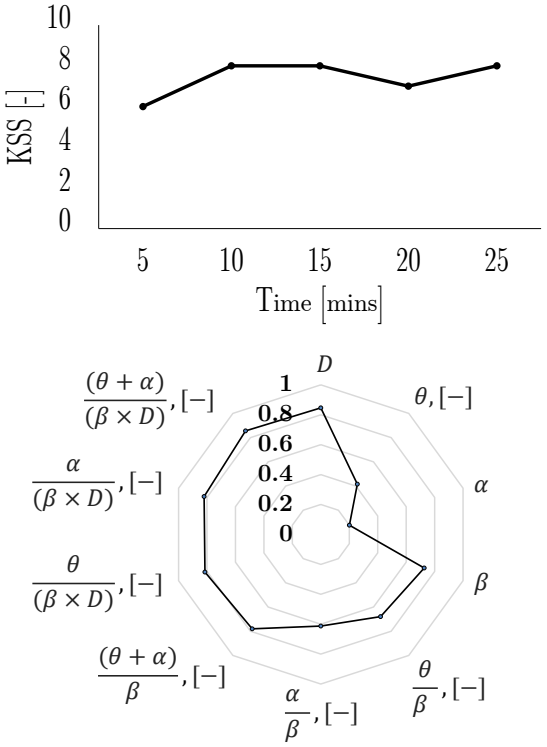

Participant C

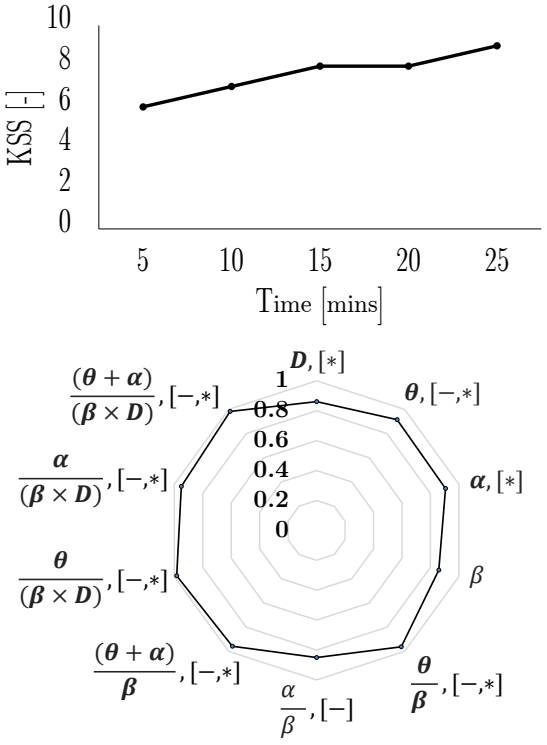

Participant D

FIGURE 6.5: KSS results and comparison of Pearson's linear correlations between all drowsy indices and KSS among the six participants. [−] indicates negative correlation, and significant correlation ($p < 0.05$) is denoted by [∗].

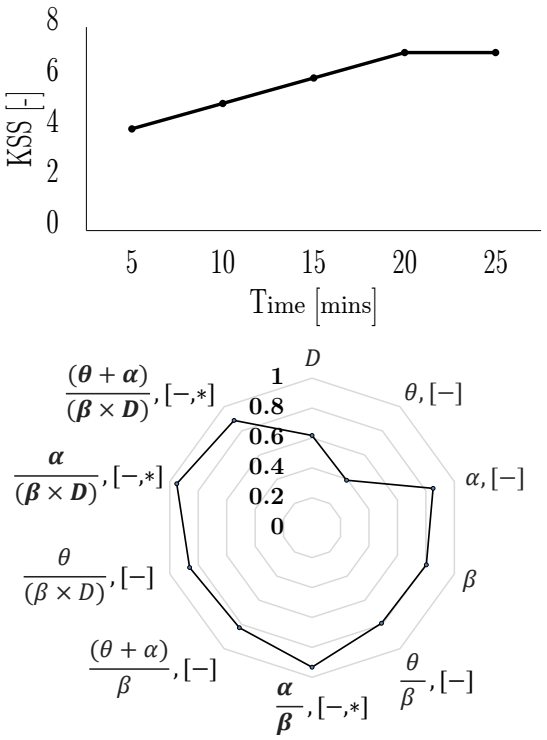

Participant E

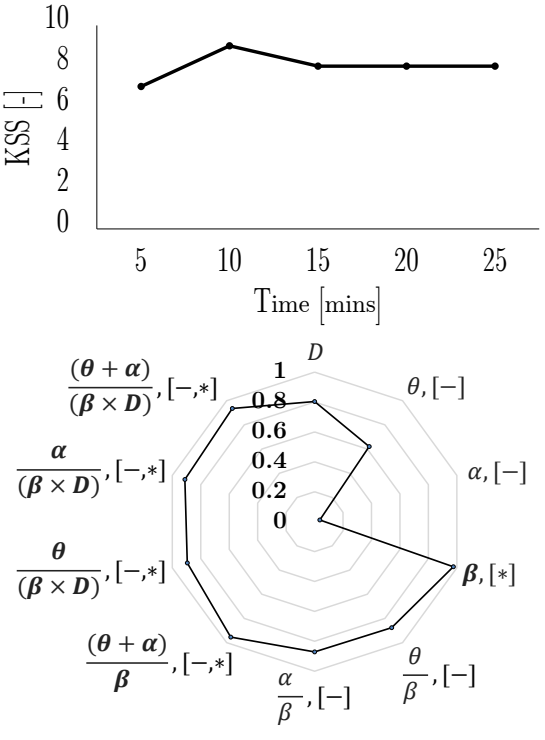

Participant F

FIGURE 6.5: KSS results and comparison of Pearson's linear correlations between all drowsy indices and KSS among the six participants. [−] indicates negative correlation, and significant correlation ($p < 0.05$) is denoted by [∗].

6.5 Summary

Here, I proposed a hybrid EEG/EOG-based BCI for drowsiness detection. EEG and EOG signals during performance of a simple response task in a drowsy environment were simultaneously recorded by a single-channel EEG amplifier. I report the first use of hybrid EEG/EOG indices to assess drowsiness. My results reveal the superiority of my proposed indices compared with conventional indices. I expect that this paper will contribute to the development of real-time drowsiness detection and sleep research in the near future.

Chapter 7

Conclusion

In this Chapter, I begin with discussion on contributions of research outcomes towards development of BCI applications. Then, I point out ongoing research issues and future works. Finally, conclusion of this thesis is summarized.

7.1 Contributions

7.1.1 Visual factor studies for an improvement of P300-based BCIs

Various visual factors, color effect, motion-modulated effect (modulated by saccade-ERP), complexity-modulated effect and orientation-modulated effect for a design of visual-based BCI are first introduced by my research. I demonstrate that introduced visual factors did enhance the P300 responses and suggested their feasibility in the practical use of BCI system. Finally, my research is supposed to be inter-connection between scientific and engineering researches. Investigated visual factors related to P300 will be summarized to be a design theory of visual stimulation for BCI. Not only medical-used applications, but also non-medical used applications can gain advantages from my proposed theory. Furthermore, I expect that my research will motivate other BCI researchers to study more about human visual factors in a design of visual stimulation.

7.1.2 PIN application using BCIs

To demonstrate performance of my developed BCI towards non-medical application, I invent a BCI-based personal identification number (PIN) application. Nowadays, users typically use keypads to input PINs. A major drawback of keypads is that PINs can be visually or optically observed when they are entered or recovered afterward by thermal

camera-based attacks. Various approaches based on biometrics and biosignals have been proposed in order to solve this problem. Fingerprints are widely used in biometric system. However, fingerprints can be duplicated by various techniques. One research group proposes gaze-based password entry, but gaze tracking requires a long time for calibration. There are two advantages of BCI-based PIN application over the above-mentioned techniques. The first is that the user can avoid the problem of the PIN being observed during entry, as is possible with keypads. The second is that BCIs allow for non-touch input, so no heat signal or fingerprint is left behind after use. Moreover, proposed PIN application is based on novel adaptive algorithm for P300 detection which is useful for other BCI applications as well.

7.1.3 Toward development of hybrid BCIs

Here, I propose novel hybrid BCI (brain/blink) which is very useful for certain populations who possess some residual motor functions. The use of oculomotor, both eye blink and eye closure (to control EEG), should not be demanding even for patient populations. I also evaluate performance of the proposed interface with PIN application, and the result is convincing. Hybrid BCI technology would be a promising method to improve user satisfaction / experience in BCI devices. Moreover, same recording setup as proposed hybrid BCI is also applied for sleepiness level measurement. Preliminary findings on drowsiness detection using hybrid index (EEG/EOG) is promising for future development.

7.1.4 Single channel EEG-based computer interfaces

Most researchers develop EEG-based BCIs using multiple channels of electrodes. Multiple electrodes require large time consuming works in skin preparation and electrode placement. Thus, the existing BCI applications are not user-friendly compared to other human computer interfaces. On the other hand, single channel EEG and a computationally inexpensive algorithm are used throughout my studies. My proposed BCI and hybrid BCI are more practical and user-friendly than conventional BCIs.

7.2 Future works

To demonstrate that research fiindings from this thesis could be extended to various research directions, I illustrate summarized diagram as seen in Figure 7.1. There are

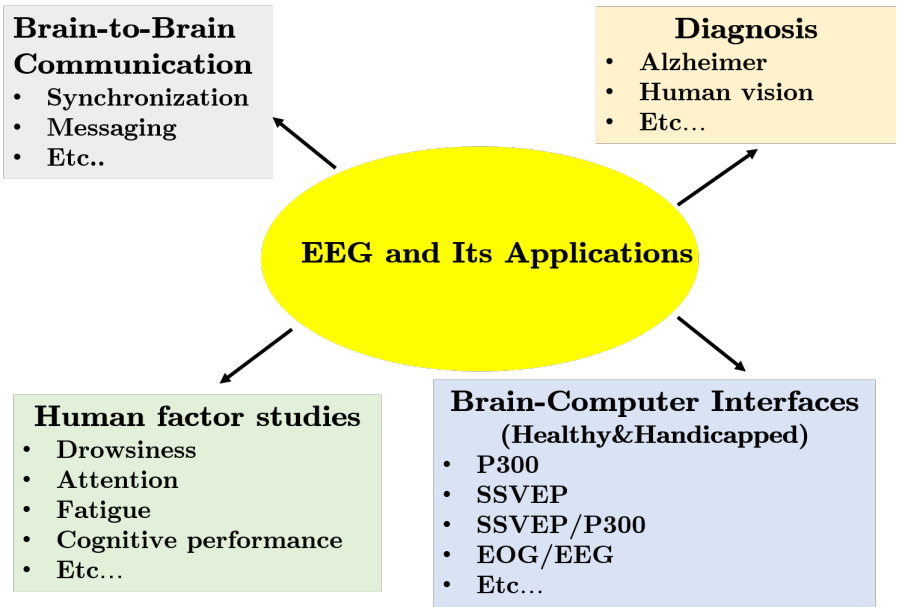

FIGURE 7.1: Present possibility to extend research findings from this thesis into four major research directions.

four major directions which are all related to EEG and BCIs. I am now working three out of four directions which are described in next three sub-sections.

7.2.1 Hybrid brain/eye-computer interface

Recently, I and my research collaborator expand the idea of hybrid brain/blink-computer interface to be hybrid brain/eye-computer interface by including eye movement signals to be input features. We have already published relevant research results on international conference proceedings [73]. In the next step, we are going to develop novel interface which can simultaneously recognize signals from brain (from eye closure), blink and eye movement. By incorporating of multiple obvious potential responses from brain and eyes, we would have high information transfer rate interface with acceptable reliability.

FIGURE 7.2: Preliminary study on EEG/EOG-based human fatigue measurement while engaing self-driving simulator. The study was conducted at Fatigue Countermeasures Group, Human Systems Integration Division, NASA Ames Research Center

7.2.2 Hybrid BCIs for drowsiness detection

According to side project on Chapter 6, I plan to conduct more research on EEG/EOG-based human fatigue measurement in driving studies as shown in Figure 7.2. Nowadays, many automobile companies are investigating driver fatigue measurement techniques. The fatigue measurement can help a car in performing a decision to select between manual and auto-pilot driving modes. Thus, further investigation on this research topics would be advantages for automobile societies in near future.

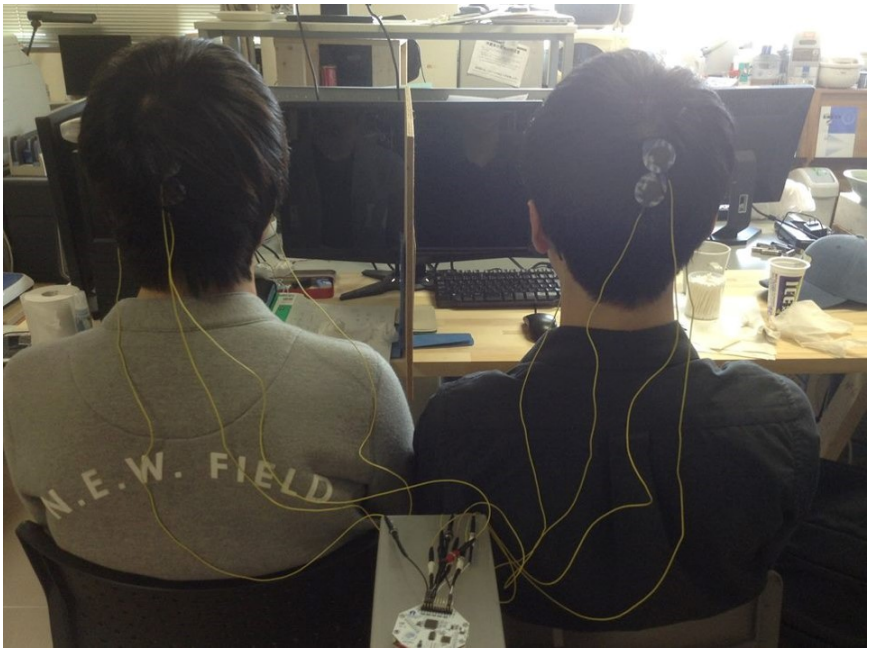

FIGURE 7.3: Preliminary study on proof of concept of brain-to-brain communcation

7.2.3 Introduction to brain-to-brain communication

To expand basis of EEG knowledge, I am now working on proof of concept of brain-to-brain communication (B2B) [74], Figure 7.3. I am trying to make synchronization between two brains (to establish communication pathway), and then allow one brain to send message (modulate EOG information into EEG signal) to the other via the established pathway. B2B experiments are based on EEG, visual stimulation, computer simulation and electronic circuit. I strongly believe that B2B concept would be an opening gate to future trends of BCI research.

7.3 Conclusion

Ultimate goal of this research is to develop practical BCI applications for both medical and non-medical purposes. I first achieve in proposing novel visual stimuli for an improvement of P300-based BCIs. Second, I introduce novel hybrid BCI which is more practical and user-friendly than conventional BCIs. To demonstrate the advantage of improved P300-baed BCI and proposed hybrid BCI, I incorporate both interfaces into PIN application. Participants in this studies perform acceptable accuracy in using BCI-based PIN application. Experimental results are promising that proposed interfaces would make scientific and engineering contributions to BCI research societies in near future. Moreover, this research lead me to threes new research issues which are drowsiness

detection using hybrid BCI, novel hybrid brain/eye interface and introduction to-brain-to-brain communication. Continue developing these issues are possibly to make scientific contributions in near future.

References

[1] Reza Fazel-Rezai, Brendan Z Allison, Christoph Guger, Eric W Sellers, Sonja C Kleih, and Andrea Kübler. P300 brain computer interface: current challenges and emerging trends. *Front Neuroeng*, 5:14, 2012. doi: 10.3389/fneng.2012.00014. URL `http://dx.doi.org/10.3389/fneng.2012.00014`.

[2] John G. Webster. Measurement, instrumentation, and sensors handbook, second edition. 2014. URL `http://gbv.eblib.com/patron/FullRecord.aspx?p=1407945`. Description based upon print version of record.

[3] Jonathan R Wolpaw, Niels Birbaumer, Dennis J McFarland, Gert Pfurtscheller, and Theresa M Vaughan. Brain–computer interfaces for communication and control. *Clinical neurophysiology*, 113(6):767–791, 2002.

[4] Luis Fernando Nicolas-Alonso and Jaime Gomez-Gil. Brain computer interfaces, a review. *Sensors (Basel)*, 12(2):1211–1279, 2012. doi: 10.3390/s120201211. URL `http://dx.doi.org/10.3390/s120201211`.

[5] Tobias Kaufmann, Elisa M Holz, and Andrea Kübler. Comparison of tactile, auditory, and visual modality for brain-computer interface use: a case study with a patient in the locked-in state. *Front Neurosci*, 7:129, 2013. doi: 10.3389/fnins.2013.00129. URL `http://dx.doi.org/10.3389/fnins.2013.00129`.

[6] TW Picton. The p300 wave of the human event-related potential. *J Clin Neurophysiol*, 9(4):456–479, Oct 1992.

[7] Lawrence Ashley Farwell and Emanuel Donchin. Talking off the top of your head: toward a mental prosthesis utilizing event-related brain potentials. *Electroencephalography and clinical Neurophysiology*, 70(6):510–523, 1988.

[8] Setare Amiri, Reza Fazel-Rezai, and Vahid Asadpour. A review of hybrid brain-computer interface systems. *Advances in Human-Computer Interaction*, 2013:1, 2013.

[9] Jiaxin Ma, Yu Zhang, Andrzej Cichocki, and Fumitoshi Matsuno. A novel eog/eeg hybrid human-machine interface adopting eye movements and erps: application to robot control. *IEEE Trans Biomed Eng*, 62(3):876–889, Mar 2015. doi: 10.1109/TBME.2014.2369483. URL `http://dx.doi.org/10.1109/TBME.2014.2369483`.

[10] Robert Leeb, Hesam Sagha, Ricardo Chavarriaga, and José Del R Millán. A hybrid brain-computer interface based on the fusion of electroencephalographic and electromyographic activities. *J Neural Eng*, 8(2):025011, Apr 2011. doi: 10.1088/1741-2560/8/2/025011. URL `http://dx.doi.org/10.1088/1741-2560/8/2/025011`.

[11] B Z Allison, C Brunner, V Kaiser, G R M?ller-Putz, C Neuper, and G Pfurtscheller. Toward a hybrid brain–computer interface based on imagined movement and visual attention. *J. Neural Eng.*, 7(2):026007, mar 2010. doi: 10.1088/1741-2560/7/2/026007. URL `http://dx.doi.org/10.1088/1741-2560/7/2/026007`.

[12] Gert Pfurtscheller, Teodoro Solis-Escalante, Rupert Ortner, Patricia Linortner, and Gernot R Müller-Putz. Self-paced operation of an ssvep-based orthosis with and without an imagery-based "brain switch:" a feasibility study towards a hybrid bci. *IEEE Trans Neural Syst Rehabil Eng*, 18(4):409–414, Aug 2010. doi: 10.1109/TNSRE.2010.2040837. URL `http://dx.doi.org/10.1109/TNSRE.2010.2040837`.

[13] C Brunner, B Z Allison, C Altst?tter, and C Neuper. A comparison of three brain–computer interfaces based on event-related desynchronization, steady state visual evoked potentials, or a hybrid approach using both signals. *J. Neural Eng.*, 8 (2):025010, mar 2011. doi: 10.1088/1741-2560/8/2/025010. URL `http://dx.doi.org/10.1088/1741-2560/8/2/025010`.

[14] Rajesh C Panicker, Sadasivan Puthusserypady, and Ying Sun. An asynchronous p300 bci with ssvep-based control state detection. *IEEE Trans Biomed Eng*, 58(6): 1781–1788, Jun 2011. doi: 10.1109/TBME.2011.2116018. URL `http://dx.doi.org/10.1109/TBME.2011.2116018`.

[15] Siamac Fazli, Jan Mehnert, Jens Steinbrink, Gabriel Curio, Arno Villringer, Klaus-Robert Müller, and Benjamin Blankertz. Enhanced performance by a hybrid nirs-eeg brain computer interface. *Neuroimage*, 59(1):519–529, Jan 2012. doi: 10.1016/j.neuroimage.2011.07.084. URL `http://dx.doi.org/10.1016/j.neuroimage.2011.07.084`.

[16] Kouji Takano, Tomoaki Komatsu, Naoki Hata, Yasoichi Nakajima, and Kenji Kansaku. Visual stimuli for the p300 brain-computer interface: a comparison of white/gray and green/blue flicker matrices. *Clin Neurophysiol*, 120(8):1562–1566,

Aug 2009. doi: 10.1016/j.clinph.2009.06.002. URL http://dx.doi.org/10.1016/j.clinph.2009.06.002.

[17] MG Woldorff. Distortion of erp averages due to overlap from temporally adjacent erps: analysis and correction. *Psychophysiology*, 30(1):98–119, Jan 1993.

[18] Reza Fazel-Rezai. Human error in p300 speller paradigm for brain-computer interface. *Conf Proc IEEE Eng Med Biol Soc*, 2007:2516–2519, 2007. doi: 10.1109/IEMBS.2007.4352840. URL http://dx.doi.org/10.1109/IEMBS.2007.4352840.

[19] Christoph Guger, Shahab Daban, Eric Sellers, Clemens Holzner, Gunther Krausz, Roberta Carabalona, Furio Gramatica, and Guenter Edlinger. How many people are able to control a p300-based brain-computer interface (bci)? *Neurosci Lett*, 462 (1):94–98, Oct 2009. doi: 10.1016/j.neulet.2009.06.045. URL http://dx.doi.org/10.1016/j.neulet.2009.06.045.

[20] Reza Fazel-Rezai and Kamyar Abhari. A comparison between a matrix-based and a region-based p300 speller paradigms for brain-computer interface. *Conf Proc IEEE Eng Med Biol Soc*, 2008:1147–1150, 2008. doi: 10.1109/IEMBS.2008.4649364. URL http://dx.doi.org/10.1109/IEMBS.2008.4649364.

[21] G Townsend, BK LaPallo, CB Boulay, DJ Krusienski, GE Frye, CK Hauser, NE Schwartz, TM Vaughan, JR Wolpaw, and EW Sellers. A novel p300-based brain-computer interface stimulus presentation paradigm: moving beyond rows and columns. *Clin Neurophysiol*, 121(7):1109–1120, Jul 2010. doi: 10.1016/j.clinph.2010.01.030. URL http://dx.doi.org/10.1016/j.clinph.2010.01.030.

[22] Jing Jin, Brendan Z Allison, Tobias Kaufmann, Andrea Kübler, Yu Zhang, Xingyu Wang, and Andrzej Cichocki. The changing face of p300 bcis: a comparison of stimulus changes in a p300 bci involving faces, emotion, and movement. *PLoS One*, 7(11):e49688, 2012. doi: 10.1371/journal.pone.0049688. URL http://dx.doi.org/10.1371/journal.pone.0049688.

[23] Fei Guo, Bo Hong, Xiaorong Gao, and Shangkai Gao. A brain-computer interface using motion-onset visual evoked potential. *J Neural Eng*, 5(4):477–485, Dec 2008. doi: 10.1088/1741-2560/5/4/011. URL http://dx.doi.org/10.1088/1741-2560/5/4/011.

[24] Tao Liu, Leslie Goldberg, Shangkai Gao, and Bo Hong. An online brain-computer interface using non-flashing visual evoked potentials. *J Neural Eng*, 7(3):036003, Jun 2010. doi: 10.1088/1741-2560/7/3/036003. URL http://dx.doi.org/10.1088/1741-2560/7/3/036003.

[25] Yu Su, Yu Qi, Jian xun Luo, Bian Wu, Fan Yang, Yi Li, Yue ting Zhuang, Xiao xiang Zheng, and Wei dong Chen. A hybrid brain-computer interface control strategy in a virtual environment. *Journal of Zhejiang University SCIENCE C*, 12(5):351–361, may 2011. doi: 10.1631/jzus.c1000208. URL `http://dx.doi.org/10.1631/jzus.C1000208`.

[26] H. Riechmann, N. Hachmeister, H. Ritter, and A. Finke. Asynchronous, parallel on-line classification of p300 and erd for an efficient hybrid bci. In *Proc. 5th Int Neural Engineering (NER) IEEE/EMBS Conf*, pages 412–415, April 2011. doi: 10.1109/NER.2011.5910574.

[27] X. Yong, M. Fatourechi, R. K. Ward, and G. E. Birch. The design of a point-and-click system by integrating a self-paced brain –computer interface with an eye-tracker. *IEEE Journal on Emerging and Selected Topics in Circuits and Systems*, 1 (4):590–602, December 2011. ISSN 2156-3357. doi: 10.1109/JETCAS.2011.2175589.

[28] Katarzyna Blinowska and Piotr Durka. *Electroencephalography (EEG)*. John Wiley & Sons, Inc., 2006. ISBN 9780471740360. doi: 10.1002/9780471740360.ebs0418. URL `http://dx.doi.org/10.1002/9780471740360.ebs0418`.

[29] Robert M. Chapman, Samuel A. Shelburne Jr., and Henry R. Bragdon. {EEG} alpha activity influenced by visual input and not by eye position. *Electroencephalography and Clinical Neurophysiology*, 28(2):183 – 189, 1970. ISSN 0013-4694. doi: http://dx.doi.org/10.1016/0013-4694(70)90186-0. URL `http://www.sciencedirect.com/science/article/pii/0013469470901860`.

[30] F Piccione, F Giorgi, P Tonin, K Priftis, S Giove, S Silvoni, G Palmas, and F Beverina. P300-based brain computer interface: reliability and performance in healthy and paralysed participants. *Clin Neurophysiol*, 117(3):531–537, Mar 2006. doi: 10.1016/j.clinph.2005.07.024. URL `http://dx.doi.org/10.1016/j.clinph.2005.07.024`.

[31] Luca Citi, Riccardo Poli, Caterina Cinel, and Francisco Sepulveda. P300-based bci mouse with genetically-optimized analogue control. *IEEE Trans Neural Syst Rehabil Eng*, 16(1):51–61, Feb 2008. doi: 10.1109/TNSRE.2007.913184. URL `http://dx.doi.org/10.1109/TNSRE.2007.913184`.

[32] Christian J Bell, Pradeep Shenoy, Rawichote Chalodhorn, and Rajesh P N Rao. Control of a humanoid robot by a noninvasive brain-computer interface in humans. *J Neural Eng*, 5(2):214–220, Jun 2008. doi: 10.1088/1741-2560/5/2/012. URL `http://dx.doi.org/10.1088/1741-2560/5/2/012`.

[33] I. Iturrate, J. M. Antelis, A. Kubler, and J. Minguez. A noninvasive brain-actuated wheelchair based on a p300 Neurophysiological protocol and automated navigation. 25(3):614–627, June 2009. ISSN 1552-3098. doi: 10.1109/TRO.2009.2020347.

[34] Halder S. Kleih S. C. Furdea A. Raco V. Hoesle A. Muenssinger, J. I. and Kubler. Brain painting: First evaluation of a new brain-computer interface application with als-patients and healthy volunteers. *Front Neurosci*, 4:182, 2010. doi: 10.3389/fnins.2010.00182. URL `http://dx.doi.org/10.3389/fnins.2010.00182`.

[35] Minkyu Ahn, Mijin Lee, Jinyoung Choi, and Sung Chan Jun. A review of brain-computer interface games and an opinion survey from researchers, developers and users. *Sensors (Basel)*, 14(8):14601–14633, 2014. doi: 10.3390/s140814601. URL `http://dx.doi.org/10.3390/s140814601`.

[36] JD Bayliss and DH Ballard. A virtual reality testbed for brain-computer interface research. *IEEE Trans Rehabil Eng*, 8(2):188–190, Jun 2000.

[37] Shiro Ikegami, Kouji Takano, Makoto Wada, Naokatsu Saeki, and Kenji Kansaku. Effect of the green/blue flicker matrix for p300-based brain-computer interface: An eeg-fmri study. *Front Neurol*, 3:113, 2012. doi: 10.3389/fneur.2012.00113. URL `http://dx.doi.org/10.3389/fneur.2012.00113`.

[38] Jaime Parra, Fernando H Lopes da Silva, Hans Stroink, and Stiliyan Kalitzin. Is colour modulation an independent factor in human visual photosensitivity? *Brain*, 130(Pt 6):1679–1689, Jun 2007. doi: 10.1093/brain/awm103. URL `http://dx.doi.org/10.1093/brain/awm103`.

[39] B Radford and R Bartholomew. Pokémon contagion: photosensitive epilepsy or mass psychogenic illness? *South Med J*, 94(2):197–204, Feb 2001.

[40] Ai Yoto, Tetsuo Katsuura, Koichi Iwanaga, and Yoshihiro Shimomura. Effects of object color stimuli on human brain activities in perception and attention referred to eeg alpha band response. *J Physiol Anthropol*, 26(3):373–379, May 2007.

[41] Taka-aki Suzuki, Yi Qiang, Satoshi Sakuragawa, Hisae Tamura, and Katsunori Okajima. Age-related changes of reaction time and p300 for low-contrast color stimuli: Effects of yellowing of the aging human lens. *J Physiol Anthropol*, 25(2):179–187, Mar 2006.

[42] D Regan and H Spekreijse. Evoked potential indications of colour blindness. *Vision Res*, 14(1):89–95, Jan 1974.

[43] John P Kelly, Michael A Crognale, and Avery H Weiss. Ergs, cone-isolating veps and analytical techniques in children with cone dysfunction syndromes. *Doc Ophthalmol*, 106(3):289–304, May 2003.

[44] Theerawit Wilaiprasitporn and Tohru Yagi. Investigation of p300 response characteristics through human color vision-based visual stimulation. *Conf Proc IEEE Eng Med Biol Soc*, 2014:4900–4903, 2014. doi: 10.1109/EMBC.2014.6944722. URL `http://dx.doi.org/10.1109/EMBC.2014.6944722`.

[45] Wilaiprasitporn Theerawit and Yagi Tohru. Preliminary study of visual attention effect on p300 response. *in Proc. IEEJ EISS*, pages 188–191, sep 2014.

[46] T. Wilaiprasitporn and T. Yagi. New visual stimulation paradigm for p300-based brain-computer interfaces. In *Proc. 7th Biomedical Engineering Int. Conf. (BMEiCON)*, pages 1–5, November 2014. doi: 10.1109/BMEiCON.2014.7017369.

[47] S Makeig, M Westerfield, TP Jung, S Enghoff, J Townsend, E Courchesne, and TJ Sejnowski. Dynamic brain sources of visual evoked responses. *Science*, 295 (5555):690–694, Jan 2002. doi: 10.1126/science.1066168. URL `http://dx.doi.org/10.1126/science.1066168`.

[48] Olaf Dimigen, Matteo Valsecchi, Werner Sommer, and Reinhold Kliegl. Human microsaccade-related visual brain responses. *J Neurosci*, 29(39):12321–12331, Sep 2009. doi: 10.1523/JNEUROSCI.0911-09.2009. URL `http://dx.doi.org/10.1523/JNEUROSCI.0911-09.2009`.

[49] Sangita Dandekar, Jian Ding, Claudio Privitera, Thom Carney, and Stanley A Klein. The fixation and saccade p3. *PLoS One*, 7(11):e48761, 2012. doi: 10.1371/journal.pone.0048761. URL `http://dx.doi.org/10.1371/journal.pone.0048761`.

[50] DH Hubel and TN Wiesel. Receptive fields and functional architecture of monkey striate cortex. *J Physiol*, 195(1):215–243, Mar 1968.

[51] T. Wilaiprasitporn and T. Yagi. Personal identification number application using brain-computer interface. In *Neural Engineering (NER), 2015 7th International IEEE/EMBS Conference on*, pages 114–117, 2015. doi: 10.1109/NER.2015.7146573. URL `http://ieeexplore.ieee.org/stamp/stamp.jsp?arnumber=7146573`.

[52] Keaton Mowery, Sarah Meiklejohn, and Stefan Savage. Heat of the moment: Characterizing the efficacy of thermal camera-based attacks. In *Proceedings of the 5th USENIX Conference on Offensive Technologies*, WOOT'11, pages 6–6, Berkeley, CA, USA, 2011. USENIX Association. URL `http://dl.acm.org/citation.cfm?id=2028052.2028058`.

[53] A. K. Jain, A. Ross, and S. Prabhakar. An introduction to biometric recognition. *IEEE Transactions on Circuits and Systems for Video Technology*, 14(1):4–20, January 2004. ISSN 1051-8215. doi: 10.1109/TCSVT.2003.818349.

[54] Manu Kumar, Tal Garfinkel, Dan Boneh, and Terry Winograd. Reducing shoulder-surfing by using gaze-based password entry. In *Proceedings of the 3rd Symposium on Usable Privacy and Security*, SOUPS '07, pages 13–19, New York, NY, USA, 2007. ACM. ISBN 978-1-59593-801-5. doi: 10.1145/1280680.1280683. URL `http://doi.acm.org/10.1145/1280680.1280683`.

[55] Ramaswamy Palaniappan and Kenneth Revett. Pin generation using eeg: A stability study. *Int. J. Biometrics*, 6(2):95–105, May 2014. ISSN 1755-8301. doi: 10.1504/IJBM.2014.060960. URL `http://dx.doi.org/10.1504/IJBM.2014.060960`.

[56] Theerawit Wilaiprasitporn and Tohru Yagi. Orientation-modulated attention effect on visual evoked potential: Application for pin system using brain-computer interface. *Conf Proc IEEE Eng Med Biol Soc*, 2015:2327–2330, Aug 2015. doi: 10.1109/EMBC.2015.7318859. URL `http://dx.doi.org/10.1109/EMBC.2015.7318859`.

[57] E. Sellers. A p300 event-related potential brain-computer interface (bci): the effects of matrix size and inter stimulus interval on performance. *Biol Psychol.*, 73:242–252, July 2006.

[58] Hiroyuki Manabe, Masaaki Fukumoto, and Tohru Yagi. Direct gaze estimation based on nonlinearity of eog. *IEEE Trans Biomed Eng*, 62(6):1553–1562, Jun 2015. doi: 10.1109/TBME.2015.2394409. URL `http://dx.doi.org/10.1109/TBME.2015.2394409`.

[59] Theerawit Wilaiprasitporn and Tohru Yagi. Motion-modulated and complexity-modulated attention effects on visual evoked potential p300: Applications for p300-Based brain-computer interfaces. *IEEJ Trans.EIS*, 135(7):826–831, 2015. doi: 10.1541/ieejeiss.135.826. URL `http://dx.doi.org/10.1541/ieejeiss.135.826`.

[60] Yanchao Dong, Zhencheng Hu, Keiichi Uchimura, and Nobuki Murayama. Driver inattention monitoring system for intelligent vehicles: A review. *Intelligent Transportation Systems, IEEE Transactions on*, 12(2):596–614, 2011.

[61] Arun Sahayadhas, Kenneth Sundaraj, and Murugappan Murugappan. Detecting driver drowsiness based on sensors: a review. *Sensors*, 12(12):16937–16953, 2012.

[62] Hong J Eoh, Min K Chung, and Seong-Han Kim. Electroencephalographic study of drowsiness in simulated driving with sleep deprivation. *International Journal of Industrial Ergonomics*, 35(4):307–320, 2005.

[63] Budi Thomas Jap, Sara Lal, Peter Fischer, and Evangelos Bekiaris. Using eeg spectral components to assess algorithms for detecting fatigue. *Expert Systems with Applications*, 36(2):2352–2359, 2009.

[64] Kosuke Kaida, Masaya Takahashi, Torbjörn Åkerstedt, Akinori Nakata, Yasumasa Otsuka, Takashi Haratani, and Kenji Fukasawa. Validation of the karolinska sleepiness scale against performance and eeg variables. *Clinical Neurophysiology*, 117(7): 1574–1581, 2006.

[65] Fu-Chang Lin, Li-Wei Ko, Chun-Hsiang Chuang, Tung-Ping Su, and Chin-Teng Lin. Generalized eeg-based drowsiness prediction system by using a self-organizing neural fuzzy system. *Circuits and Systems I: Regular Papers, IEEE Transactions on*, 59(9):2044–2055, 2012.

[66] Chin-Teng Lin, Che-Jui Chang, Bor-Shyh Lin, Shao-Hang Hung, Chih-Feng Chao, and I-Jan Wang. A real-time wireless brain–computer interface system for drowsiness detection. *Biomedical Circuits and Systems, IEEE Transactions on*, 4(4): 214–222, 2010.

[67] Jianping Liu, Chong Zhang, and Chongxun Zheng. Eeg-based estimation of mental fatigue by using kpca–hmm and complexity parameters. *Biomedical Signal Processing and Control*, 5(2):124–130, 2010.

[68] Rami N Khushaba, Sarath Kodagoda, Sara Lal, and Gamini Dissanayake. Driver drowsiness classification using fuzzy wavelet-packet-based feature-extraction algorithm. *Biomedical Engineering, IEEE Transactions on*, 58(1):121–131, 2011.

[69] Muhammed B Kurt, Necmettin Sezgin, Mehmet Akin, Gokhan Kirbas, and Muhittin Bayram. The ann-based computing of drowsy level. *Expert Systems with Applications*, 36(2):2534–2542, 2009.

[70] Michael Ingre, TorbjÖRn ÅKerstedt, BjÖRn Peters, Anna Anund, and GÖRan Kecklund. Subjective sleepiness, simulated driving performance and blink duration: examining individual differences. *Journal of sleep research*, 15(1):47–53, 2006.

[71] SR Quartz, M Stensmo, MS Makeig, and TJ Sejnowski. Eye blink rate as a practical predictor for vigilance. *Society for Neuroscience, San Diego*, 1995.

[72] Torbjörn Åkerstedt, Anna Anund, John Axelsson, and Göran Kecklund. Subjective sleepiness is a sensitive indicator of insufficient sleep and impaired waking function. *Journal of sleep research*, 23(3):242–254, 2014.

[73] Theerawit Wilaiprasitporn Alexandru Popovici and Tohru Yagi. Single-channel electrooculography application using unsupervised calibration. In *Conf Proc Telecommunications and Signal Processing (TSP)*, 2016.

[74] Theerawit Wilaiprasitporn Christopher Micek and Tohru Yagi. A study on ssvep-based brain synchronization: Road to brain-to-brain communication. In *Proc. 9th Biomedical Engineering Int. Conf. (BMEiCON)*, 2016.

Relevant Publications

Journals

1. **T. Wilaiprasitporn** and T. Yagi, "Motion-Modulated and Complexity-Modulated Attention Effects on Visual Evoked Potential P300: Applications for P300-Based Brain-Computer Interfaces", IEEJ Transactions on Electronics, Information and Systems (C), Vol. 135, No. 7, pp. 826-4831, 2015 [Chapter 3]

2. **T. Wilaiprasitporn** and T. Yagi, "Personal Identification Number Application Using Adaptive P300 Brain–Computer Interface", IEEJ Transactions on Electronics, Information and Systems (C), Vol. 136, No. 9, pp. 1277-1282, 2016 [Chapter 4]

3. **T. Wilaiprasitporn**, A. Popovici and T. Yagi, "Hybrid Brain/Blink Computer Interface toward a Personal Identification Number Application", IEEJ Transactions on Electronics, Information and Systems (C), Vol. 136, No. 9, pp. 1312-1317, 2016 [Chapter 5]

Proceedings

1. **T. Wilaiprasitporn** and T. Yagi, "Investigation of P300 Response Characteristics through Human Color Vision-Based Visual stimulation", Conf Proc IEEE Eng Med Biol Soc, 4900-4903, 2014 [Chapter 3]

2. **T. Wilaiprasitporn** and T. Yagi, "New Visual Stimulation Paradigm for P300-Based Brain-Computer Interfaces", In Proc. 7th Biomedical Engineering Int. Conf. (BME-iCON), 1-5, 2014 [Chapter 3]

3. **T. Wilaiprasitporn** and T. Yagi, "Personal Identification Number Application Using Brain-Computer Interface", In Neural Engineering (NER), 27th International IEEE/EMBS Conference on, 114-117, 2015 [Chapter 4]

4. **T. Wilaiprasitporn** and T. Yagi, "Orientation-Modulated Attention Effect on Visual Evoked Potential: Application for Pin System Using Brain-Computer Interface", Conf Proc IEEE Eng Med Biol Soc, 2327-2330, 2015 [Chapter 3, 4]

5. **T. Wilaiprasitporn** and T. Yagi, "Feasibility Study of Drowsiness Detection Using Hybrid Brain-Computer Interface", In Proc. of i-CREATe, 2016 [Chapter 6]

6. A. Popovici, **T. Wilaiprasitporn**, and T. Yagi, "Single-Channel Electrooculography Application Using Unsupervised Calibration", In Conf Proc Telecommunications and Signal Processing (TSP), 2016 [Chapter 7]

7. C. Micek, **T. Wilaiprasitporn** and T. Yagi, "A Study on SSVEP-Based Brain Synchronization: Road to Brain-to-Brain Communication", In Proc. 9th Biomedical Engineering Int. Conf. (BMEiCON), 2016 (in press) [Chapter 7]